STUDIES IN THE ABSORPTION OF CARBON DIOXIDE IN WATER AT HIGH PARTIAL PRESSURES

A thesis submitted by

A. M. McLean, B.Sc., A.R.I.C.,

to the University of Glasgow in fulfilment of the requirements of the Degree of Doctor of Philosophy in Applied Science.

Technical Chemistry Department,
Royal Technical College,
Glasgow.

December, 1956

ProQuest LLC.
789 East Eisenhower Parkway
P.O. Box 1346
Ann Arbor, MI 48106 – 1346

PUBLICATIONS

Parts of this thesis have been submitted as papers to the Journal "Chemical Engineering Science" and the following two papers have been accepted for publication:-

1. Compressibility, Fugacity and Water-Solubility of Carbon Dioxide in the Region 0-36 atm. and 0-100°C. (Part 2 of this thesis).
2. Absorption of Carbon Dioxide in Water under Pressure, Using a Gas-Bubble Column. (Part 3 of this thesis).

A third paper, based on Part 4 of this thesis, called "The Mechanism of Formation of Gas Bubble-Beds" has also been submitted but at present no decision has been reached on its publication.

ACKNOWLEDGMENTS

The author wishes to express his gratitude to his supervisor, Dr. G. Houghton, for his interest and advice during the course of this work, and to Professor P.D. Ritchie, for affording the facilities of the Technical Chemistry Department of the Royal Technical College, Glasgow. The author is also indebted to his colleague Mr. J.A. Thomson for many stimulating discussions.

Grateful thanks are expressed to all members of the Technical Chemistry Department Workshop and in particular to Messrs. A. Clunie and G. Waddell for their help during the design and construction of the pilot plant.

Finally the author wishes to express his gratitude to the Admiralty for providing the research grant, which enabled this work to be carried out.

SUMMARY

This thesis is concerned with the absorption of carbon dioxide in water at partial pressures of the order 1-20 atmospheres.

In the introduction, the literature on the various types of gas scrubbers has been surveyed with reference to the absorption of a sparingly soluble gas at high concentrations and partial pressures. From this discussion, it was decided to investigate the absorption phenomena of carbon dioxide in water using a countercurrent bubble type absorber.

Part 2 of this thesis discusses the compressibility and equilibrium data for carbon dioxide in the pressure range 0-36 atmospheres and in the temperature range 0-100°C. A new equation of state for carbon dioxide, based on the Beattie equation, is derived and compressibility and fugacity charts have been drawn up using data calculated from this equation. The solubility data of carbon dioxide in water, from various sources, are reviewed and compared and a large scale solubility chart has been constructed. The applicability of Henry's law and the fugacity correction to Henry's law are also discussed.

In Part 3 the absorption phenomena of carbon dioxide in water using a countercurrent bubble type absorber has been studied. The effect of the following operating variables on the absorption rate has been determined; (i) liquid velocity, in the range 0.03-0.20 ft./sec.; (ii) gas velocity, in the range 0.06-0.25 ft./sec.; (iii) partial pressure of carbon dioxide, in the range 2.5-14 atmospheres; (iv) bed height, in the range 0.5-5.5 ft.; (v) temperature, in the range 10-30°C; and (vi) porosity of gas distributor, in the range 70-10,000 microns. In general, the bubble type absorber has proved successful for the absorption of large quantities of carbon dioxide from mixtures containing high percentages of carbon dioxide and is superior

to packed and spray towers for the absorption of this particular gas.

Finally, in Part 4 of this thesis, the mechanism of formation of gas bubble beds is investigated. Experimental data on the size, number, and distribution of bubbles in the bubble bed are discussed in relation to the formation of fluidised and foam beds. The effect of different porosities of gas distributor on the bed density and bubble size and shape are also investigated for various liquids. It is shown that the bed density at any superficial gas velocity is a function of the number of bubbles per ml. and the average volume of the bubbles produced.

CONTENTS.

PART 4. THE MECHANISM OF FORMATION OF GAS BUBBLE BEDS

PART 1

INTRODUCTION

1.1.

This thesis is concerned with gas absorption at high partial pressures, in particular with the absorption of carbon dioxide by water at partial pressures of the order 1-20 atmospheres.

The problem of removal of carbon dioxide from gas mixtures is commonly encountered in industry, where many processes produce quantities of gas containing from 10 to 90% carbon dioxide, the remainder being oxygen, nitrogen, carbon monoxide, hydrogen or mixtures of these components. There are several possible methods of removing carbon dioxide from these gases:-

1) Absorption in caustic alkali or ammonia to form the carbonates and bicarbonates;

2) Absorption in ethanolamine, followed by regeneration of the base;

3) Absorption in water.

In recent years much work has been done on absorption of carbon dioxide in ethanolamine by various workers such as Cryder and Maloney[1], working with packed towers, and Dixon[2] and also Chambers and Wall[3], using centrifugal scrubbers of the Piazza stillhead type. High absorption rate coefficients have been obtained but ethanolamine solutions suffer from the disadvantages that they deteriorate by oxidation and are corrosive to iron[4].

Water scrubbing, however, presents interesting possibilities for gases containing large percentages of carbon dioxide, especially if pressures greater than atmospheric are used. The effect of increase in

pressure is to decrease the amount of scrubbing water required, owing to the greater solubility of the gas at higher pressures, and to reduce the volume of gas being handled, which is especially important if large quantities of gas are to be treated. This reduction in the quantities of material involved will decrease the size of the absorber, possibly to a size comparable with or smaller than that of a scrubber using a chemical absorption process. Consequently, the relative advantages of water and chemical absorption are closely linked with the relative costs of gas compression compared with the cost of caustic or ammonia solutions, in case (1), and the cost of heat for the regeneration of ethanolamine, in case (2). Practical evidence for a beneficial effect of increased total pressure on the absorption rate of carbon dioxide has been noted from observations on overall plate efficiencies in plate absorbers. O'Connell[5] and also Drickamer and Bradford[6] have shown that plate efficiencies increase with total pressure.

1.2. CARBON DIOXIDE AS A SPARINGLY SOLUBLE GAS

Carbon dioxide is one of the less soluble gases, having a Bunsen absorption coefficient of 1 $ft.^3$ of carbon dioxide (calculated at N.T.P.) per $ft.^3$ of water at 15°C and 1 atmosphere partial pressure of carbon dioxide. This can be compared with an absorption coefficient of 785 for ammonia, one of the more soluble gases. Consequently, very large quantities of water are required for the absorption of carbon dioxide compared with that required for ammonia. According to Sherwood and Pigford[7] the ratio of liquid to gas flows by weight, for carbon dioxide, must exceed 880, while a similar liquid to gas ratio for ammonia is only about 5.

The Whitman theory[8] of absorption of a gas by a liquid assumes that

when a gas and a liquid are brought into contact the main bulk of both fluids is in turbulent flow and thus uniformly mixed. Adjacent to the interface, however, and on either side of it, there are assumed to be thin films of gas and liquid in streamline flow. It is further assumed that the resistance of the soluble gas to mass transfer is located wholly in these films and the main bulk of both fluids offer no resistance. There is no evidence of an appreciable diffusion resistance at the actual interface. Therefore, this resistance is assumed to be zero and the two phases are in equilibrium at all points on the surface. In a later paper Lewis and Whitman[9] relate the individual mass transfer coefficients of the films with the overall mass transfer coefficients and show that for slightly soluble gases the resistance of the liquid film to mass transfer controls the rate of absorption.

$$\frac{1}{K_L} = \frac{1}{k_L} + \frac{H}{k_G} \quad \text{---- ---- ----} \quad (1)$$

(where K_L is the overall mass transfer coefficient based on the liquid phase; k_L and k_G are the individual film mass transfer coefficients of liquid and gas respectively; and H is the Henry's law constant for the gas).

The coefficient H is a measure of the solubility of the gas in the liquid. It is evident from equation (1) that if H is sufficiently small, the gas film resistance may be negligible in comparison with the liquid film resistance.

A rather more accurate criterion for determining the absorption controlling film is described by Morris and Jackson[10] using the dimensionless ratio ρ_g/HP, where ρ_g is the density of the soluble gas at its actual temperature and pressure and P is the total pressure. For an absorption operation in the absence of any chemical reaction, Morris and Jackson give

the following rough guide for determining the relative magnitudes of the gas and liquid film resistances;

1) When $\rho_g/HP < 5 \times 10^{-4}$, gas film control is likely;

2) When $\rho_g/HP > 0.2$, liquid film control is likely;

3) For intermediate values, the resistance of both films may be significant.

Applying this guide to the case of carbon dioxide and water, and using values of ρ_g and H calculated from data in the International Critical Tables, it is found that $\rho_g/HP = 1.06$ at N.T.P. It can therefore be assumed that the absorption of carbon dioxide by water is liquid film controlled at N.T.P. An increase in total pressure may cause the gas film resistance to increase, since it will reduce the dimensionless ratio. However, an increase in the dimensionless ratio will also be caused by an increase in the partial pressure of the soluble gas since this will increase ρ_g. For pure carbon dioxide up to pressures of 10 atm. it can safely be assumed that the liquid film resistance will predominate and control the rate of absorption.

1.3. ABSORPTION RATES

Before discussing the types of gas absorption equipment available for a liquid film controlled absorption process, it will be helpful to outline the various units used in measuring the performance and efficiency of an an absorption operation.

The principal unit used in reporting the rate of an absorption process is the overall mass transfer coefficient. This is derived in the Whitman two film theory of absorption and is defined as:

$$B = K_L(x^* - x) \quad -- \quad -- \quad -- \quad -- \quad (2)$$

(where B is the rate of mass transfer, x^* is the concentration of a

solution in equilibrium with the solute partial pressure in the main gas stream and x is the concentration of gas already dissolved in the main liquid stream).

For the calculation of K_L it is necessary to evaluate the interfacial surface area between the liquid and gas phases. This value is difficult, if not impossible, to ascertain and for this reason it is convenient to introduce a variable a, which represents the interfacial surface area per unit volume. Since both a and K_L depend on the nature of the absorption column and the flow rates of the gas and liquid streams, they may be combined as a product, K_La, which represents the overall capacity coefficient on a volume basis. Thus K_La represents the rate of interphase diffusion as moles per unit time per unit volume per unit driving force in terms of concentrations for a liquid film controlled absorption process, and is defined by the equation:

$$Ba\ dV = K_La(x^* - x)dV \quad -- \quad -- \quad -- \quad (3)$$

(where Ba is the rate of mass transfer as moles per unit volume of equipment and V is the volume of the absorption process).

For a countercurrent absorption operation equation (3) can be simplified to:

$$K_La = \frac{B}{hA\Delta x_M} \quad -- \quad -- \quad -- \quad -- \quad (4)$$

(where h is the height of the absorption process, A is the cross-sectional area of column, and Δx_M is the mean driving force in terms of concentrations throughout the absorption volume).

A more convenient method of reporting the performance of an absorption process is based on the height of a transfer unit which was first introduced by Chilton and Colburn[11]. This method is used frequently in practical

design work as it is simple and easy to calculate and the resistance to mass transfer is expressed in the terms of an experimentally determined number which has the dimensions of length only. The basic concept is that estimation of the height of a tower always depends upon the evaluation of a definite integral, such as the following for a liquid film controlled absorption process:

$$(N.T.U.)_{OL} = \int_{x_1}^{x_2} \frac{dx}{x^* - x} \quad -- \quad -- \quad -- \quad (5)$$

where the subscripts 1 and 2 refer to concentrations of the gas in liquid in the inlet and outlet liquid streams respectively. The value of the integral, which is dimensionless, expresses the difficulty of absorbing the solute from the gas; it is greater the smaller the mean driving force and the larger the required change in gas composition. Chilton and Colburn have called it the number of transfer units based on the overall liquid phase driving force.

If the equilibrium and operating lines are straight, then the value of the integral can be evaluated using the logarithmic mean driving force. Then:

$$(N.T.U.)_{OL} = \frac{x_2 - x_1}{\Delta x_{lm}} \quad -- \quad -- \quad -- \quad -- \quad -- \quad -- \quad (6)$$

Where

$$\Delta x_{lm} = \frac{(x_2^* - x_2) - (x_1^* - x_1)}{\ln \frac{(x_2^* - x_2)}{(x_1^* - x_1)}} \quad -- \quad -- \quad -- \quad (7)$$

If, however, the equilibrium and/or operating lines are curved then the integral must be solved graphically, taking into account the effect of changes in the mean driving force throughout the column.

From the number of transfer units and the experimentally measured tower height the value of the height of an overall transfer unit, for a liquid film controlled absorption process, becomes:

$$(H.T.U.)_{OL} = \frac{h}{(N.T.U.)_{OL}} \quad -- \quad -- \quad -- \quad -- \quad (8)$$

The relationship between $K_L a$ and $(H.T.U.)_{OL}$ is:

$$(H.T.U.)_{OL} = \frac{L}{\rho_L K_L a} \quad -- \quad -- \quad -- \quad -- \quad (9)$$

(where L is the liquid rate and ρ_L is the density of the liquid).

An even simpler method of reporting the absorption rate data is the use of the absorption efficiency, E_A, which is defined as follows:

$$E_A = \frac{x_2 - x_1}{x_2^* - x_1} \quad -- \quad -- \quad -- \quad -- \quad (10)$$

(based on the inlet gas concentrations) and as:

$$E'_A = \frac{x_2 - x_1}{x_1^* - x_1} \quad -- \quad -- \quad -- \quad -- \quad (11)$$

(based on the outlet gas concentrations).

The overall absorption efficiencies, E_A and E'_A, have advantages over the $(H.T.U.)_{OL}$ and $K_L a$ concepts for correlating the data from countercurrent absorbers where large amounts of gas are absorbed and mean driving forces change throughout the absorption operation. E_A is more convenient to use in design calculations, since it avoids the computation of mean concentration gradients, and in addition can be used directly in calculating power requirements for pressure absorbers. (See Section 5.2.). In this respect, E_A is more useful than E'_A, since the latter may have values considerably greater than 100 for countercurrent operations.

1.4. ABSORPTION TOWERS

Industrial equipment for gas absorption can usually be classified as one of three types, each having as its principal objective the promotion of interphase contact between gas and liquid. In order to investigate the absorption of carbon dioxide by water under pressure the literature on the three standard types of absorption equipment has been surveyed to find which is most suitable for the absorption of large percentages of a gas whose absorption rate is controlled by the liquid film resistance.

1.4.1. Spray towers.

Spray towers consist of large empty chambers into the top of which the liquid is sprayed by means of nozzles or other atomising devices; the droplets thus formed are then allowed to fall to the botton of the tower through a stream of gas circulating upwards. Although diffusion is slow inside the drops, the continuous formation of fresh liquid surface at the spray nozzles allows absorption to take place rapidly. The gas film resistance around the drops being relatively small owing to the high velocities with which the liquid drops are propelled into the gas.

The main disadvantages of this type of absorber is that the droplets first formed may coalesce, thus reducing the surface area for absorption, and that the liquid is liable to be entrained in the gas stream even at low gas velocities.

In general, spray towers have been found more suitable for applications involving small changes in composition of the gas being treated, and where the gas film resistance controls the rate of absorption. This is exactly opposite to the conditions specified above, so that this type of

tower has been rejected for the study of the absorption of carbon dioxide.

1.4.2. Packed towers

The most common type of absorption equipment is the packed tower. It consists of a vertical shell set on adequate foundations, and filled with one of the numerous types of inert packing material. The operation is usually countercurrent, the solvent being distributed over the packing at the top of the tower and passing down over the packing in thin liquid films, while the gas passes up through the free space between the wetted particles of packing.

To ensure maximum absorption efficiencies it is necessary to obtain maximum wetting of the packing material by a good liquor distribution. Even if this is obtained the liquid has a tendency to flow towards the walls leaving unwetted packing in the middle. This leads to "channelling" of the liquid and gas streams through the tower without obtaining the maximum possible interphase contact. Another serious disadvantage of packed towers is that the large volumes of solvent needed to absorb a sparingly soluble gas may flood the packing and interrupt the absorption process.

Cooper, Christl and Peery[12] have investigated the absorption of carbon dioxide in water in a tower packed with Raschig rings and have found the $(H.T.U.)_{OL}$ values to vary from 2 to 10 ft. depending on the liquid to gas flow ratio. These values may be compared with (H.T.U.) values of the order of 0.3 to 2 ft. for a very soluble gas such as ammonia. For equivalent absorption a packed column for absorbing carbon dioxide must be about 5 times longer than a tower for ammonia.

Consequently packed towers are more suitable where the gas is very

soluble, the liquid rate is low, and the change in composition of the gas is small and therefore not suitable for absorbing large quantities of carbon dioxide.

1.4.3. Gas bubble and plate columns

Quite opposite in principle to spray towers are the gas bubble units in which the gas is dispersed in pools of liquid, or a continuous descending liquid phase, in the form of fine bubbles. The subdivision of the gas stream may be accomplished by forcing the gas through a porous plate or cylinder placed at the bottom of the absorption vessel. The small bubbles manufactured thus present a very large surface of contact between the phases, interphase diffusion taking place as the bubbles are formed and as they rise up through the liquid. The liquid phase resistance is reduced by the motion of the bubbles as they rise upwards.

A plate tower is a special case of a gas bubble column, where the liquid flows across a series of plates through which the gas stream is rising. The depth of liquid on each plate is about 3 in. so that the contact time is only about 0.25 sec. Nevertheless Bonnet[13] and also Walter and Sherwood[14] have observed high mass transfer rates for carbon dioxide in water. Walter and Sherwood using a bubble-cap tray report $(H.T.U.)_{OL}$ values for carbon dioxide in water in the range 0.1 to 1 ft. at superficial gas velocities in the range 0.25 to 4 ft./sec. and liquid velocities in the range 0.025 to 0.05 ft./sec.

Datta, Napier and Newitt[15] have shown that a carbon dioxide bubble of 5 mm. diameter can be completely absorbed by rising only 3-4 ft. in water at room temperature and pressure. By using depths of the order of 3 ft. and passing the liquid countercurrent to the gas the contact time may be increased to 3 sec. or more, thus increasing the time of contact during which absorption may take place.

Shulman and Molstad[16] have studied the use of countercurrent gas bubble columns for absorption and desorption of slightly soluble gases, carbon dioxide and hydrogen, at atmospheric pressure. They concluded that bubble columns are superior to packed and spray towers where high liquid rates are required and where the liquid film resistance controls the rate of absorption. However, most of the work of Shulman and Molstad was carried out at atmospheric pressure and was concerned with desorption. In addition the gases used were dilute so that the gas velocity did not change appreciably during absorption or desorption.

The absorption of carbon dioxide in water using a bubble type absorber under pressure has been discussed by Howard[17] who describes a few experiments in which the carbon dioxide content of a burner gas was reduced from 12 to 1% by absorption in water at 75 lb./in.^{2} gauge. For this particular burner gas, Howard used three bubble type absorbers in series in order to accomplish the stripping and he came to the conclusion that a continuous bubble type scrubber using ethanolamine was preferable to water scrubbing. As with the work of Shulman and Molstad the gas velocity did not change appreciably throughout the absorber and his partial pressures of inlet carbon dioxide were only of the order of 10 lb./in.^{2}

1.5. CONCLUSIONS

In conclusion it can be said that gas bubble columns are superior to packed and spray towers for the absorption of carbon dioxide in water where high liquid rates are required and where the liquid film resistance controls the rate of absorption. Gas bubble columns would therefore be most suitable for removing large quantities of carbon dioxide from concentrated mixtures.

Very little work has been done on the effect of pressure on the rate

of absorption of carbon dioxide in water or the rate of absorption from concentrated mixtures where the gas velocities change considerably throughout the column and where the operating line is curved.

From these considerations a countercurrent bubble type absorber suitable for high pressures and high concentrations of carbon dioxide has been built in order to study the effect of these variables on the absorption rate of carbon dioxide in water. A bubble type absorber being preferred to a plate tower owing to the difficulties of manufacturing and maintaining the latter.

PART 2

COMPRESSIBILITY, FUGACITY AND SOLUBILITY DATA FOR CARBON DIOXIDE

2.1. INTRODUCTION

In order to evaluate the efficiency of a gas absorption operation it is necessary to know the equilibrium data between the gas and the absorbing liquid over the range of temperature for which the scrubber will be used. Furthermore, in a pressure absorber using a non-ideal gas as the solute, a knowledge of the compressibility data for the gas is essential in order to make accurate calculations of gaseous volumes and velocity changes taking place throughout the absorber. As a preliminary investigation, therefore, a literature survey on compressibility and solubility in water of carbon dioxide was made for the range 0-100°C and 0-36 atmospheres.

2.1.1. Solubility data

The following data on the solubility of carbon dioxide in water were available:

a) Bohr and Bock[18] (Wied. Ann. Phys. (3), 1899, 68, 505.)

This paper gives the solubility of carbon dioxide in water at 1 atm. partial pressure of carbon dioxide for the temperature range 0-60°C. Solubilities are given in Bunsen Absorption coefficients, i.e., the volume of gas (calculated at N.T.P.) absorbed by one volume of liquid at a certain temperature and partial pressure of gas, e.g., ml. of gas/ml. of liquid.

b) Zelvinskii[19] (J. Chem. Ind. (U.S.S.R.), 1937, 4, 1250.)

This paper gives the solubilities of carbon dioxide in water for the isotherms 0, 12.48, 25, 50, 75 and 100°C over a pressure range 0-90 atm. The data given are fairly complete for the lower two isotherms, but at the higher temperatures only a few isolated points are included in the

range 0-36 atm. The solubilities are given as the volume of gas (calculated at N.T.P.) absorbed by one volume of water reduced to 0°C at a certain partial pressure of gas. A method is also given for calculating solubilities at any temperature and pressure using the empirical equation:-

$$S = ap - bp^2 \quad -- \quad -- \quad -- \quad (12)$$

where S = solubility of gas, ml. of gas/ml. of water at 0°C,

p = partial pressure of carbon dioxide in atm.,

and a & b = empirical constants dependent on temperature.

c) Wiebe and Gaddy[20] (J.Amer.Chem.Soc.,1939,61,315.;1940,62,815.)

These papers deal with the solubility of carbon dioxide in water at very high pressures within the range 0-700 atm., only isolated points on certain isotherms being in the range 0-36 atm. The solubilities are expressed as the volume of gas (calculated at N.T.P.) absorbed by one gram of water at a certain total pressure, in this case 25 atm.

Total Pressure (atm.)	Temperature (°C)	Solubility (ml./g.H_2O)
25	18	19.51
25	31.04	14.18
25	35	12.95
25	40	11.62
25	50	9.71
25	75	6.82
25	100	5.37

As will be seen from above the data available are very incomplete, and as a consequence, the possibility was investigated of using Henry's law to calculate the required solubility data.

2.1.2. Henry's Law

This law states that the solubility of a gas is directly proportional

to the partial pressure of the gas.

$$p = kx \quad -- \quad -- \quad -- \quad -- \quad (13)$$

where p = partial pressure of gas in atm.

x = mole fraction of gas absorbed in liquid at saturation

and k = the Henry's law constant.

Using Henry's law to calculate the solubility of carbon dioxide in water at 0°C and 30 atm. from the experimental absorption coefficient of Bohr and Bock of 1.713 at 1 atm., it is found that x, the mole fraction, is 41.65×10^{-3}. The experimental value obtained by Zelvinskii is 25.95×10^{-3}, which is only 60% of the amount predicted by Henry's law (see Table 6). This calculation shows that Henry's law is not accurate enough for normal calculations. However, it may be possible to use the fugacity and activity corrections to Henry's law for non-ideal gases and non-ideal liquids respectively.

The corrections to Henry's law can be written thus:-

$$f = ka \quad -- \quad -- \quad -- \quad -- \quad (14)$$

where f = fugacity of gas in atm.

and a = the activity of the gas in solution.

As the solubility of carbon dioxide in water is relatively small, i.e., the solutions are dilute, it can be assumed that a = x (the mole fraction) i.e., f = kx.

The fugacity may be obtained from the equation:-

$$\ln f = \int_0^p \frac{V}{RT} dp \quad -- \quad -- \quad -- \quad (15)$$

where V = volume of gas in litres/g.mole,

T = temperature in °K,

p = pressure in atm.,

and R = the ideal gas constant.

To calculate the fugacity an explicit volume equation of state is necessary in order to evaluate the integral above. The equation of state is also useful in calculating compressibility data and therefore the literature survey also covered equations of state for carbon dioxide.

2.2. p-V-T RELATIONSHIPS FOR CARBON DIOXIDE

2.2.1. Equations of state

The algebraic representation of the p-V-T relationship of fluids is an equation of state. For practical purposes the most useful equations of state are those explicit in volume, although the most accurate and common ones are those explicit in pressure.

Over 100 equations of state are recorded but only about 15 are in common use. It has been found that most known equations of state used at present, whether derived theoretically or empirically, can be reduced to one of two forms,

$$pV = a + bp + cp^2 + dp^3 + \text{--} \quad \text{--} \quad (16) \text{ (explicit volume type)}$$

$$pV = a + \frac{b}{V} + \frac{c}{V^2} + \frac{d}{V^3} + \quad \text{--} \quad \text{--} \quad (17) \text{ (explicit pressure type)}$$

a, b, c, d, etc. are functions dependent entirely on temperature and the nature of the gas. The constants are evaluated from the experimental p-V-T data for the fluid.

If we reduce the above equations of state to the compressibility form, i.e., divide through by RT, then

$$\frac{pV}{RT} = C = \frac{a}{RT} + \frac{bp}{RT} + \frac{cp^2}{RT} + \frac{dp^3}{RT} + \quad \text{--} \quad (18)$$

or

$$\frac{pV}{RT} = C = \frac{a}{RT} + \frac{b}{VRT} + \frac{c}{V^2RT} + \frac{d}{V^3RT} + \quad \text{--} \quad (19)$$

where C = compressibility factor of the fluid.

If in (18) we then substitute $p = RT/V_i$, where V_i is the ideal gas volume, then

$$C = \frac{a}{RT} + \frac{b}{V_i} + \frac{cRT}{V_i^2} + \frac{d(RT)^2}{V_i^3} + \quad -- \quad -- \quad -- \quad (20)$$

If RT is included within the temperature functions the virial forms of the equation are obtained thus

$$C = \alpha_1 + \frac{\alpha_2}{V_i} + \frac{\alpha_3}{V_i^2} + \frac{\alpha_4}{V_i^3} + \quad -- \quad -- \quad -- \quad (21) \text{ (explicit volume)}$$

and $$C = \alpha_1 + \frac{\alpha_2}{V} + \frac{\alpha_3}{V^2} + \frac{\alpha_4}{V^3} + \quad -- \quad -- \quad -- \quad (22) \text{ (explicit pressure)}$$

where $\alpha_1, \alpha_2, \alpha_3, \alpha_4$, etc. are known as the virial coefficients and are dependent upon some function of temperature and the nature of the gas.

If the most common equations of state are transposed into the compressibility forms, we obtain the table of virial coefficients shown at the end of this thesis, where the constants R, a, b, c, etc. are dependent on the nature of the gas (Table 1).

Some of the equations seem to have more constants than is stated in column (4), but this is because the later constants are derived from the earlier ones, e.g., van der Waals' equation, constant $b_1 = a_1 \times a_2$.

Other common equations of state such as the Dieterici, Keyes and Goodenough equations can also be reduced to approximately the same form, but complications occur due to the use of exponentials (Dieterici and Keyes) and fractional powers of temperature (Goodenough). The Benedict-Webb-Rubin equation falls into this class and is included in Table 1. to show how nearly it approaches the general form. It will be noted that the exponential term is a function of volume as well as of temperature in the Benedict-Webb-Rubin equation.

Table 1 compares briefly the most common equations of state and leads to the following conclusions:

a) On the whole, explicit volume equations require a greater number

of virial terms to give the same accuracy as explicit pressure equations over the same range of temperature and pressure.

b) A large number of terms is required to give even reasonable accuracy over small ranges, especially near the critical point. A minimum of five empirical constants is required to give reasonable accuracy.

c) The virial coefficients appear to follow a definite series in 1/T.

2.2.2. Explicit volume equation of state for carbon dioxide

The critical temperature of carbon dioxide is 31.04°C which occurs near the middle of the temperature range 0-100°C used in this thesis. This fact increases the difficulty of obtaining an equation of state which will accurately portray the experimental data both above and below the critical temperature.

The literature survey produced the following data on equations, of state, explicit in volume, for carbon dioxide.

a) Cawood and Patterson[21] (Trans. Roy. Soc. 1936, A236, 77).

This paper gives an equation of state for carbon dioxide of the form:-

$$\frac{pV}{RT} = 1 - Ap \quad -- \quad -- \quad -- \quad (23)$$

where A is a constant dependent upon temperature.

This equation is only accurate over small pressure ranges (0-5 atm. at most) and is of no use in accurate determinations of physical properties over appreciable ranges.

b) Linhart[22] (J. Phys. Chem., 1953, 37, 645; 1954, 38, 1091)

These papers give an equation of the form:-

$$\frac{V_1 - V_\infty}{V_p - V_\infty} = p^k \quad -- \quad -- \quad -- \quad (24)$$

where V_∞ = the ultimate molal volume of carbon dioxide,

$V_1 = V_o T/T_o$ where $V_o = 1$ at $T_o = 273.13^oK$ and 1 atm.
(i.e., Charles law is assumed to be obeyed by carbon dioxide at 1 atm.)

V_p = volume at pressure p,

and k = a constant dependent on temperature.

This equation is not sufficiently accurate for exact calculations.

c) Michels and Michels[23] (Proc. Roy. Soc. 1936, A153, 201)

This gives an equation of the form:-

$$pV = A + Bd + Cd^2 + Dd^3 + \text{--} \quad \text{--} \qquad (25)$$

where d = Amagat density of the gas, and A, B, C, D, etc., are constants dependent on temperature.

This portrays the data accurately, but no simple method seems to be available for interpolating the constants for isotherms other than the ones used.

d) Maron and Turnbull[24] (J. Amer. Chem. Soc., 1942, 44, 2195)

This paper gives an equation of the form:-

$$C = 1 + \left[\frac{\beta_1}{T_r} + \frac{\beta_2}{T_r^2} + \frac{\beta_3}{T_r^4}\right]\frac{P_r}{R} + \left[\frac{\beta_4}{T_r^3} + \frac{\beta_5}{T_r^5} + \frac{\beta_6}{T_r^7}\right]\frac{P_r^2}{R}$$
$$+ \left[\frac{\beta_7}{T_r^3} + \frac{\beta_8}{T_r^5} + \frac{\beta_9}{T_r^7}\right]\frac{P_r^3}{R} + \left[\frac{\beta_{10}}{T_r^3} + \frac{\beta_{11}}{T_r^5} + \frac{\beta_{12}}{T_r^7}\right]\frac{P_r^4}{R} \qquad (26)$$

where P_r and T_r = reduced pressure and temperature respectively, and $\beta_1, \beta_2, \beta_3$, etc., are empirical constants.

This equation gives accurate results for a very wide range of temperature and pressure above the critical point. The lowest limit of application is $T_r = 1.50$, which for carbon dioxide corresponds to a temperature of 123°C. This is 23°C outside the range 0–100°C, the range over which data are required.

e) Beattie[25] (Proc. Nat. Acad. Sci., Wash.,), 1930, 16, 14.)

This paper gives the explicit volume equation derived from the Beattie-Bridgeman explicit pressure equation. For carbon dioxide this explicit volume equation gives an average deviation of 5% (maximum 6.5%) over small temperature and pressure ranges. When the equation was derived, Beattie pointed out the possibility of adding extra empirical constants to increase its accuracy for specific gases.

In conclusion therefore, it was decided to use the Beattie equation as a starting point in the calculation of the p-V-T relationships of carbon dioxide.

2.2.3. Experimental p-V-T data for carbon dioxide

A search of the literature provided the following data on the experimental p-V-T relations for carbon dioxide.

a) Amagat[26] (Int. Crit. Tables, Vol. III, p.11).

Amagat gives the p-V-T data for carbon dioxide over a wide pressure and temperature range but outside the range 0-36 atm.

b) Andrews[27] (Phil. Trans., 1876, 166, 421.)

This paper gives various isotherms of p-V data for carbon dioxide. Three of these isotherms (6.5, 64, 100°C) have experimental results in the pressure range 0-36 atm. and will be used in verifying the accuracy of Beattie's equation of state.

c) Michels and Michels[23] (Proc. Roy. Soc., 1936, A153, 201.)

This paper lists pV data for carbon dioxide over eight isotherms (0-100°C) in the pressure range 0-36 atm. and will be used in verifying the accuracy of Beattie's equation of state.

Comparison of Experimental Methods of Andrews and Michels and Michels.

a) Temperature: Andrews measured his temperatures with a precision of

0.01°C but had difficulty in maintaining constant temperature control at each isotherm. The lowest isotherm varied from 6.05 to 6.90°C, temperature being maintained by cold running water. The temperature was controlled at 64°C by vapour from boiling methyl alcohol and at 100°C by steam.

Michels and Michels used thermometers divided by 1/100th°C and maintained rigid temperature control by using a thermostat.

b) Pressure: Andrews used a mercury reservoir suspended below two glass tubes containing air and carbon dioxide respectively. A screw arrangement forced mercury up the tubes compressing the gases, the volumes of which could be read to 0.1cc. The pressure was measured from the air volume using the equation

$$p_A = \frac{V_o(1 + \alpha t)}{V_i} \mp \frac{q}{760} \quad -- \quad -- \quad (27)$$

where p_A = pressure in atm.,

V_o = volume of air at N.T.P.,

V_i = volume of air observed at t°C,

α = the coefficient of expansion of air,

and q = the difference in mercury level in the air and carbon dioxide tubes.

Throughout his work Andrews assumed the compressibility of air to be unity (i.e., the volume for an ideal gas), because at that time no p-V-T data for air were available. If q is known it is possible to correct Andrews' data to true pressures, but since he gives no values for this correction his data can be corrected only approximately. Andrews states that q was never greater than 0.25 atm., but usually considerably less. The maximum possible error arising from this source is therefore 2.5% occurring at 12 atm., Andrews' lowest pressure value.

In correcting for the compressibility of air q has therefore been

ignored leaving the pressure equation as

$$p_A = \frac{V_o(1 + \alpha t)}{V_i} \quad -- \quad -- \quad -- \quad -- \quad (28)$$

Holborn and Otto[35] give the equation of state for air at 0°C as:

$$pV = (1.0006 - 0.000603p + 0.00000302p^2) \quad -- \quad (29)$$

At N.T.P. $p = p_o = 1$ atm. and $V = V_o$

Therefore $p_o V_o = 1.000$

Since the manometer in Andrews' work is at 6-7°C in all cases, a correction has to be applied to the above equation. The assumption of Charles' law is reasonably correct over such a small temperature range, which gives the equation as:

$$p_T V_i = (1.0006 - 0.000603p + 0.00000302p^2)\ T/273.13 \quad (30)$$

where T = temperature of air manometer in °K.

Let the numerical value of $p_T V_i$ calculated from the above equation be X. Then:

$$\frac{p_T V_i}{p_o V_o} = X \text{ (where } p_o = 1 \text{ atm. and } p_T = \text{true pressure)}$$

i.e., $$p_T = XV_o/V_i \quad -- \quad -- \quad -- \quad -- \quad -- \quad (31)$$

dividing (31) by (28) we get that:

$$\frac{p_T}{p_A} = \frac{X}{(1 + \alpha t)} \quad -- \quad -- \quad (32)$$

This gives a method of calculating the true pressure from Andrews' data to within 2.5%.

Michels and Michels used a graduated tube over mercury. The pressure was increased by an oil pump till the mercury touched a special make or break contact in the tube at a known volume level. The pressure was measured by a pressure balance and corrections applied for the height of mercury and the hydrostatic head of oil. This gave pressure measurements

accurate to the fourth decimal place.

c) Carbon dioxide preparation: Andrews obtained his carbon dioxide by the action of CO_2 free sulphuric acid on marble chips. The carbon dioxide was dessicated by passing it through U-tubes containing chloride-ion free pumice moistened with sulphuric acid.

Michels and Michels obtained their carbon dioxide from a special three stage low temperature distillation process.

d) Conclusion: From the above considerations it will be seen that the results of Michels and Michels are the most accurate data available and will therefore be used as the basis for testing the accuracy of the equations of state for carbon dioxide.

2.2.4. Data used in calculations.

$0^{\circ}C = 273.15^{\circ}K$,

$R = 0.08206$ litre, atm./g.mol./$^{\circ}K$,

Gram molecular volume of CO_2 at N.T.P. = 22.2611 litres.

The gram molecular volume of carbon dioxide can be obtained from the compressibility data thus:

Michels and Michels[23] give the value of $(1 + \lambda)$, the compressibility coefficient of carbon dioxide at N.T.P. as 1.006824 and the gram molecular volume is given by the equation

$$P_s V_s = \frac{RT_o}{1 + \lambda} = \frac{0.08206 \times 273.13}{1.006824} = 22.2611$$

2.2.5. The Beattie equation

The Beattie Equation is generally written as:

$$V = (\pi + B)(1 - \epsilon) - A/RT \quad -- \quad -- \quad -- \quad (33)$$

for one mole of gas,

where $A = A_o(1 - a/\pi)$; $B = B_o(1 - b/\pi)$

$\epsilon = c/\pi T^3$; $\pi = RT/p$

and for carbon dioxide

$$A_o = 5.0065 \qquad a = 0.07132$$

$$B_o = 0.10476 \qquad b = 0.07235$$

$$c = 660{,}000$$

The simplified equation used in calculation is

$$V = 0.10476 + \frac{RT}{p} - \frac{5.0065}{RT} - \frac{0.007579p}{RT} + \frac{0.357064p}{R^2T^2}$$

$$- \frac{660{,}000}{T^3} - \frac{69141.6p}{RT^4} + \frac{5002.39p^2}{R^2T^5} \qquad -- \qquad (34)$$

If this is written in the general compressibility form (see section 2. 2.1.) this gives:

$$C = 1 + \frac{1}{V_i}\left(0.10476 - \frac{61.0102}{T} - \frac{660{,}000}{T^3}\right)$$

$$- \frac{1}{V_i^2}\left(0.007579 - \frac{4.35126}{T} + \frac{69141.6}{T^3}\right)$$

$$+ \frac{1}{V_i^3}\left(\frac{5002.39}{T^3}\right) \qquad -- \quad -- \quad -- \quad -- \qquad (35)$$

The volumes of carbon dioxide at various temperatures and pressures have been calculated and compared with the experimental values of Michels and Michels (Table 2A) and Andrews (Table 3A). The fourth column shows the difference between calculated and experimental volumes, and the fifth column the percentage deviation.

Tables 2B and 3B show the average and maximum deviations of Beattie's explicit volume equation from experimental results. There is an average deviation of 2.36% and a maximum of 11.69% at 0°C and 33.4 atm. for the results of Michels and Michels.

From these tables it is clear that the Beattie equation of state for carbon dioxide does not represent the data accurately enough for the computation of physical properties, e.g., compressibility factors and fugacity

coefficients, and a more exact equation is required.

2.2.6. The new equation of state for carbon dioxide

From the discussion on equations of state it is seen that the greater the accuracy required the more constants are needed. The Beattie equation is suitable for addition of extra terms and two further empirical terms have been added from a consideration of the deviations of Beattie's equation from the experimental results of Michels and Michels.

The compressibility form of the new equation is:

$$C = 1 + \frac{1}{V_i}\left(0.10476 - \frac{61.0102}{T} - \frac{660{,}000}{T^3} - \frac{2.47 \times 10^{27}}{T^{12}}\right)$$
$$- \frac{1}{V_i^2}\left(0.007579 - \frac{4.35126}{T} + \frac{69141.6}{T^3}\right)$$
$$+ \frac{1}{V_i^3}\left(\frac{5002.39}{T^3} - \frac{2.69354 \times 10^{10}}{T^5}\right) \quad -- \quad -- \quad (36)$$

The term $(-2.47 \times 10^{27}/T^{12})$ has been added to the second virial coefficient and the term $(-2.69354 \times 10^{10}/T^5)$ has been added to the fourth virial coefficient of the Beattie equation. The number of empirical constants has been increased to seven.

The volume explicit form used in the calculations is:

$$V = 0.10476 + \frac{RT}{p} - \frac{61.0102}{T} - \frac{660{,}000}{T^3} - \frac{2.47 \times 10^{27}}{T^{12}}$$
$$- \frac{1}{V_i}\left(0.007579 - \frac{4.35126}{T} + \frac{69141.6}{T^3}\right)$$
$$+ \frac{1}{V_i^2}\left(\frac{5002.39}{T^3} - \frac{2.69354 \times 10^{10}}{T^5}\right) \quad -- \quad (37)$$

for 1 mole of gas and where $V_i = RT/p$.

Using this new equation the volumes of carbon dioxide at the temperatures and pressures used for the Beattie equation have been calculated and compared with the experimental results as before. (See the last two columns of Tables 2A and 3A.)

The average and maximum deviations are shown underneath the values for the Beattie equation in Tables 2B and 3B. There is an average deviation of 0.17% and a maximum of 0.35% at 0°C and 16.5 atm. for the results of Michels and Michels.

A further test for accuracy was carried out with some random experimental points and the results are shown in Table 4. The deviations are well within the average and maximum deviations already found.

These deviations are well within reasonable limits of error and this equation of state for carbon dioxide will be used to calculate the physical properties of carbon dioxide.

2.2.7. The compressibility factor of carbon dioxide.

The compressibility factor of carbon dioxide has been calculated from the new equation for the isotherms 0, 10, 15, 20, 25, 35, 50, 75 and 100°C over the pressure range 0-36 atmospheres. The results are shown in Table 5 under the column C and have been plotted on a large scale to show the variation of C with pressure and temperature over the required range. A photographic reproduction of this graph is shown in Plate I. These curves will also be used for calculating gaseous volumes and velocities of carbon dioxide in the pressure absorber.

At 0°C carbon dioxide liquifies at approximately 34 atm. and the 0°C isotherm has therefore been stopped at 33 atm.

From the graph it will be seen that as temperature increases the compressibility approaches unity, the value for an ideal gas. The curves also tend to approach straight lines the higher they are above the critical temperature of 31.04°C.

2.2.8. The fugacity coefficient of carbon dioxide

The fugacity is obtained from the equation

$$\ln f = \int_0^P \frac{V}{RT}\, dp. \qquad (15)$$

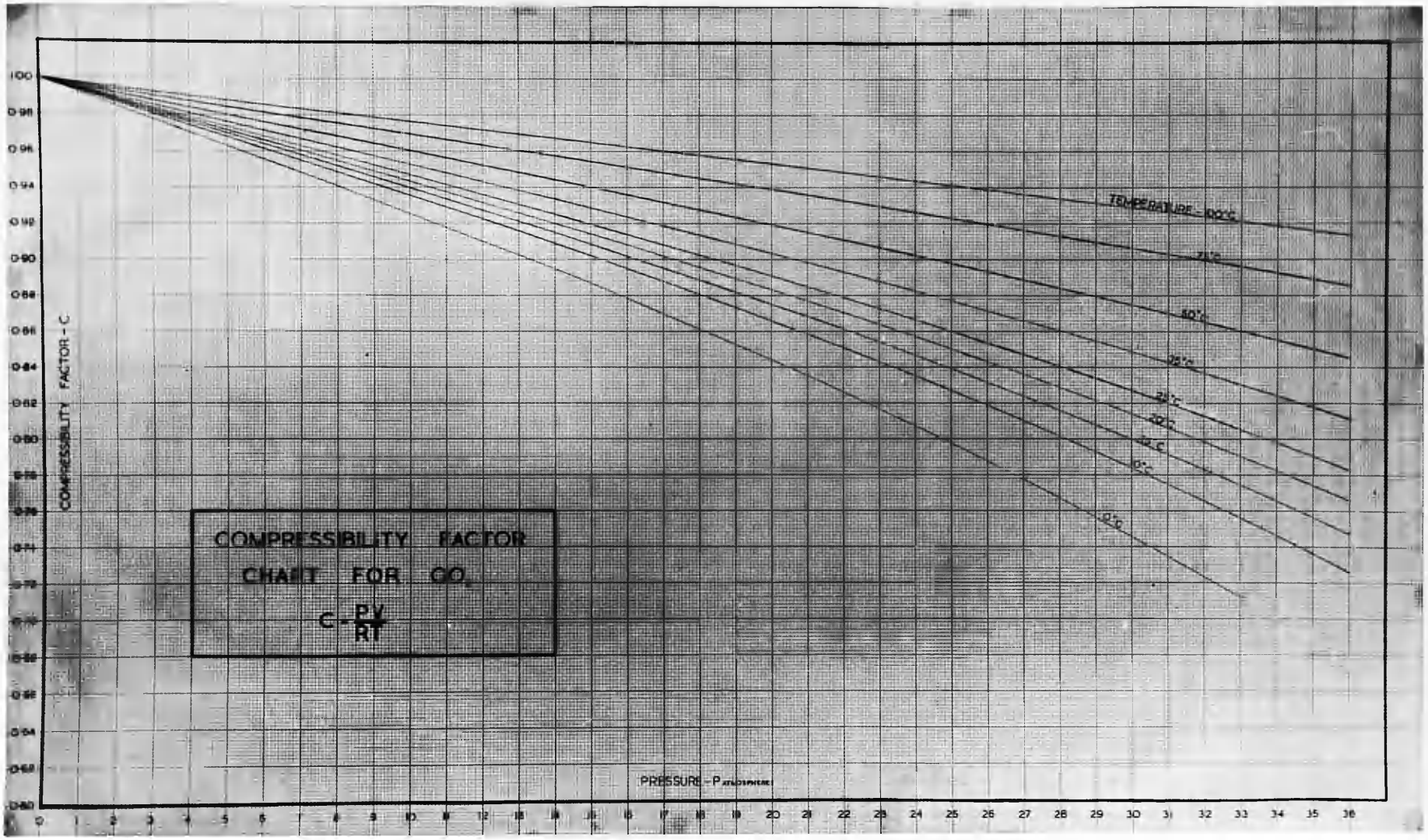
COMPRESSIBILITY FACTOR - C
PRESSURE - P ATMOSPHERE
TEMPERATURE - 100°C
75°C
50°C
25°C
0°C
COMPRESSIBILITY FACTOR CHART FOR CO_2
$C = \frac{PV}{RT}$

PLATE I

Substituting the new equation of state for V we get, on integrating and simplifying,

$$\ln \frac{f}{p} = \frac{1}{V_i}\left(0.10476 - \frac{61.0102}{T} - \frac{6.6 \times 10^5}{T^3} - \frac{2.47 \times 10^{27}}{T^{12}}\right)$$

$$- \frac{1}{2V_i^2}\left(0.007579 - \frac{4.35126}{T} + \frac{69141.6}{T^3}\right)$$

$$+ \frac{1}{3V_i^3}\left(\frac{5002.39}{T^3} - \frac{2.69554 \times 10^{10}}{T^5}\right) \quad -- \quad -- \qquad (38)$$

where $V_i = RT/p$ and f/p = the fugacity coefficient.

The fugacity is obtained simply by multiplying the fugacity coefficient, f/p, by the pressure, p.

The fugacity coefficient has been calculated for the isotherms 0, 10, 15, 20, 25, 35, 50, 75 and 100°C over the pressure range 0-36 atm. The values obtained are listed in Table 5 under f/p. These results have been plotted on a large scale chart showing the fugacity coefficients for the various temperatures and pressures over the required range. A photographic copy of this chart is shown in Plate II.

From the graph it will be seen that as the temperature increases the fugacity coefficient approaches unity, the value for an ideal gas. The curves also tend to approach straight lines as the temperature increases.

2.3. THE SOLUBILITY OF CARBON DIOXIDE IN WATER

2.3.1. Units

As will be seen in the introduction (section 2.1.1.) the data available for the solubility of carbon dioxide are in different units. For comparison all units have been transformed into Bunsen absorption coefficients, i.e., the volume of gas (calculated at N.T.P.) absorbed by 1 volume of water at a certain temperature and partial pressure of carbon dioxide.

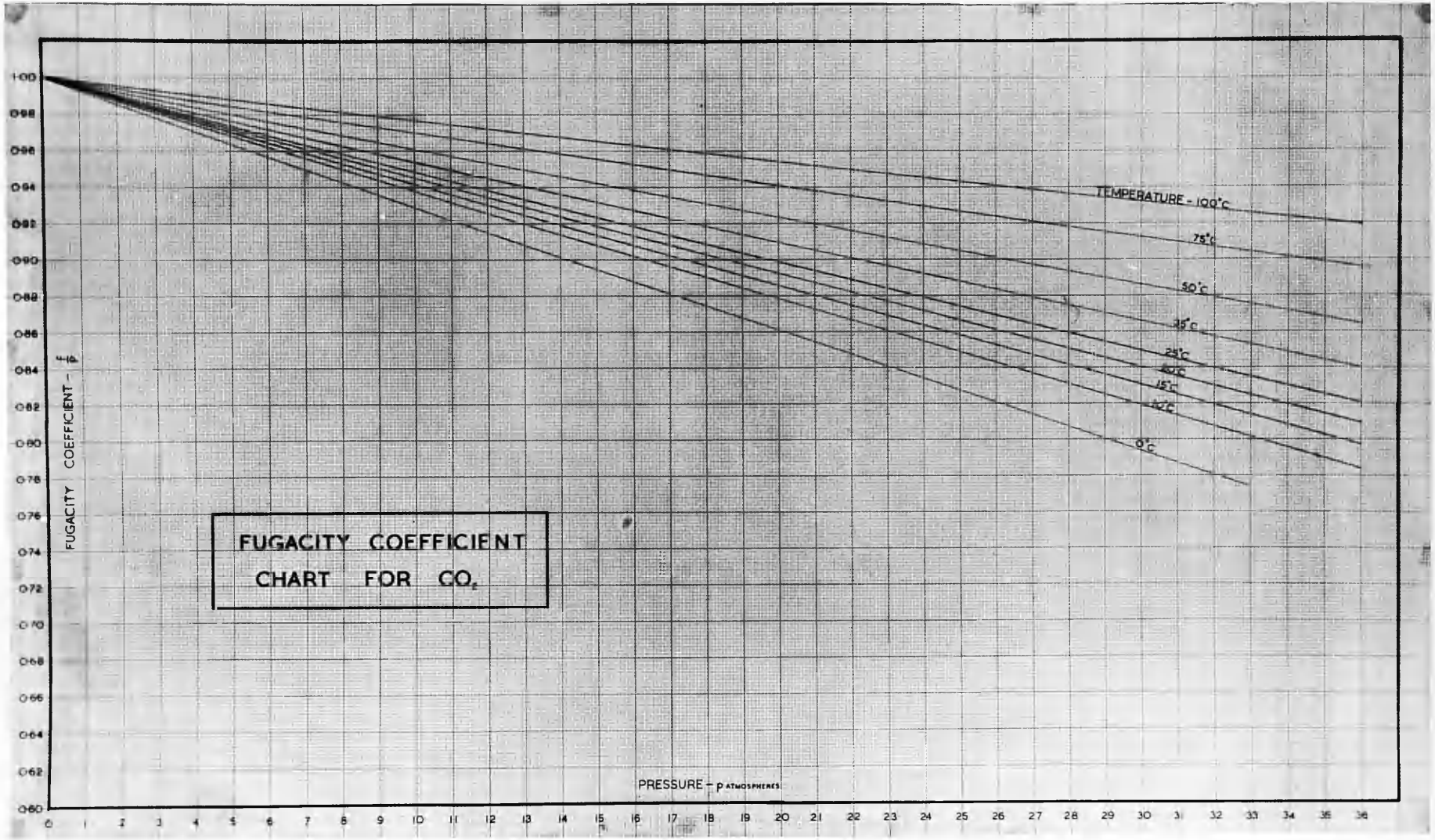
FUGACITY COEFFICIENT – f/p
PRESSURE – p ATMOSPHERES
TEMPERATURE - 100°C
75°C
50°C
35°C
25°C
15°C
0°C
FUGACITY COEFFICIENT CHART FOR CO_2

PLATE II

Zelvinskii used units of ml. of gas (calculated at N.T.P.) per ml. of water reduced to 0°C and a certain partial pressure of carbon dioxide.

These units are changed to Bunsen coefficients by multiplying the Zelvinskii solubility by the ratio of the density of water at t°C to the density of water at 0°C.

e.g., At 25°C ρ_{H_2O} = 0.99707 g./ml.

at 0°C ρ_{H_2O} = 0.99987 g./ml.

and the ratio = 0.99721

The calculated Zelvinskii solubility at 25°C and 10 atm. is 7.13 ml. gas/ml. water which is equivalent to a Bunsen coefficient of 7.13 x 0.99721 = 7.11

The units used by Wiebe and Gaddy are in ml. of gas (calculated at N.T.P.) per 1g. of water at a certain total pressure and temperature. To change solubility to volume/volume it is only necessary to multiply by the density of water at that temperature.

To change total pressure to partial pressure it is necessary to correct for the effect of total pressure on the partial pressure of water vapour. The correct partial pressure can be calculated from the Poynting relationship below:

$$\left[\frac{dp}{dP}\right]_T = \frac{V}{v} \quad -- \quad -- \quad -- \quad -- \quad (39)$$

where p and P are the vapour pressure and the total pressure on the water respectively, V the partial molal volume of water, and v the partial molal volume of water vapour.

As the partial molal volumes are not known the molal volumes are used in each case. At 100°C the perfect gas law does not hold accurately enough for saturated steam and the vapour pressure must be calculated

from Poynting's relationship in conjunction with the Callender equation of state for steam, while at all other temperatures the perfect gas law can be used.

Wiebe and Gaddy, using Poynting's relationship and the Callender equation of state for steam, obtained the partial pressure of water vapour at 100°C and 25 atm. total pressure as 1.018 atm.

Partial pressures for the lower isotherms are evaluated as follows:

$$\frac{\partial p}{\partial P} = \frac{V}{v} = \frac{M}{\rho v}, \quad V = M/\rho \quad \text{(for water)} \quad -- \quad (40)$$

where M = molecular weight and ρ = density of water at T°K.

Now $v = RT/p$ (the perfect gas law) so that:

$$\frac{\partial p}{\partial P} = \frac{Mp}{RT\rho} \quad -- \quad -- \quad -- \quad -- \quad (41)$$

i.e., differential form can be written as

$$\frac{dp}{p} = \frac{M\,dP}{RT\rho} \quad -- \quad -- \quad -- \quad (42)$$

Integrating this between p_o and p for left hand side and p_o and P for the right hand side, we get:

$$\ln \frac{p}{p_o} = \frac{M}{RT\rho}(P - p_o) \quad -- \quad -- \quad -- \quad (43)$$

where p_o = water vapour pressure and p = water vapour pressure at P atm.

e.g., At 18°C p_o = 15.480 mm. of Hg = 0.0204 atm.

P = 25 atm. ρ = 0.99862 g./ml.

then $\log_{10} p = \log_{10} P + \dfrac{18.016\,(25 - 0.0204)}{2.303 \times 0.08206 \times 291.13 \times 0.9986}$

$\therefore$ p = 0.0208 atm.

i.e., partial pressure of carbon dioxide = 25 - 0.0208

= 24.9792 atm.

Mole fraction:

In solubility calculations it is more usual to use the mole fraction

of the gas in the liquid. This is obtained from the solubility coefficient by use of the equation:

$$x = \frac{\left(\frac{S_t}{S_t + 22.2611}\right) \times \rho H_2O}{18.016} \quad -- \quad -- \quad (44)$$

where x is the mole fraction of carbon dioxide, ρH_2O is the density of water at t°C and S_t is the Bunsen absorption coefficient at t°C.

2.3.2. Zelvinskii's data

The data available in the pressure range 0-36 atm. have been listed under Zelvinskii experimental mole fraction in Table 6 for the isotherms 0, 25, 50, 75, and 100°C. As will be seen these data are very incomplete, especially at the higher temperatures, and it is necessary to use Zelvinskii's equations to fill in the blanks. These, as mentioned in the introduction (section 2.1.1.) are empirical equations of the form

$$S = ap - bp^2 \quad -- \quad -- \quad -- \quad (12)$$

where S = solubility in ml. of CO_2 (calculated at N.T.P.) per ml. of water at 0°C.

p = partial pressure of CO_2 in atm.

and a&b = empirical constants dependent on temperature.

The constants given by Zelvinskii for the various isotherms are listed below:

T°C	a	b
0	1.84	0.025
25	0.755	0.0042
50	0.425	0.00156
75	0.308	0.000966
100	0.231	0.000322

Comparing the 28 experimental points in the tables with the corresponding calculated values from the above equations, it was found that the

average deviation was 0.94% with a maximum of 2.64%.

Zelvinskii plotted these constants against temperature and obtained a curve which would enable the constants to be read off at any required temperature. He checked this curve by calculating expected solubilities at 12.43°C and confirmed them by experiment. The results obtained are shown below, the empirical equation being

$$S = 1.08p - 0.0108p^2 \quad -- \quad -- \quad (45)$$

p atm.	Calculated $x \times 10^3$	Experimental $x \times 10^3$	% dev.
1	0.865	0.878	1.48
5	4.135	4.151	0.39
10	7.806	7.751	0.71
15	11.023	10.912	1.02
20	13.763	13.660	0.76
25	16.127	16.174	0.29
30	18.027	18.471	2.40

The curve, therefore, seems to give a fairly accurate method of interpolating solubilities and a replica of Zelvinskii's chart has been drawn (Fig. 1). This curve was used to find the constants for the isotherms 10, 15, 20 and 35°C, from which the values of the solubilities at these temperatures were calculated.

The constants were found to be

T°C	a	b
10	1.231	0.0133
15	1.000	0.0089
20	0.862	0.0061
35	0.568	0.0025

The solubilities calculated from Zelvinskii's equations are tabulated in Table 6. Since these calculated values give a complete coverage of the temperature and pressure ranges, they were used as a basis for

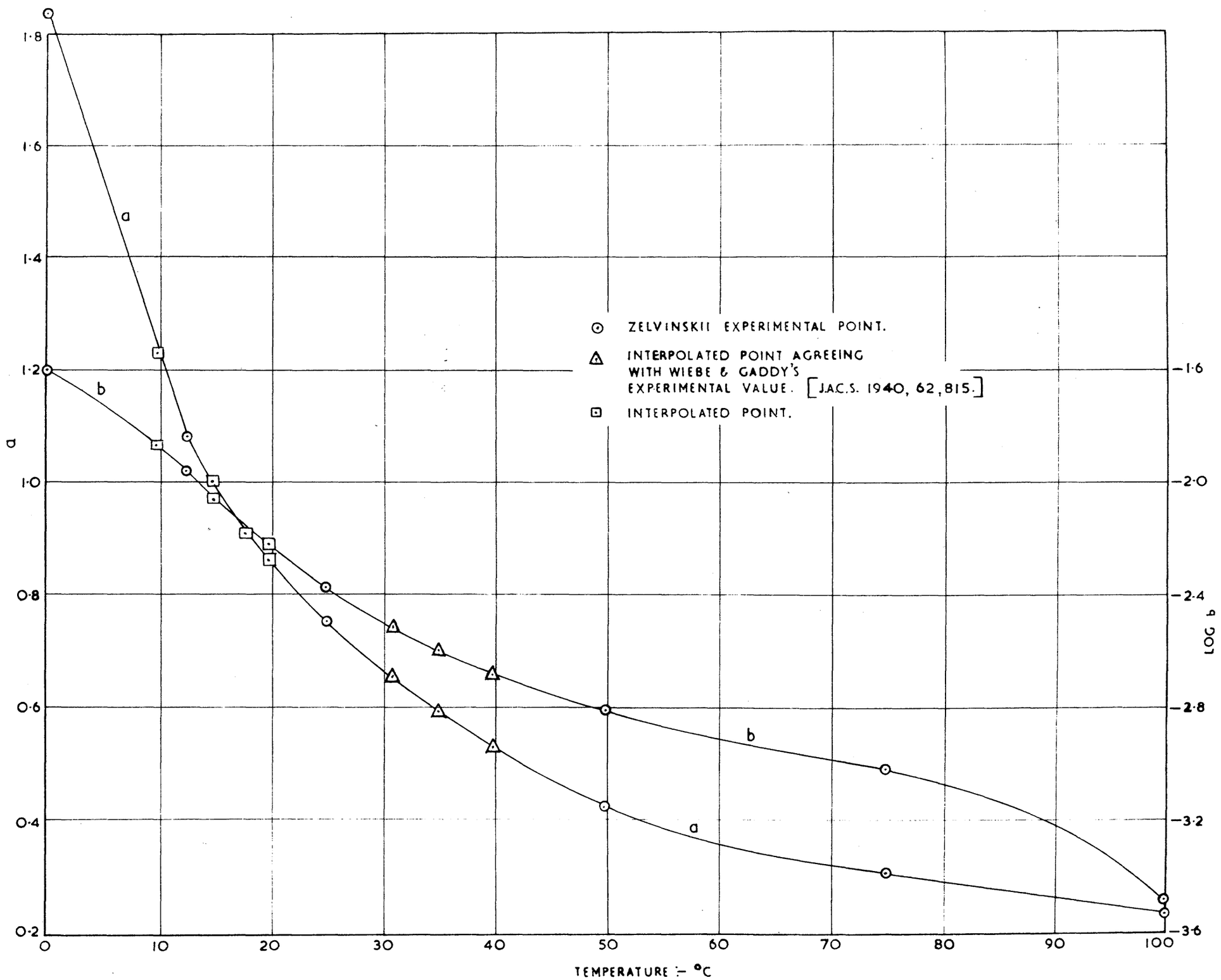

Fig. 1. GRAPH OF THE CONSTANTS OF ZELVINSKII'S EQUATION FOR THE SOLUBILITY OF CO_2 IN WATER AT DIFFERENT TEMPERATURES

$$S_z = aP - bP^2$$

WHERE S_z IS IN CC'S OF GAS AT S.T.P. PER CC. OF WATER AT 0°C.

[J. CHEM. IND. (U.S.S.R.) 1937, 14, 1250]

comparison of the experimental data, Henry's law and the fugacity correction to Henry's law.

2.3.3. The data of Bohr and Bock

The data of Bohr and Bock for the isotherms 0, 10, 15, 20, 25, 35 and 50°C at 1 atm. partial pressure of carbon dioxide have been used to calculate theoretical solubilities according to Henry's law and the results are tabulated in Table 6.

The Henry's law constant for each isotherm was calculated from the data of Bohr and Bock thus:

At 0°C and 1 atm. $S = 1.713$ ml.gas/ml.water

$\therefore \quad x = 0.001385$

$\therefore \quad K = p/x = 1/0.001385 = 722.0$

Using this value of K in the equation $x = p/K$ the mole fraction of carbon dioxide in water can be calculated for any pressure.

The deviations from Zelvinskii's calculated solubilities are shown in the column adjacent to the Henry's law data and show that Henry's law cannot be applied with any accuracy above 1-2 atm. for the low temperatures though at 35 and 50°C the accuracy is within 5% up to 10 atm.

At 75 and 100°C the value of Zelvinskii's calculated solubility at 1 atm. was used to find the Henry's constant and it will be seen that the accuracy rapidly improves till at 100°C it is possible to get within 6% of the correct value at 36 atm.

A deviation summary for Henry's law is shown in Tables 7 & 8.

The fugacity correction to Henry's law was also applied to the results of Bohr and Bock and the values obtained together with the deviations are shown in Table 6. Here again at low temperatures the agreement is not good but it is still a considerable improvement over Henry's law itself. The deviation falls rapidly with increase in temperature and at 25°C it

will be seen that there is a maximum deviation of 6% at 36 atm. Above 25°C the deviations level out and depend more on the deviation of the data of Bohr and Bock from the data of Zelvinskii at 1 atm. rather than on the inapplicability of the fugacity correction to Henry's law. A deviation summary is given in Tables 7 and 8.

Table 9 compares the deviation of the data of Bohr and Bock from Zelvinskii's experimental and calculated values at 1 atm. partial pressure of carbon dioxide. The average deviation is 3%.

Fig. 2 gives a graphical representation of the deviation from experimental values of Henry's law and the fugacity correction to Henry's law.

2.3.4. The data of Wiebe and Gaddy

The data of Wiebe and Gaddy at 25 atm. total pressure for the isotherms 35, 50, 75 and 100°C were changed to Bunsen absorption coefficients by the method shown in the discussion on solubility units (section 2.3.1.). From these results the constants for the fugacity correction to Henry's law were calculated and the values obtained from the use of the correction are tabulated in Table 6 along with the deviations from Zelvinskii's calculated results. Deviation summaries are given in Tables 7 and 8 and it will be seen that the data obtained are in agreement with Zelvinskii's results with a maximum deviation of 3.6% though the average is of the order of 1%.

Table 10 gives a comparison of interpolated Zelvinskii solubilities (from Fig. 1) with the available experimental data of Wiebe and Gaddy. The deviations show that the accuracy of using Zelvinskii's interpolated equations is within an average of ± 2% of the true experimental data. The deviation at 18°C of 6% from the experimental value is rather high but as

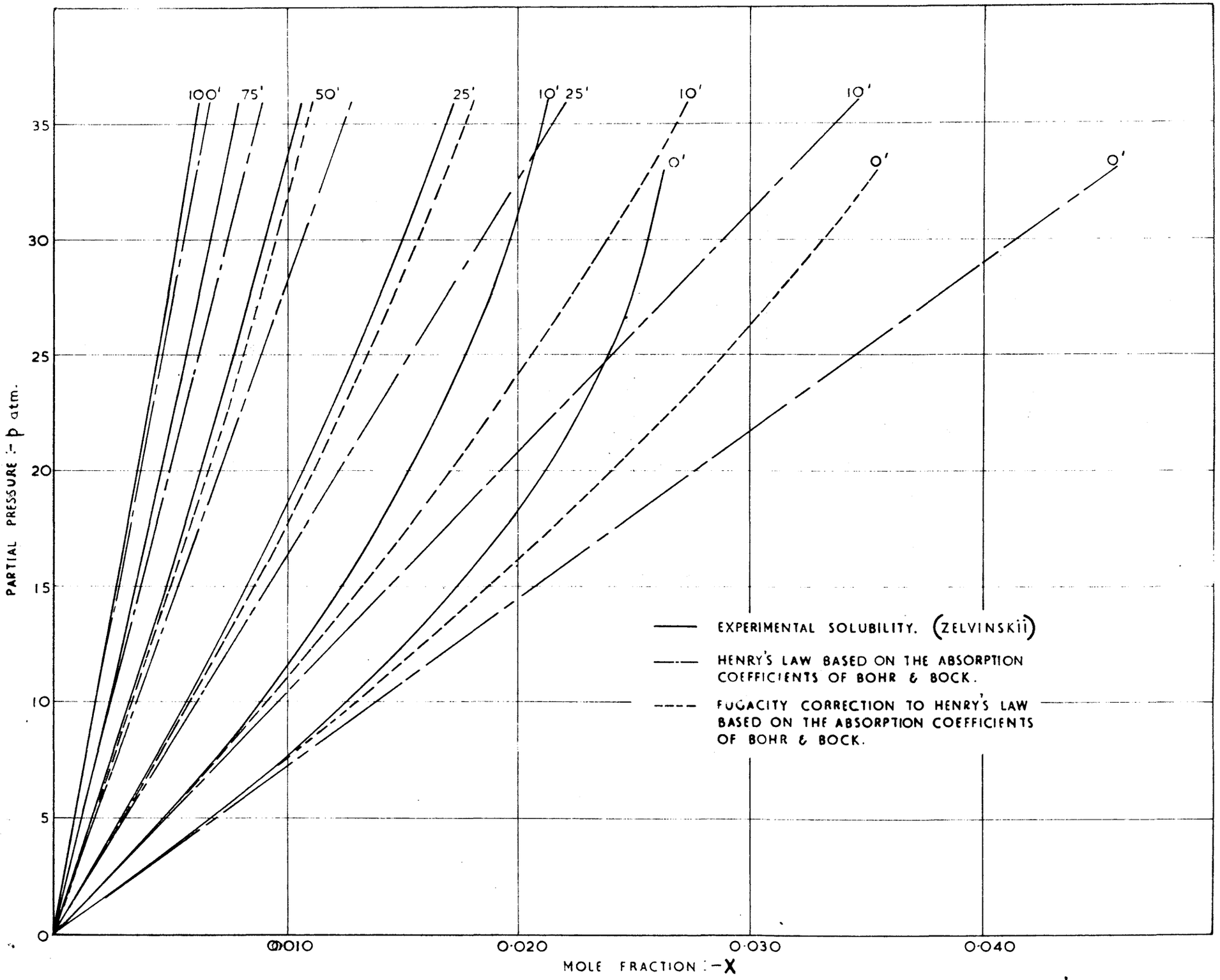

Fig. 2. COMPARISON OF EXPERIMENTAL SOLUBILITIES OF CO_2 IN WATER WITH HENRY'S LAW AND WITH THE FUGACITY CORRECTION TO HENRY'S LAW

the other points agree so well it seems reasonable to assume that the experimental result of Wiebe and Gaddy is in error.

2.3.5. Conclusions

1. The solubilities of carbon dioxide in water at high partial pressures calculated from Henry's law and the fugacity correction to Henry's law, based on the absorption coefficients of Bohr and Bock, are always higher than actual experimental solubilities. (Table 6, 7, 8 and Fig. 2).
2. Henry's law can only be used up to 5 atm. with an accuracy of ± 5% though the accuracy rapidly improves with increase in temperature above 35°C.
3. The fugacity correction to Henry's law using the data of Bohr and Bock at 1 atm. improves the accuracy. Below 25°C the correction can be used up to 10 atm. with an accuracy of ± 5%. Above 25°C the deviations are positive by a constant value of about 2-4% which indicates a constant experimental error in the data of either Bohr and Bock or Zelvinskii. Allowing for this constant deviation the fugacity correction applies almost exactly at temperatures above 30°C. (Tables 6, 7 and 8.)
4. The results obtained by Bohr and Bock disagree with those extrapolated from Zelvinskii's equations at 1 atm. by about 3% and this is the experimental error indicated above. (Table 9).
5. In general the application of the fugacity correction to Henry's law using a single value of Wiebe and Gaddy gives excellent agreement with Zelvinskii's data above 25°C. (Tables 6, 7 and 8).
6. Since the fugacity correction applies well only above 30°C, it is reasonable to assume that below 30°C solutions of carbon dioxide are not ideal and that some sort of compound is formed. Consequently the original assumption that $x = a$ is invalid below 30°C.
7. Because saturated solutions of carbon dioxide appear non-ideal below

30°C the fugacity correction to single points of both Bohr and Bock and Wiebe and Gaddy is inaccurate. Consequently it was found better to interpolate Zelvinskii's constants at 10, 15, 20 and 35°C from Fig. 1. The accuracy of the interpolation was checked at 18, 31.04. 35 and 40°C and was found to be good within ± 2%. Table 10 shows how well this interpolation can be made.

In conclusion it can be said that Zelvinskii's equations can be used to calculate solubilities to within ± 2% of the true experimental values. This is sufficiently accurate for engineering designs and for the calculation of mean driving forces for absorption rates. Therefore, the values of the solubility calculated from Zelvinskii's equations were plotted on a large scale graph, plotting the partial pressure of carbon dioxide against the mole fraction of carbon dioxide in water for the isotherms 0, 10, 15, 20, 25, 35, 50, 75 and 100°C. As rather a large gap in the experimental values occurs between 0 and 25°C Zelvinskii's experimental data at 12.43°C have also been plotted on the chart. A photograph of this chart is shown in Plate III.

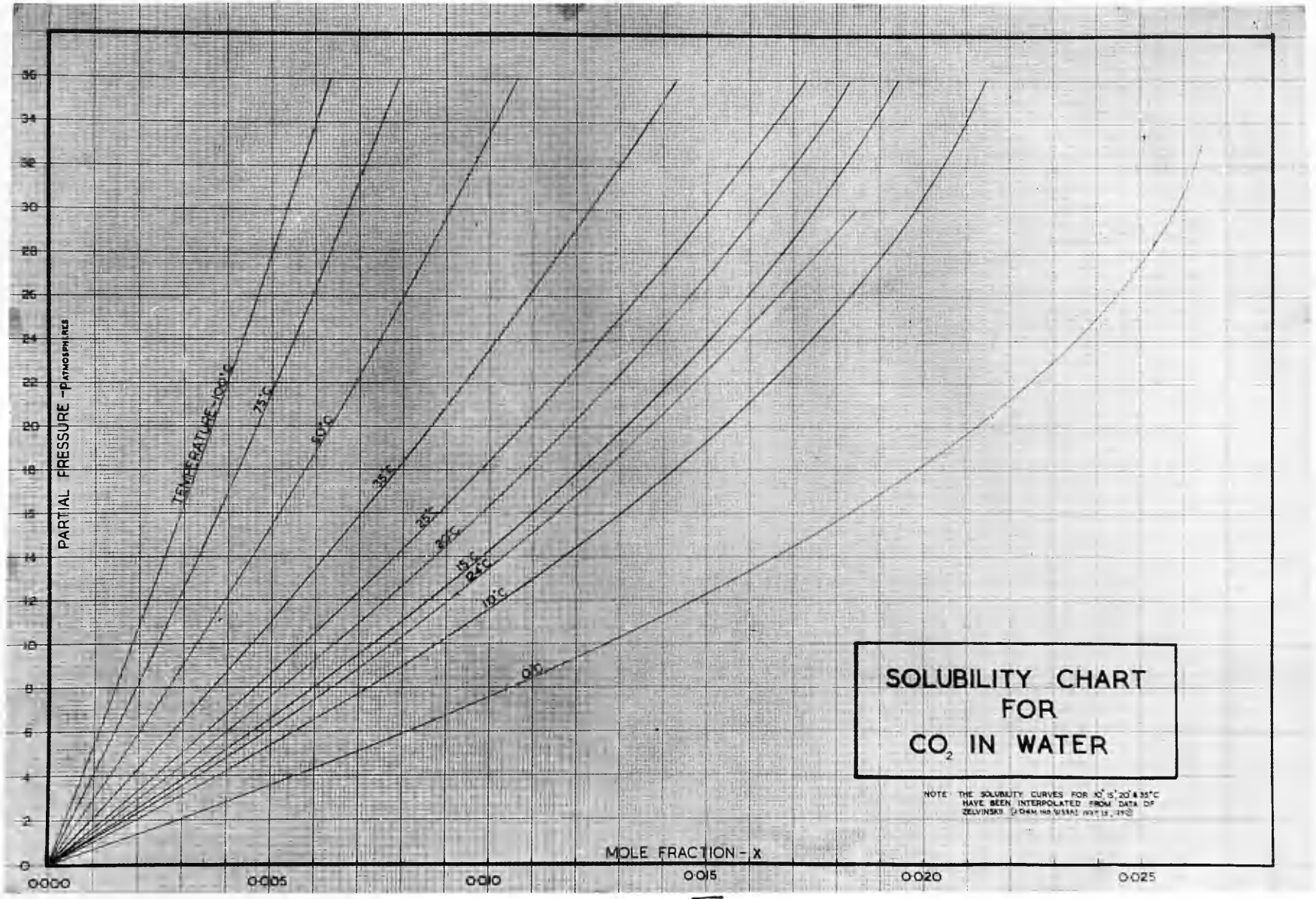
PARTIAL PRESSURE – ATMOSPHERES
MOLE FRACTION – X
0·000
0·005
0·010
0·015
0·020
0·025
0
2
4
6
8
10
12
14
16
18
20
22
24
26
28
30
32
34
36
TEMPERATURE 100°C
75°C
50°C
35°C
25°C
20°C
15°C
10°C
0°C
SOLUBILITY CHART FOR CO_2 IN WATER
NOTE: THE SOLUBILITY CURVES FOR 10°, 15°, 20° & 25°C HAVE BEEN INTERPOLATED FROM DATA OF ZELVINSKII

PLATE III

PART 3

THE ABSORPTION OF CARBON DIOXIDE IN WATER UNDER PRESSURE USING A GAS BUBBLE COLUMN

3.1. INTRODUCTION

From the conclusions drawn in the introduction to this thesis a gas bubble column was built capable of working at high pressures and handling gas mixtures containing high concentrations of carbon dioxide.

This absorber was used to study the effect of the following operating variables on the absorption rate of carbon dioxide:

a) pressure,
b) temperature,
c) gas rate,
d) liquid rate,
e) liquid level,
f) types of gas distributors.

3.2. EQUIPMENT AND OPERATION

A flow sheet of the absorption process and equipment used is shown in Fig. 3.

Absorption column:- The bubble column consisted of a 3 in. nominal bore class "C" steel pipe, 8 ft. long and flanged at both ends. The column was fitted with sight glasses for reading the liquid level and with ten pet-cocks for removing liquid samples at various heights for analysis. A bursting disc holder was also fitted and after testing the column up to 1200 lb./in^2 gauge a bursting disc set for 500 lb./in^2 was fitted in the holder.

Water phase:- Water from the Glasgow City water mains was pumped in at the top of the column, via a 300 gallon storage tank, by an E.C.D. Ltd., treble-cylinder plunger pump. This pump was capable of delivering up to

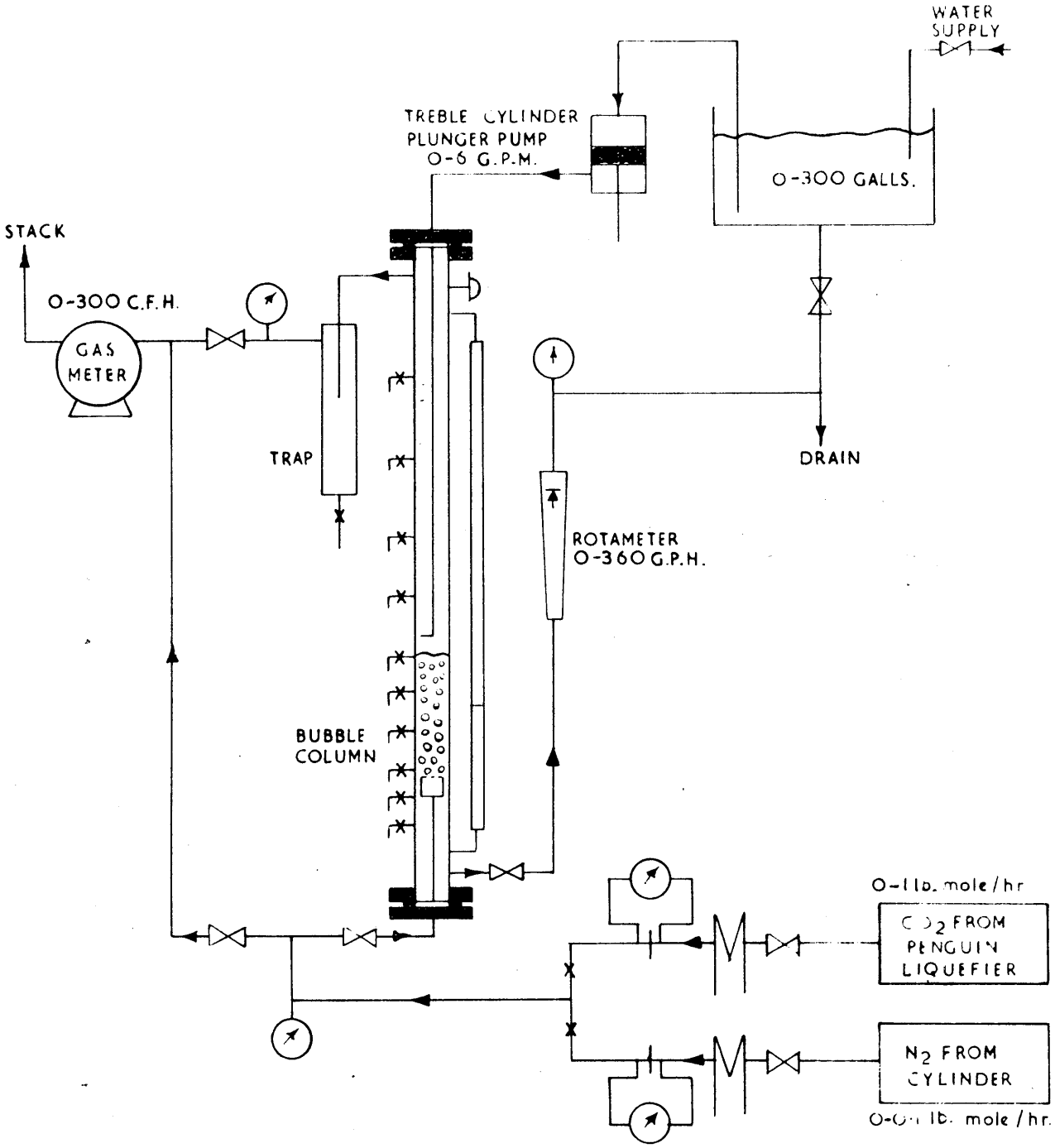

Fig. 3 EQUIPMENT

6 gal./min. of water at pressures up to 450 lb./in.^{2} gauge and the flow rate could be continuously adjusted while the pump was in operation. The exit water rate from the column was measured by a rotameter. As this measurement was taken at atmospheric pressure it was impossible to read the water rate during an absorption operation owing to the carbon dioxide absorbed at high pressures coming out of solution. The method employed, therefore, was to set the pump to give the desired flow rate before starting a run and to check this reading at the end.

Gas phase:- The carbon dioxide was generated from an I.C.I. Ltd. Penguin Liquifier which was charged initially with about 56 lb. of solid carbon dioxide ("Drikold"). Nitrogen, the diluent gas, was supplied from a cylinder of 165 ft.^{3} capacity. Both gases were metered through orifices and mixed before passing into the base of the column by means of a suitable gas distributor.

These orifices consisted of brass blocks through which was drilled a small hole of 0.063 in. diameter. Bourdon gauges at each end of the block gave the pressure drop corresponding to the desired flow rate. A detailed drawing is shown in Fig. 4.

Different flow ranges could be obtained by partially filling the orifices with wires of various diameters. Before and after each run the orifices were calibrated at their operating pressure by allowing each gas in turn to be bipassed to a dry gas meter to measure the flow rate at atmospheric pressure. The combined gas rate was also measured and an analysis sample of the gas mixture taken to confirm the individual readings. The same gas meter measured the exit gas rate from the column after absorption, so that all gas flow rates were obtained on the same basis.

The pressure drop across the orifice varied from 50 to 400 lb./in.^{2}

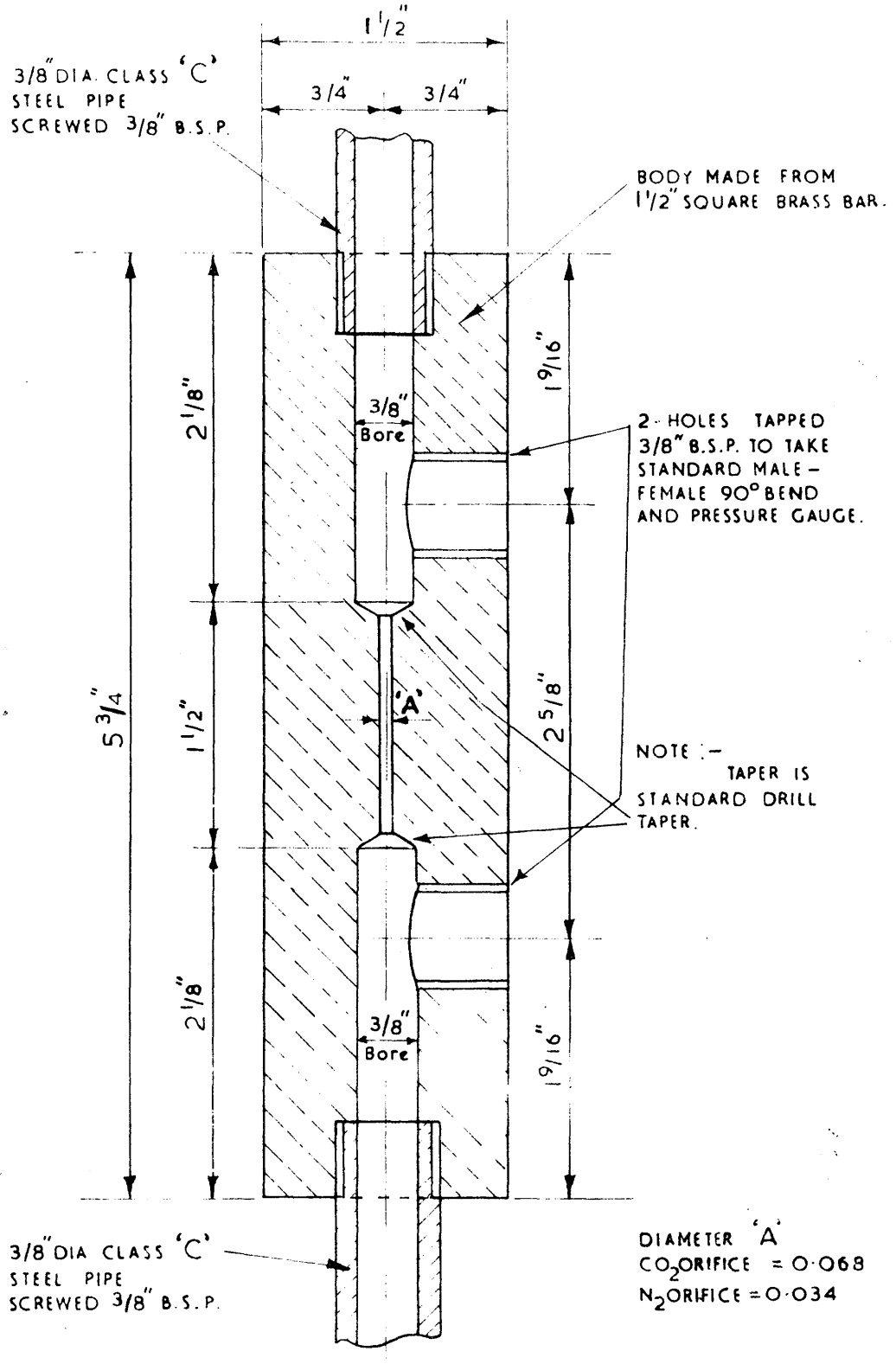

Fig. 4. DETAIL OF ORIFICE PLATE

so that a preheater was provided before each orifice to prevent its blockage with ice due to the temperature drop caused by the Joule-Thomson effect.

The inlet gas compositions normally used were in the range 80 to 90% carbon dioxide, the rest being nitrogen.

Operation:- The absorber pressure could be adjusted anywhere in the range 0 to 450 lb./in.^{2} gauge by throttling back the exit gas and water valves, all the time keeping the liquid level in the sight glass constant.

When the plant had reached steady state, the exit gas rate after absorption was measured on the gas meter and samples of the gas taken for analysis. Samples of the liquid could be taken from the column at various liquid levels by using the pet-cocks. The procedure was to release the sample under an accurately known volume of standard caustic soda solution (0.1 or 0.25N) in a measuring flask until the required volume of liquid (usually 25 ml.) had been collected. For this purpose 100 ml. measuring flasks were recalibrated to allow for the volume of the delivery tube under the caustic solution already in the flask.

The gas samples were analysed in a Macfarlane Gas Analysis Unit using mercury as the containing fluid. The amount of carbon dioxide in the sample was obtained by taking a measured volume, absorbing the carbon dioxide with 33% caustic potash solution and measuring the residual volume.

The carbon dioxide in the water was obtained by first measuring the total alkali (carbonate and hydroxide) with standard acid (0.1N) using methyl orange as indicator. The carbonate was then precipitated with barium chloride solution and the hydroxide in solution titrated with standard acid using phenolphthalein as indicator. At least three determinations were carried out on each sample.

The feed water was also analysed for carbon dioxide at the end of

each run. The carbon dioxide content of this inlet water was always in the range 0.08×10^{-3} to 0.12×10^{-3} lb.mole/ft.^{3} of water. By the complete analysis of both the liquid and gas streams in this way, it was possible to obtain a material balance around the plant based upon carbon dioxide. The accuracy of the sampling and analysing techniques is confirmed by the consistency of the material balance obtained which averaged at 99.4% for 66 runs with an average deviation of 1.2%.

3.3. GAS DISTRIBUTORS

The gas was bubbled countercurrent to the water by forcing the gas through sintered bronze discs obtained from Metal and Plastic Compacts Ltd. Coarse, medium and fine porous discs were available the porosities of which were measured by the method described in Part 4 of this thesis (section 4.3.). These discs were fitted into a cylindrical holder, a detailed drawing of which is shown in Fig. 5.

Another type of gas distributor was constructed from indented nickel strip 1 in. wide with indentations every 2 mm. along its length on one side only. These strips were packed into a square brass holder with either the indentations of one strip facing the plain surface of the next strip or with the indentations of alternate strips facing each other. Diagrams of the holder and the two arrangements of strips are shown in Figs. 6 and 7. The pressure drop across the packed indented strips was about 30 times less than that across the porous discs.

Other gas distributors investigated were an open 3/8 in. pipe and a brass plate of area 0.0307 ft. drilled with four 1/8 in. diameters holes.

Table 11 summarises the dimensions and porosities of the various gas distributors used in the bubble column.

Almost all the measurements on the effects of gas velocity, liquid velocity, bed height, temperature and pressure were made with the finest

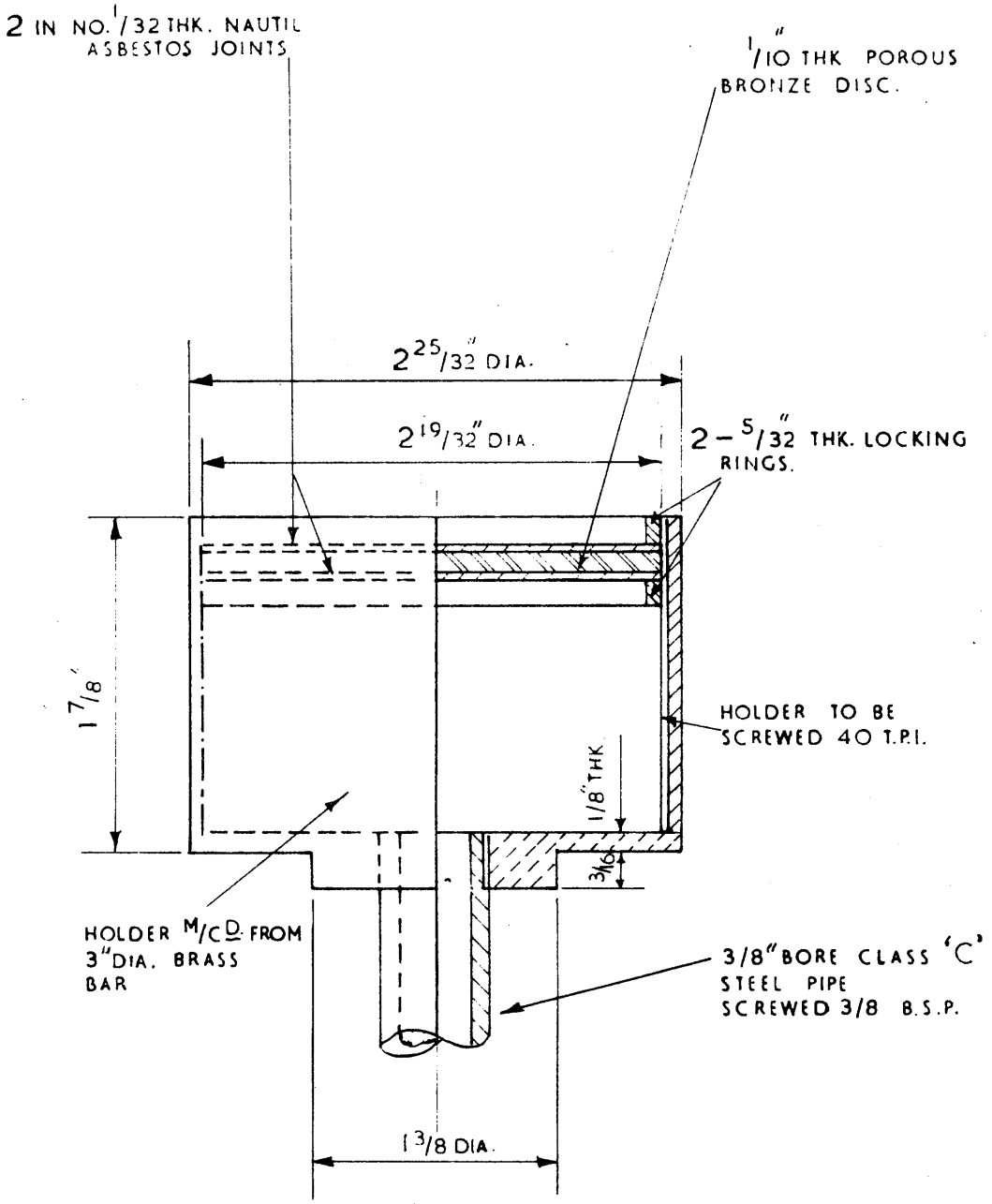

Fig 5. DETAIL OF HOLDER FOR POROUS BRONZE DISC.

SCALE:- FULL SIZE.

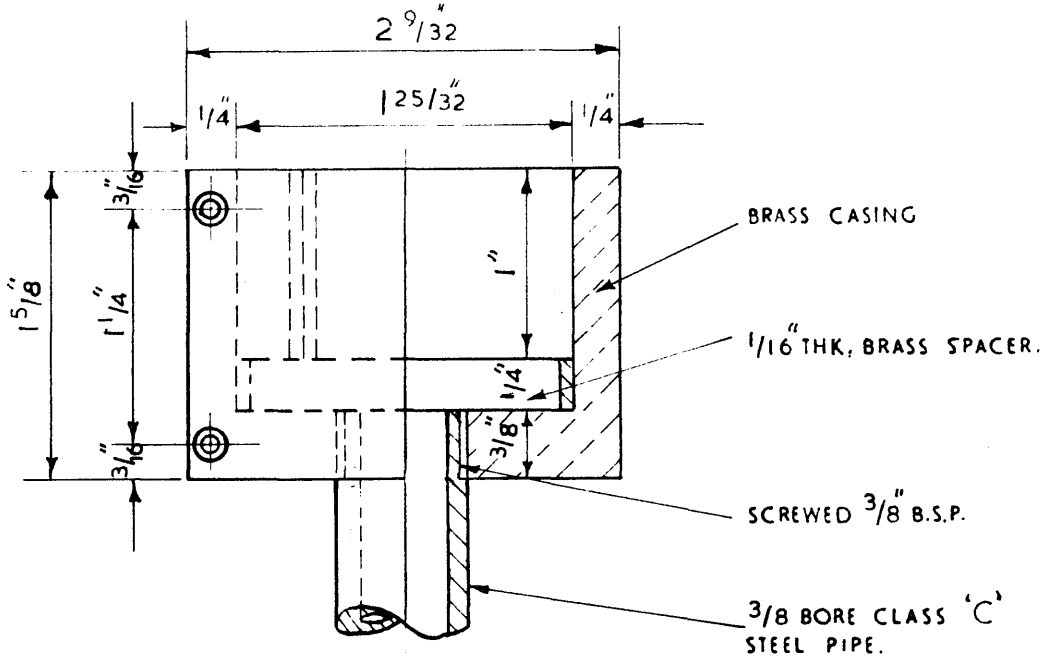

HALF SECTION THRO. CENTRE.

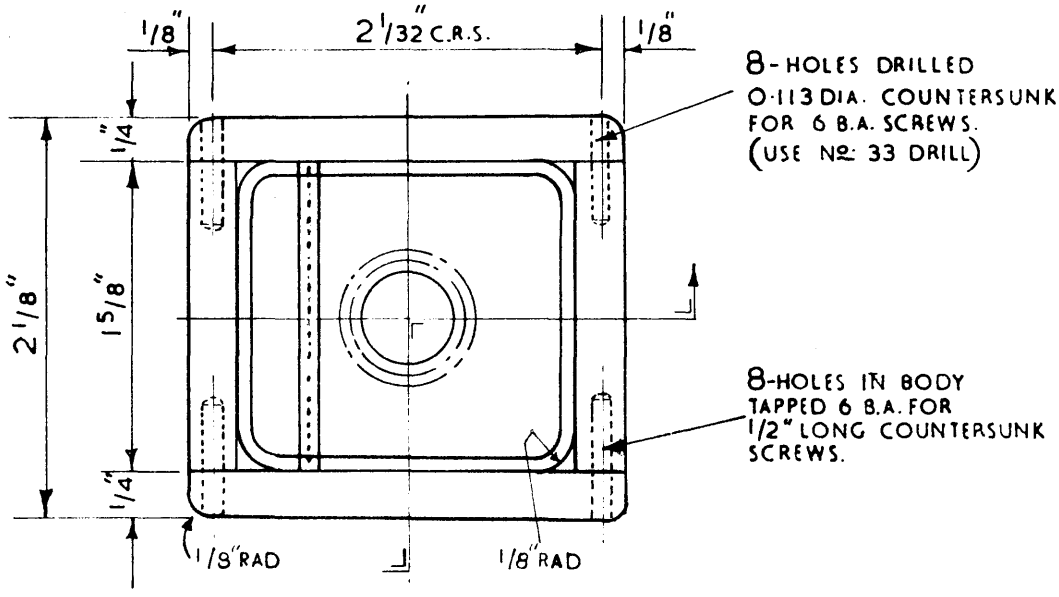

PLAN
SHOWING POSITION
OF STRIPS.

Fig.6. HOLDER FOR INDENTED NICKEL STRIPS.

SCALE:- FULL SIZE

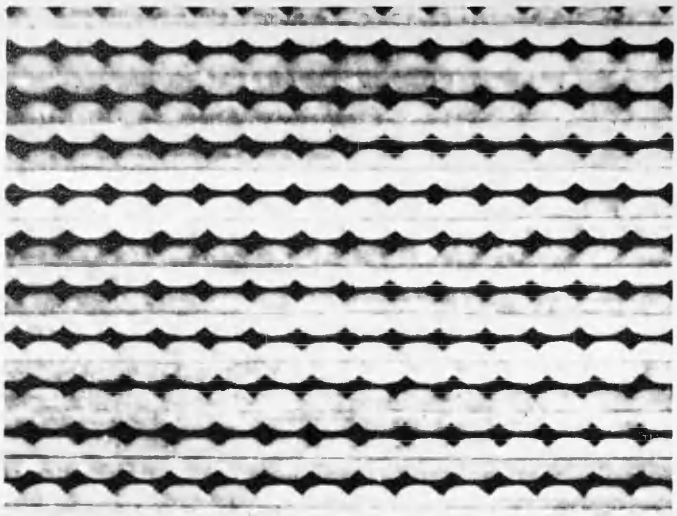

A

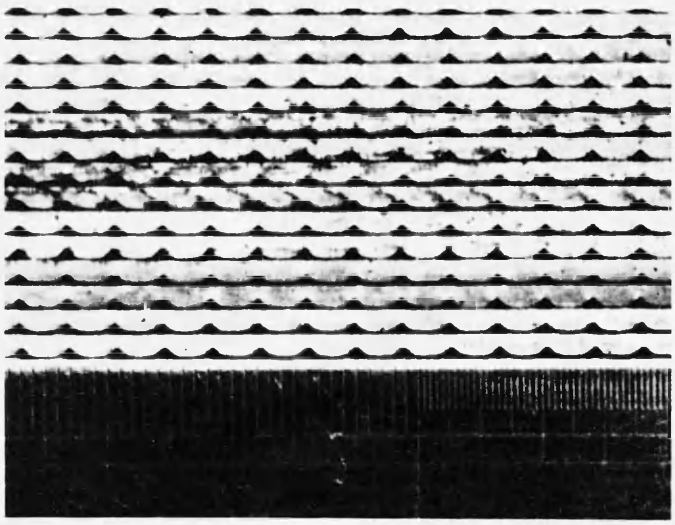

B

FIG 7. Arrangements of indented strip.

(1 Division = 1/50 th inch)

of the sintered bronze discs. When in operation, this disc gave a small pressure drop of between 5 and 10 lb./in.^{2} across the gas distributor or bubbler. The values of this pressure drop under various conditions is clearly seen by referring to the large table of results included in the folder at the back of this thesis.

3.4. DENSITIES OF FLUIDISED BUBBLE-BEDS

In the absorber the gas is bubbled countercurrent to the liquid. At any instant the liquid holds a certain volume of gas so that the density of the bubble bed is less than that of pure water. As a consequence, the level of the liquid registered by the sight glass at the side of the column is always less than the bed level inside the column. In order to be able to estimate the bed level inside the absorber experiments were conducted in a 3 in. diameter glass column to find the bed levels inside the column at various sight glass levels for different gas and liquid velocities. In the glass unit the locations of the bubbler and the sight glass were arranged to be the same as the arrangements in the metal pressure column.

Fig. 8 shows the results for the fine porous disc at the various velocities of gas and liquid used in the absorber. Fig. 9 gives the results for the other gas distributors used.

In the calculation of bed densities it has been assumed that the liquid and gas velocities are so low that frictional and contractional effects can be neglected. If this is so the bed density ρ_B can be calculated from the equation:

$$\rho_B = \frac{h_L \rho_L}{h_B} \qquad -- \qquad -- \qquad -- \qquad (46)$$

where h_B and h_L are the bed and sight glass heights respectively, above the surface of the disc and ρ_L is the density of water. The results from

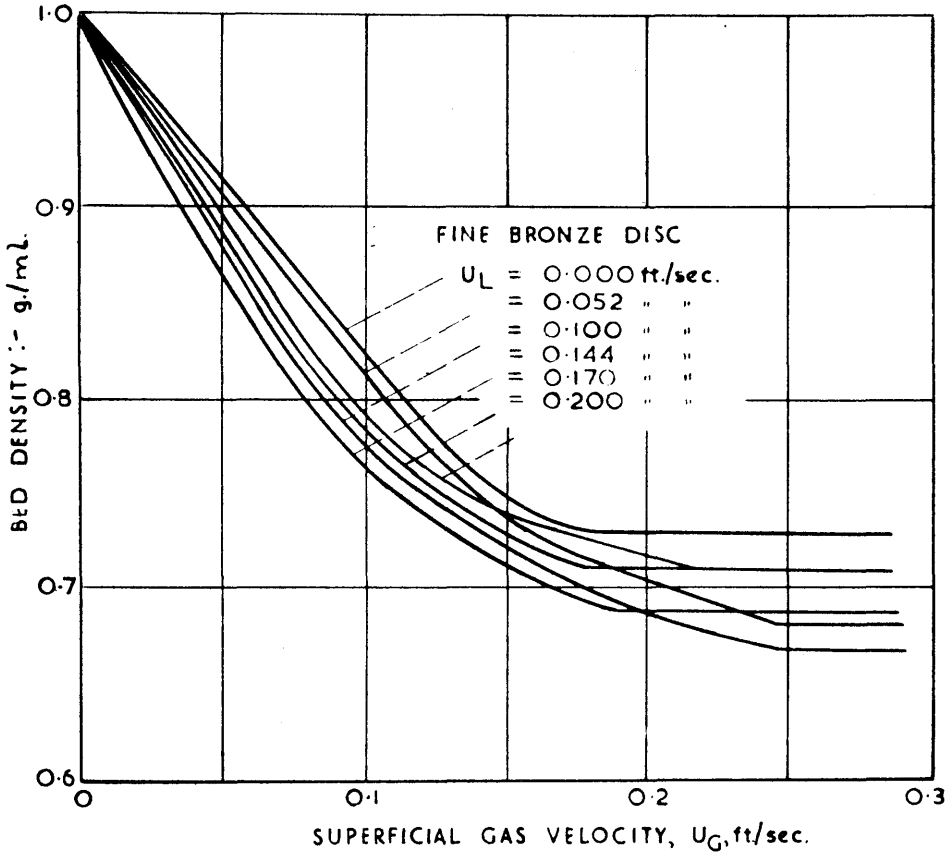

Fig. 8. EFFECT OF LIQUID AND GAS VELOCITIES ON BED DENSITY.

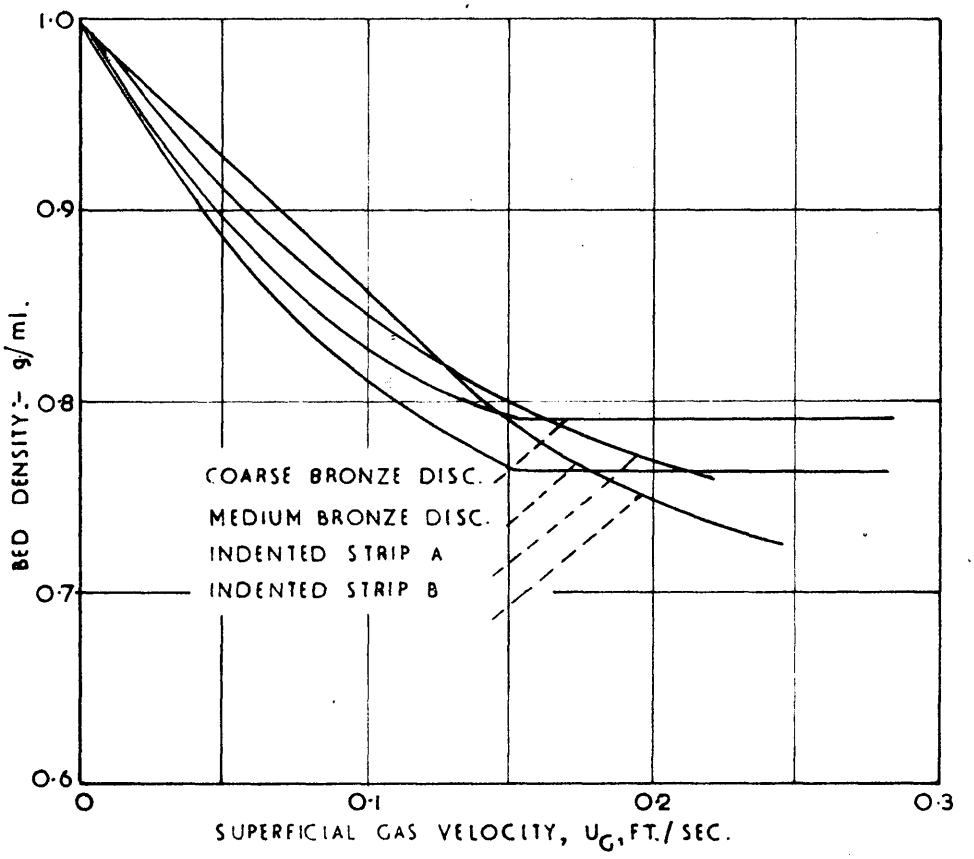

Fig.9. EFFECT OF GAS VELOCITY ON BED DENSITY FOR OTHER GAS DISTRIBUTORS AT A LIQUID VELOCITY OF 0·144 FT./SEC.

the glass column were confirmed on the metal pressure absorber where the bed was not visible by using the pet-cocks to locate the bed level inside the unit.

Bed densities at different gas velocities for stationary liquid are illustrated by Fig. 10 for the fine, medium and coarse discs and for the two arrangements of indented strip in Fig. 11.

In general all the curves show the same characteristics, namely that the bed density decreases with an increase in gas velocity until a more or less constant average value is obtained. Similar characteristics are well known in the fluidisation of solid particles by gases and liquids. At low gas velocities the gas bubbles rise independent of one another, but as the velocity increases the bed becomes a turbulent mass of rising and recirculating bubbles. As the velocity is increased further, the bed reaches a point where large plugs of gas are formed which cause the bed level to rise and fall about some mean value. The maximum and minimum levels are shown by the limits of the shaded areas in Figs. 9 and 10. In general, the curves show that the finer porous discs give the lower bed densities.

The effect of liquid velocity illustrated by Fig. 8 is to lower the bed density presumably by reducing the terminal velocity of rise by the bubbles in the bed, thus causing more bubbles to be held in suspension. However, increases in liquid velocity above 0.144 ft./sec. seem to cause the bed density to increase again. This increase may be caused either by slight frictional or contractional effects across the bubbler or by the effect of liquid velocity on the size or number of bubbles produced by the disc. At no point, however, do the bed densities at the higher liquid velocities differ by more than 10% from the values for the stationary liquid. The accuracies of the bed levels computed from Figs. 8 and 9 are

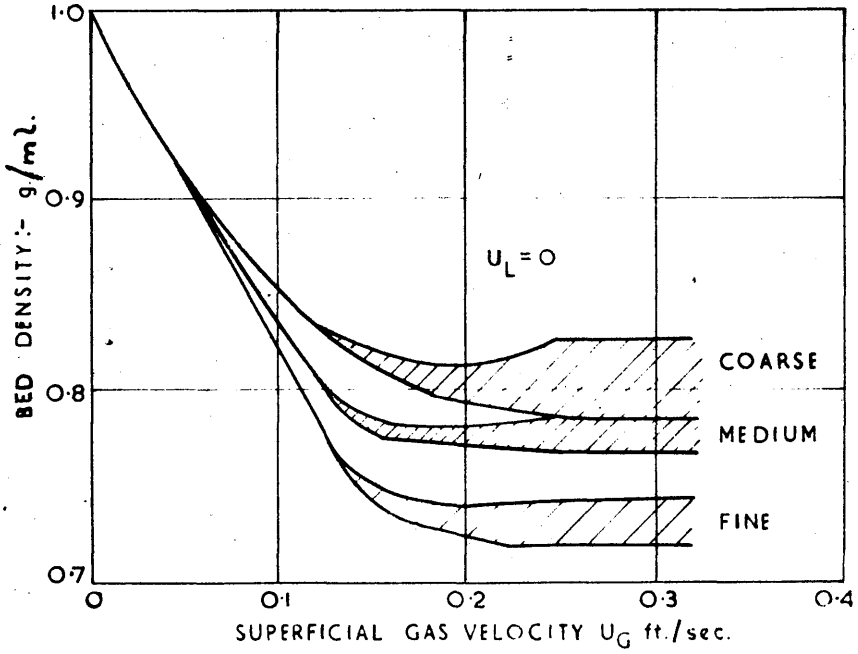

Fig. 10. COMPARISON OF POROUS DISCS.

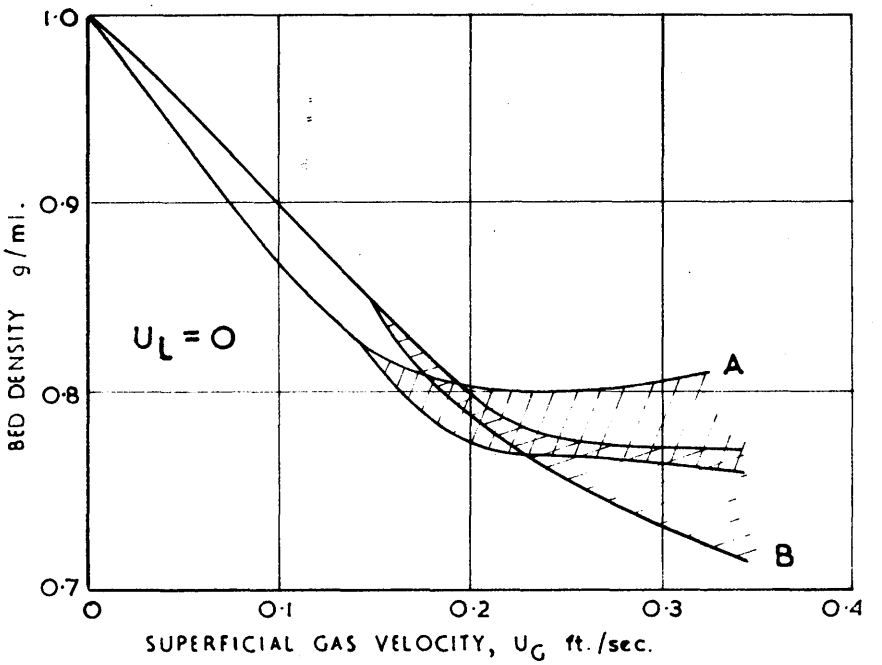

Fig. 11. BED DENSITIES FOR INDENTED STRIP

estimated to be about ± 2% for gas velocities lower than 0.15 ft./sec. and ± 5% for higher gas velocities.

Further work has been done on this subject and also on the effects of the properties of the liquid on the size and distribution of bubbles in fluidised foam beds and this work is presented as Part 4 of this thesis.

3.5. CARRY-OVER

A bubble of a certain size will rise with a certain terminal velocity of rise in water. If the water is given a downward velocity equal to that of the terminal velocity of rise, then the bubble will remain stationary with respect to the column. Further increases in liquid velocity will carry the bubble in the same direction as the liquid. Hence, the effect of too great a relative liquid to gas velocity will be to carry bubbles out of the exit water line. Carry-over in the region of the bubbler may be caused by the sudden acceleration of the water in the annular space between the bubbler and the 3 in. pipe. This effect has been observed in the glass column. The overall effect of carry-over is an apparent loss of gas revealed by a decrease in the material balance around the plant. The effect of increased relative superficial gas-liquid velocity on the material balance is shown in Fig. 12. As the relative velocity is increased beyond 0.3 ft./sec. there is a drop in the material balance corresponding to "carry-over". Hence, with the particular arrangement used in this case it is advisable to operate under conditions such that the sum of the superficial liquid and gas velocities does not exceed 0.3 ft./sec.

3.6. THE EXPRESSION OF ABSORPTION RATES

3.6.1. Equilibrium curve for carbon dioxide in water.

For the calculation of the mean driving forces causing absorption

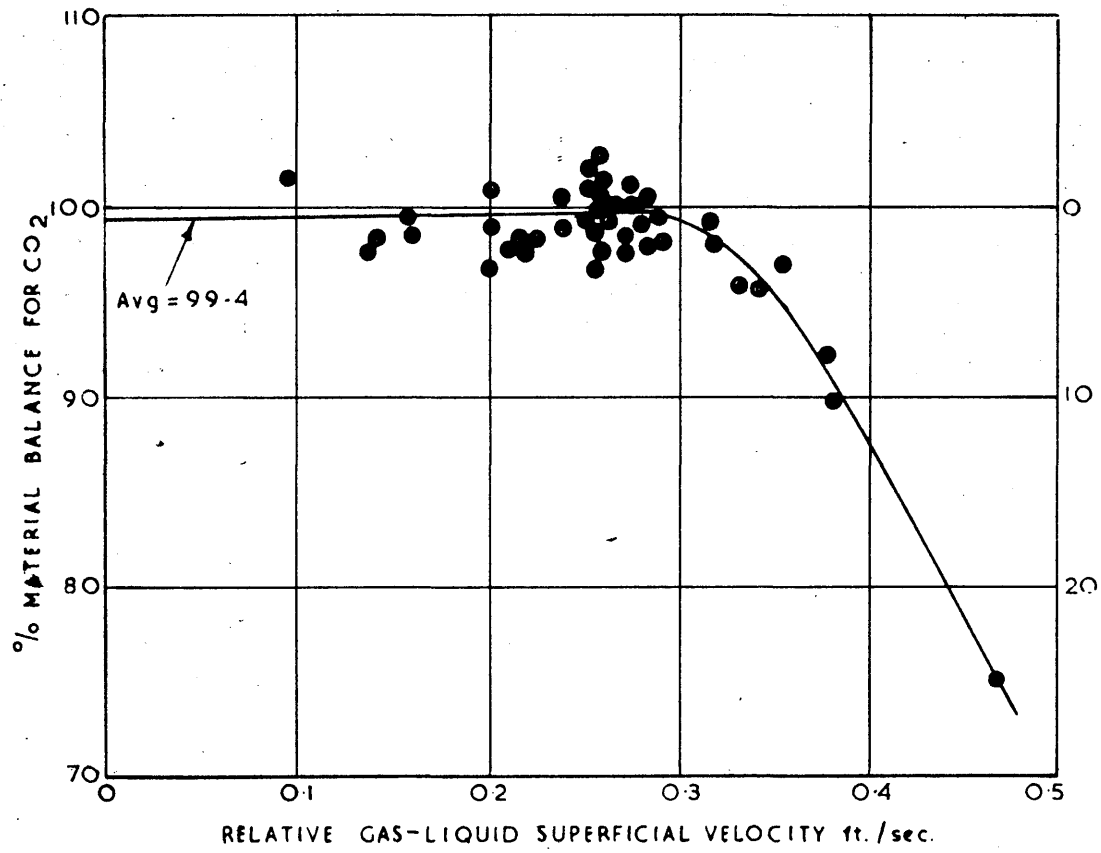

Fig.12. EFFECT OF CARRY-OVER.

it is necessary to have available accurate values for the solubilities of carbon dioxide in water over the temperature and pressure range to be studied. This has been done in Part 2 of this thesis and these results will be used in the calculations.

3.6.2. Operating line.

Since as much as 90% of the carbon dioxide entering the plant may be absorbed, the composition of the gas may change from 85% down to 30% carbon dioxide. As a consequence the operating lines may have a pronounced curvature, while the equilibrium curve may be almost straight. Operating lines for various changes in gas composition are plotted in Fig. 13. Inspection of the curves shows that the curvature becomes less pronounced as the change in gas composition between inlet and outlet becomes smaller. It was therefore decided to investigate the point at which the curvature of the operating line was so small that the logarithmic mean concentration gradient could be used to calculate the values of $(H.T.U.)_{OL}$ and K_La. In addition, the method of Carey and Williamson[28] was investigated. This method allows for the curvature of the operating line by determining the driving force midway between the inlet and outlet liquid compositions and then correcting the arithmetic mean driving force based on the inlet and outlet compositions for the much larger driving force in the middle. The comparison of the logarithmic mean driving force, the driving force obtained by the method of Carey and Williamson and the driving force obtained by graphical integration is shown in Table 12. The results are expressed in the number of transfer units for convenience.

A comparison of the method of Carey and Williamson with the method of graphical integration shows that the two methods agree with a maximum deviation of better than 4%. The logarithmic mean driving force deviates from the driving force calculated by graphical integration by less than

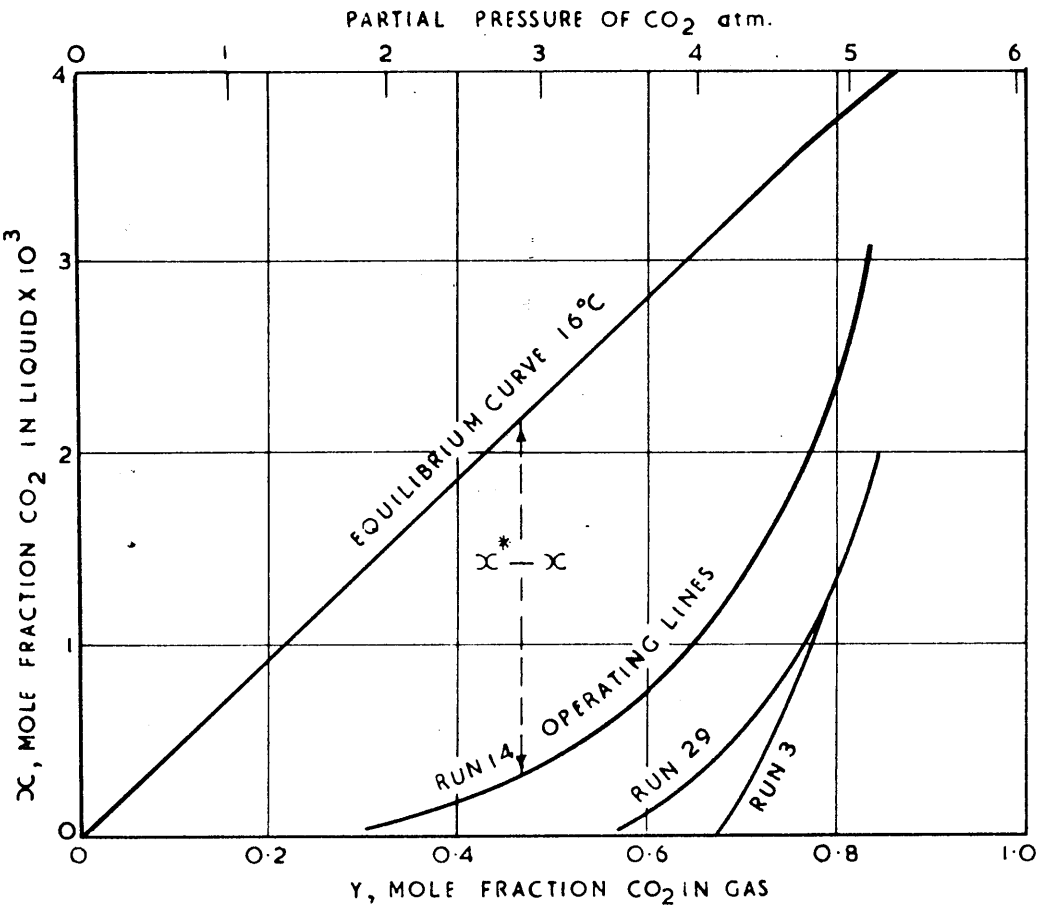

Fig. 13. OPERATING LINES

4% for gas composition changes less than 18%, by 8% for composition changes less than 28%, and by 16% for composition changes less than 40%. In this connection the change in gas composition is merely the difference in composition between the inlet and outlet gas. As a result of the comparisons in Table 12, the logarithmic mean driving force was used for gas composition changes less than 18%, the three point method of Carey and Williamson for composition changes less than 40% and greater than 18%, and graphical integration for all composition changes greater than 40%.

It must be pointed out that in the computation of mean driving forces it is assumed that a fluidised bubble-bed operates under true countercurrent conditions. In actual practice, Fig.19 shows that the liquid may be completely mixed for distances up to 1.5 ft. from the gas inlet. As a consequence, the mean concentration gradient computed from the inlet and outlet liquid concentrations may be higher than that obtained in practice.

3.6.3. Absorption rates

Absorption rates can be expressed by an overall absorption efficiency, E_A, based on the inlet gas, by an overall efficiency E_A', based on the outlet gas, by the $(H.T.U.)_{OL}$ or by the K_La concepts, where

$$E_A = \frac{x_2 - x_1}{x_2^* - x_1} \quad -- \quad -- \quad -- \quad (10)$$

$$E_A' = \frac{x_2 - x_1}{x_1^* - x_1} \quad -- \quad -- \quad -- \quad (11)$$

$$(H.T.U.)_{OL} = \frac{h}{(N.T.U.)_{OL}} \quad -- \quad -- \quad -- \quad (8)$$

$$K_La = \frac{B}{h\, A \Delta x_M} \quad -- \quad -- \quad -- \quad (4)$$

For an explanation of these symbols see the introduction (section 1.5.)

It must be noted, however, that the gas velocity through the unit may change considerably since as much as 90% of the incoming carbon dioxide may be absorbed. For instance, in a typical run where 80% of the incoming gas was absorbed, the inlet superficial gas velocity was 0.11 ft./sec. and the outlet gas velocity was only 0.044 ft./sec. Therefore, the values of $(H.T.U.)_{OL}$ and K_La calculated from equations (8) and (4) are overall average values, since the instantaneous values at any point in the column may vary considerably from the inlet to the outlet.

The overall absorption efficiencies, E_A and E'_A, have advantages over the $(H.T.U.)_{OL}$ and K_La concepts for correlating the data from countercurrent bubble absorption plants where large amounts of gas are absorbed. E_A is more convenient to use in design calculations since it avoids the computation of mean concentration gradients by graphical integration or by the method of Carey and Williamson. In addition E_A can be used directly in the calculation of power requirements for pressure absorbers. In this respect, E_A is more useful than E'_A since the latter may have values considerably greater than 100% for countercurrent operations. The use of E_A in calculating these power requirements is shown in Appendix I of this thesis.

From these considerations, therefore, the results obtained from the absorption column have been expressed as overall absorption efficiencies based on the inlet gas, E_A.

Average $(H.T.U.)_{OL}$ and K_La values have also been included for the comparison of the performance of bubble absorbers with packed towers and to illustrate the general effects of gas velocity, liquid velocity, pressure, temperature, bed height and porosity on the absorption rate.

It is important to realise that absorption from rising bubbles is a complex physical phenomenon and that the rate coefficients E_A, $(H.T.U.)_{OL}$

and $K_L a$ are more in the nature of empirical correlation variables than rate constants of an exact physical significance. These rate constants by themselves may have very little practical significance, since the attainment of high absorption rates does not necessarily indicate large amounts of absorption. On the contrary, it is possible to obtain exceedingly high absorption rates under conditions where there is very little material absorbed. The designer of absorption equipment is more often faced with the problem of attaining a practical operating condition, where high rates of absorption are coupled with large amounts of material absorbed by the plant.

3.7. RESULTS

A complete list of all the runs carried out in the absorber together with various data calculated from these results is given in the large table enclosed in a folder at the back of this thesis. Appendix II summarises the data used to plot the results.

3.7.1. The effect of superficial gas and liquid velocities on E_A.

In order to determine the effects of superficial gas and liquid velocities on the absorption efficiency experiments were conducted under conditions such that the bed height, inlet partial pressure of carbon dioxide, total absorber pressure and the temperature were constant. A plot of E_A against inlet superficial gas velocity u_G is shown in Fig. 14, using the superficial liquid velocity u_L as a parameter. The results are corrected to an inlet partial pressure of carbon dioxide of 75 lb./in.^{2} abs., a bed height of 1.5 ft. and a temperature of 15°C. Since the gas velocity changes considerably as absorption proceeds it is difficult to decide whether the inlet, outlet or average gas velocities should be used to correlate the data. As a consequence, the data were plotted using each of the variables separately. The inlet and average superficial gas

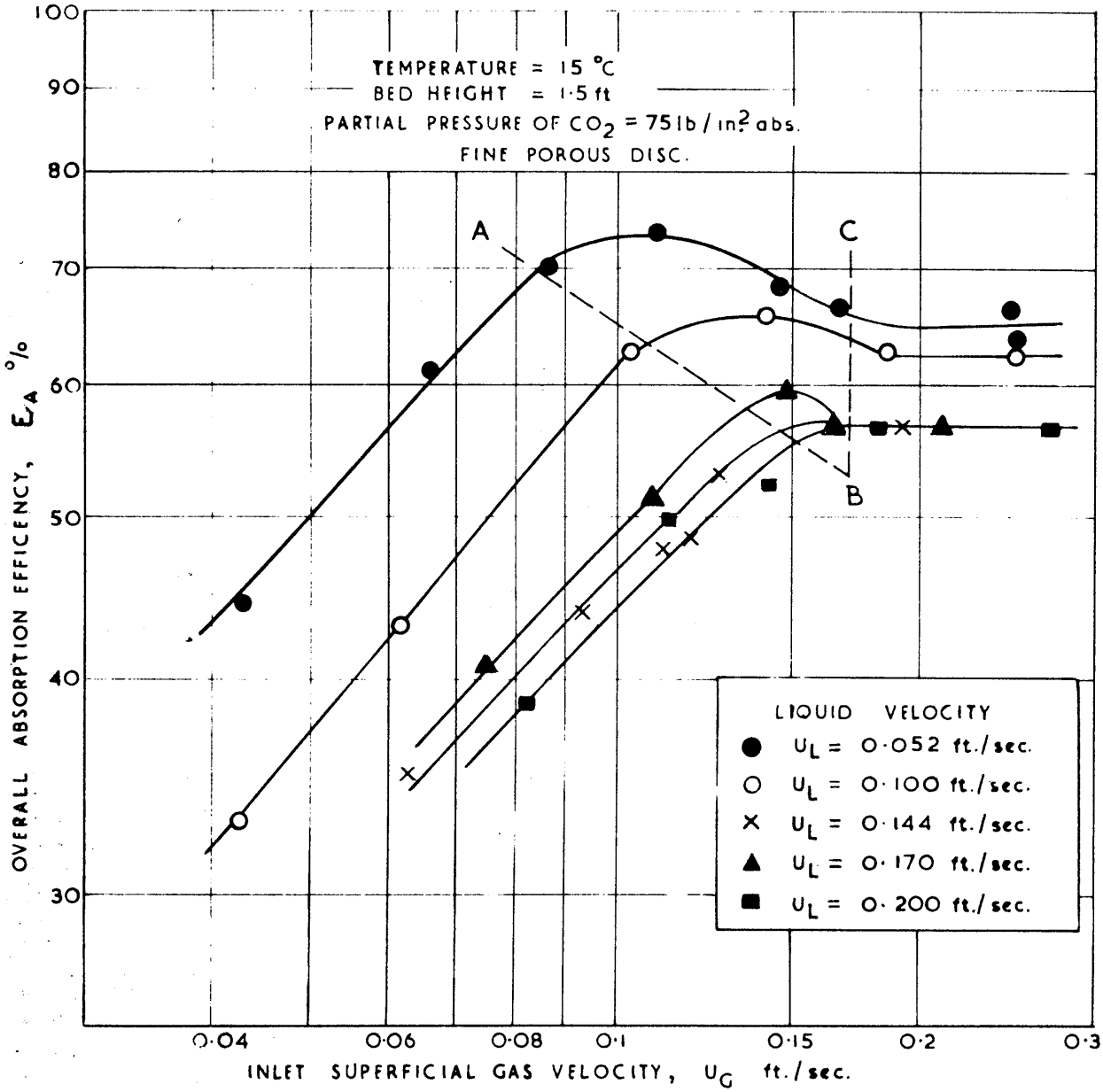

Fig.14. EFFECT OF LIQUID AND GAS VELOCITIES ON ABSORPTION EFFICIENCY.

velocities correlated the data equally well; therefore it was decided to use the inlet superficial gas velocity as the correlating variable since it is more convenient for design purposes.

The superficial gas velocities are calculated from the gas rates measured at atmospheric pressure using the compressibility data for carbon dioxide already given in Part 2 of this thesis. For the purpose of this calculation the compressibility of nitrogen was assumed to be unity, the value for an ideal gas, over the range of pressures and temperatures used.

At constant liquid velocity the absorption efficiency is observed to increase with increases in gas velocity until a constant value of absorption efficiency is obtained which is independent of further increases in gas velocity. At the lower liquid velocities of 0.052 and 0.100 ft./sec. the absorption efficiency rises to a maximum before reaching a constant value. In all cases, a constant value of the absorption is attained at gas velocities greater than about 0.17 ft./sec. An explanation of this phenomenon can be obtained by referring to the bed density curves of Fig. 8. It will be noted that the bed density decreases to a constant value at a gas velocity of about 0.17 ft./sec. so that the initial rise in absorption efficiency with gas velocity is probably due to an increase in the amount of gas in the bed, and the absorption efficiency becomes constant when the bed density becomes constant.

Experiments that will be presented in Part 4 of this thesis show that the average bubble volume in the bed does not change much with gas velocity, but that as the gas velocity increases the number of bubbles per unit volume of bed increases. The initial rise of absorption efficiency with gas velocity can therefore be explained as an increase in the gas hold-up which increases the surface area for absorption. From these

considerations, the region where the absorption efficiency increases with gas velocity will be referred to as the "rising hold-up" region and the condition where the absorption efficiency becomes independent of gas velocity will be termed the "constant hold-up" region. The region between the two will be termed the "transition" region.

In the rising hold-up region and at constant liquid velocity the absorption efficiency is proportional to $u_G^{0.61}$.

The effect of liquid velocity is also illustrated by Fig. 14. At constant gas velocity the effect of increasing the liquid velocity is to decrease the absorption efficiency up to a liquid velocity of 0.144 ft./sec. At this point further increases in liquid velocity up to 0.200 ft./sec. have a relatively small effect upon the absorption efficiency particularly in the constant hold-up region. In the rising hold-up region the absorption efficiency is directly proportional to $u_L^{-0.48}$ and in the constant hold-up region it is proportional to $u_L^{-0.15}$ at constant gas velocities.

Fig. 15 shows the effect of liquid velocity in both the rising hold-up and the constant hold-up regions. In the rising hold-up region the liquid velocity has a greater effect upon the absorption efficiency than in the constant hold-up region.

Figs. 20 and 21 show the effect of liquid and gas velocities on the average K_La and $(H.T.U.)_{OL}$ values. The rising hold-up and the constant hold-up regions are also apparent when plotting these variables as is the relatively small effect of liquid velocity on the absorption coefficient above 0.144 ft./sec. This latter effect has been noticed in packed towers by Van Ardsel[29], who found that an increase in liquid velocity relative to the gas flow caused an increase in the absorption coefficient until a "critical" velocity was reached, after which further increases had little effect.

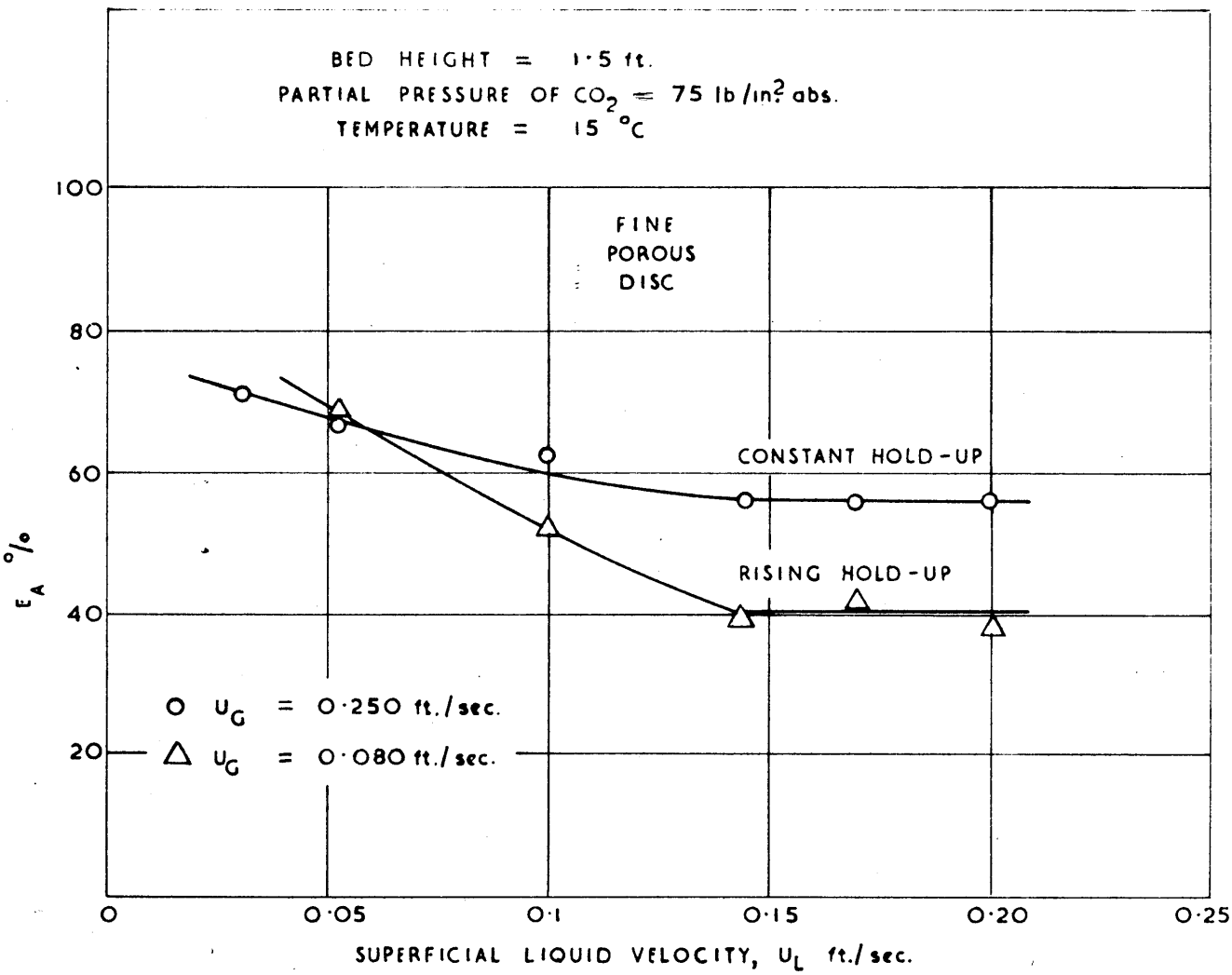

Fig. 15 EFFECT OF LIQUID VELOCITY

3.7.2. The effect of bed height

The effect of bed height on the absorption efficiency was investigated by holding all other variables at constant levels. Fig. 16 illustrates the effect of bed height on E_A, average $(H.T.U.)_{OL}$ and K_La when the partial pressure of carbon dioxide is 75 lb./in.^{2} abs. and the temperature is 15°C at various liquid and gas velocities.

In the rising hold-up region the overall absorption efficiency is proportional to $h^{0.33}$, while in the constant hold-up region the efficiency is proportional to $h^{0.22}$ for bed heights between 0.4 and 5.5 ft. However, the plots of E_A versus bed height on log-log paper exhibit a slight curvature and this is attributed to the effect of the ratio of bed height to column diameter at large bed heights.

The effect of bed height on the average $(H.T.U.)_{OL}$ is to cause an increase in this value proportional to $h^{0.5}$ in the rising hold-up region and to $h^{0.64}$ in the constant hold-up region.

Average K_La values decrease with increases in bed heights according to $h^{-0.5}$ in the rising hold-up region and $h^{-0.37}$ in the constant hold-up region. However, at bed heights greater than 4 ft., an increase in average K_La and a corresponding decrease in average $(H.T.U.)_{OL}$ values are observed, indicating that for long columns, where absorption is almost complete, there is a region at the top which does not behave as a fluidised bed. In this region it might be expected that the residual bubbles are so small that they rise independently with very little recirculation.

3.7.3. The effect of pressure

The effect of pressure was investigated by making measurements at constant bed heights and temperatures. The results shown in Fig. 17 are corrected to a bed height of 1.5 ft. and a temperature of 15°C.

The effect of pressure on the overall absorption efficiency is the

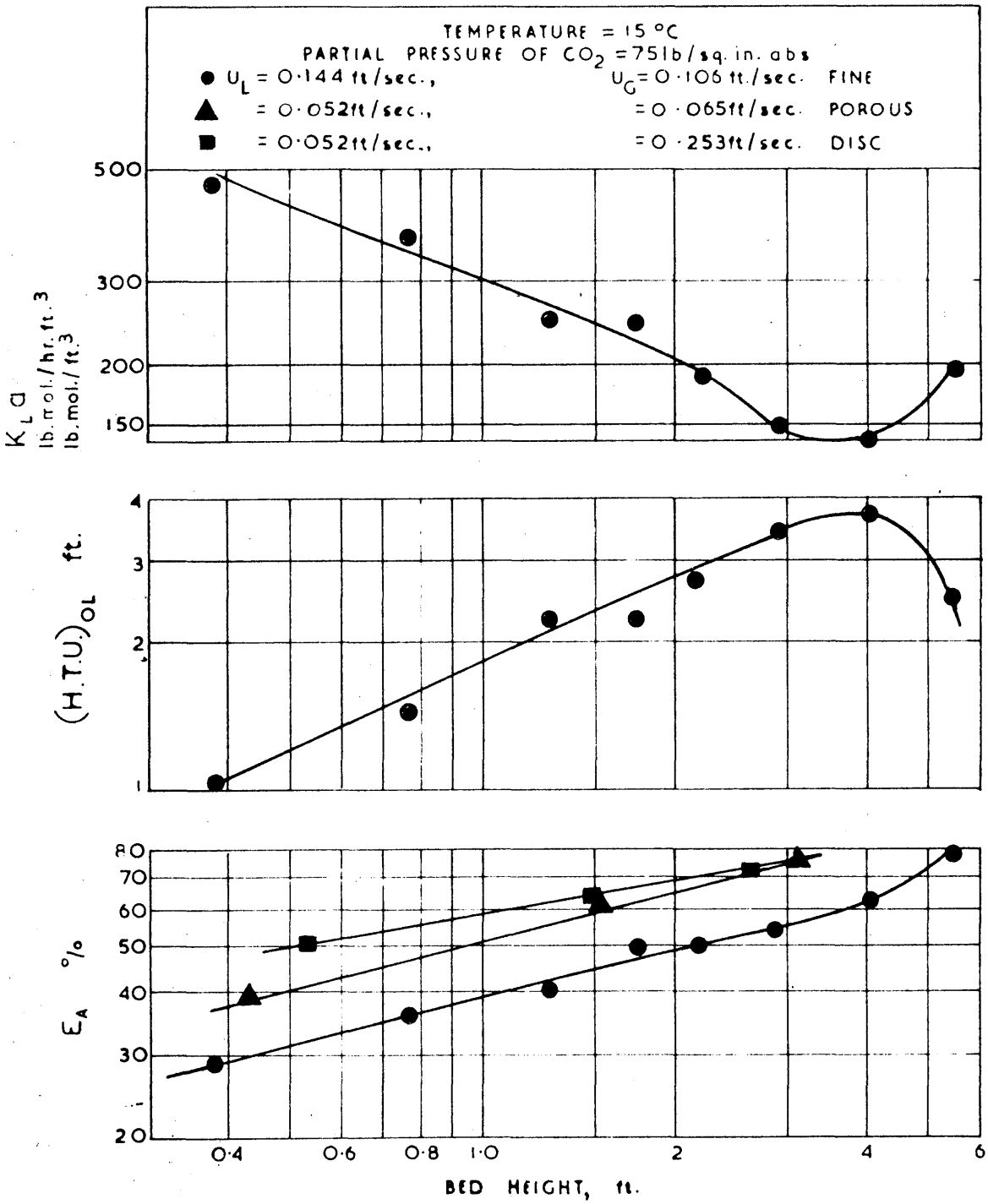

Fig. 16 EFFECT OF BED HEIGHT.

same in both the rising hold-up and constant hold-up regions and is virtually independent of gas and liquid velocities in these regions. For inlet partial pressures of carbon dioxide in the range 2.5 atm. to 14.0 atm. the absorption efficiency is proportional to $p^{-0.33}$.

In the rising hold-up region average K_La decreases with increasing partial pressure of carbon dioxide according to $p^{-0.5}$ while in the constant hold-up region the effect of pressure is much greater, being proportional to $p^{-1.4}$.

The average $(H.T.U.)_{OL}$ was found to be proportional to $p^{0.5}$ in the rising hold-up region and $p^{0.68}$ in the constant hold-up region.

The effect of increasing the pressure is to decrease the absorption rate, so that it may be impracticable to absorb carbon dioxide in water at partial pressures higher than 200 lb./in.^{2} abs., since the effect of increasing the pressure on the size of the absorber may be offset by the decrease in the absorption efficiency.

3.7.4. The effect of temperature

The effect of temperature on E_A, average $(H.T.U.)_{OL}$ and average K_La is shown in Fig. 18. The data are correlated to a bed height of 1.5 ft. and an inlet partial pressure of carbon dioxide of 75 lb./in.^{2} abs.

The effect of temperature is to increase the absorption rate in both the rising and constant hold-up regions. However, the effect is slight being proportional to $t^{0.1}$ for E_A and $t^{-0.1}$ for average $(H.T.U.)_{OL}$ in both regions and for the temperature range 10 to 30°C. The temperature effect is independent of gas and liquid velocities in both regions. Temperature has a slightly greater effect on K_La since the exponent of t was found to be 0.15 for both regions.

3.7.5. General correlation equations

For the rising hold-up region the overall absorption efficiency is

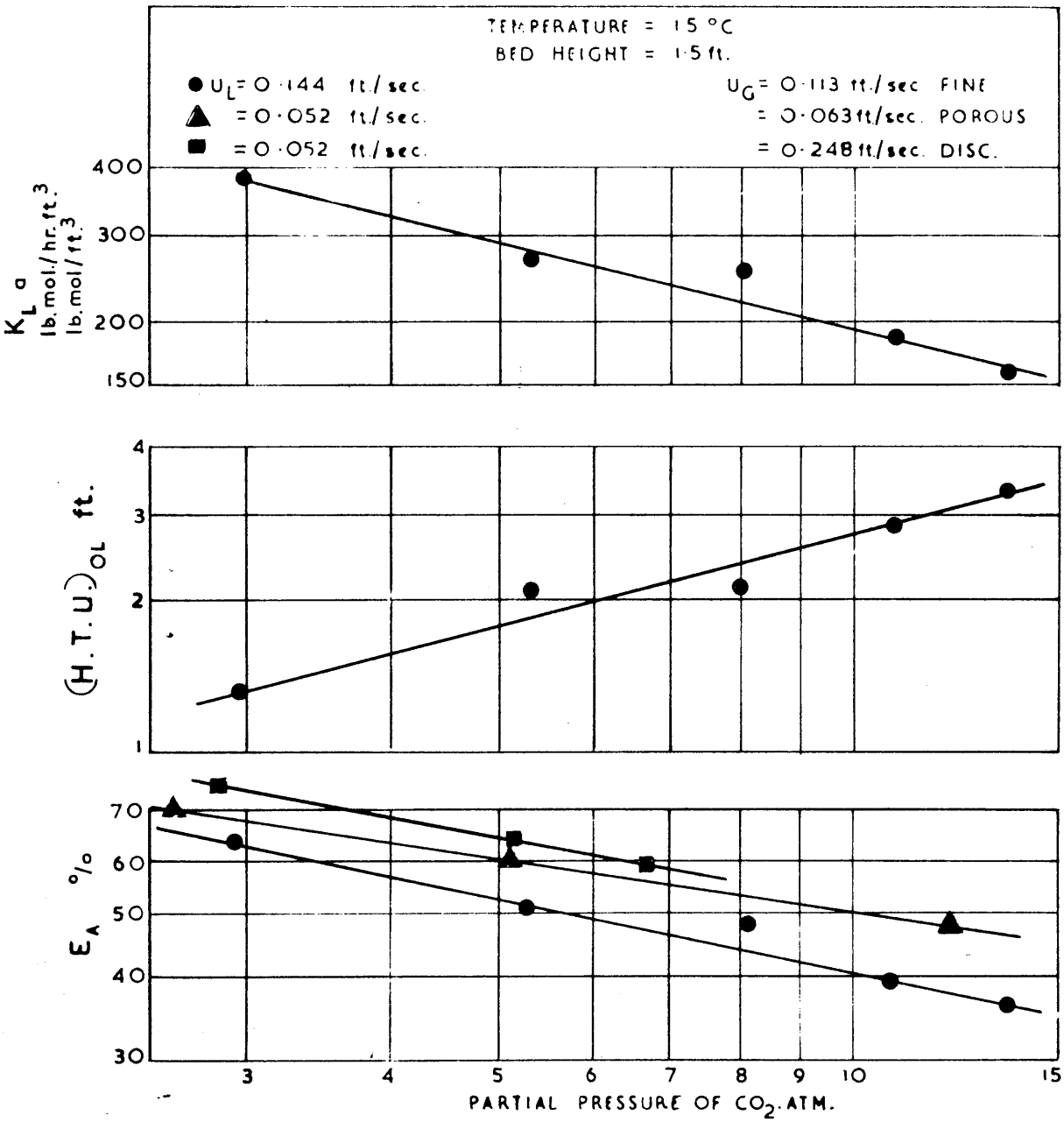

Fig. 17. EFFECT OF PRESSURE

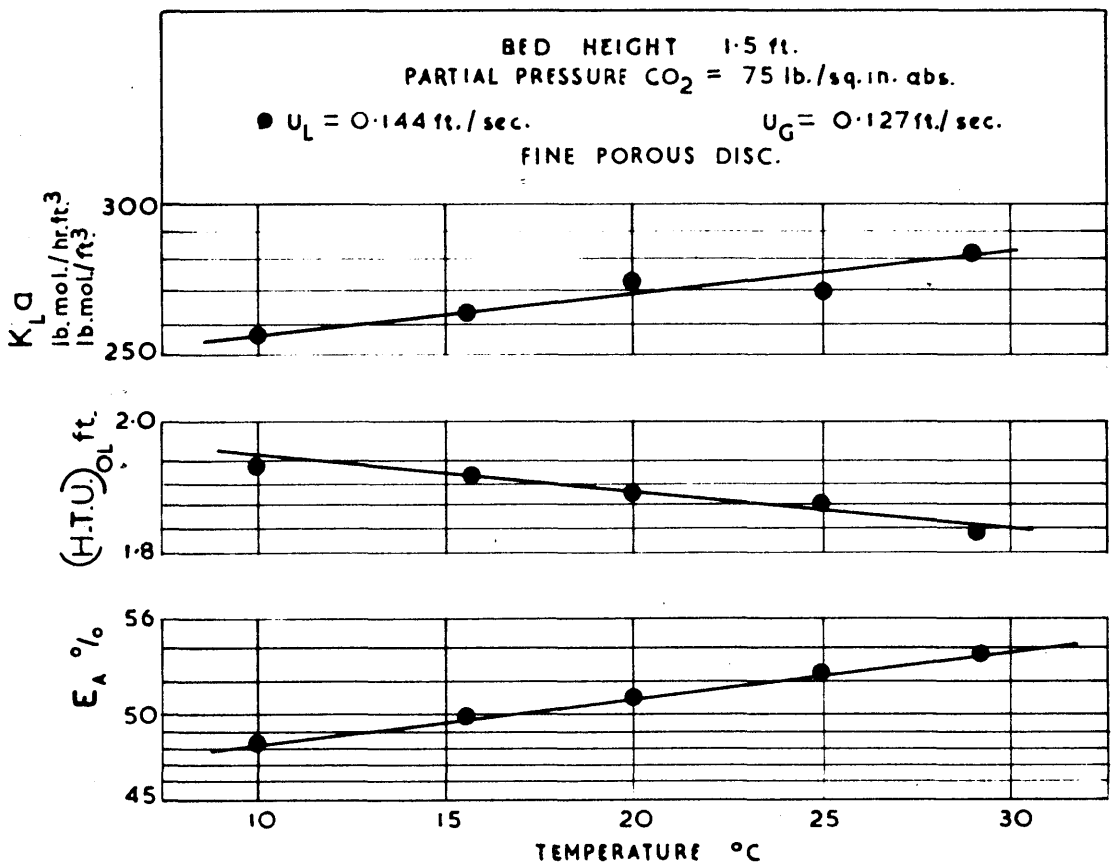

Fig. 18. EFFECT OF TEMPERATURE

given with an average deviation of ± 6% from the experimental value by the equation:

$$E_A = 0.86 \frac{u_G^{0.61}}{u_L^{0.49}} \times \frac{h^{0.33} \times t^{0.1}}{p^{0.33}} \quad -- \quad -- \quad -- \quad (47)$$

A deviation summary is given in Table 13.

Equation (47) can be used for superficial liquid velocities in the range 0.052 to 0.200 ft./sec., superficial gas velocities in the range 0.04 to 0.15 ft./sec., bed heights in the range 0.4 to 5.5 ft., partial pressures of carbon dioxide from 2.5 to 14.0 atm. and temperatures in the range 10 to 30°C.

Equation (47) can only be used if the values of E_A calculated does not exceed the value of E_A calculated from the equation below

$$E_A = \frac{0.30}{u_G^{0.40}} \times \frac{h^{0.33} \times t^{0.1}}{p^{0.33}} \quad -- \quad -- \quad -- \quad (48)$$

Equation (48) defines the limits of the rising hold-up region, and is the equation of the broken line, AB, shown in Fig. 14, for various bed heights, temperatures and partial pressures of carbon dioxide.

For the constant hold-up region the absorption efficiency is independent of the superficial gas velocity and is given by the equation:

$$E_A = \frac{0.52}{u_L^{0.15}} \times \frac{h^{0.22} \times t^{0.1}}{p^{0.33}} \quad -- \quad -- \quad -- \quad (49)$$

Equation (49) gives values of E_A with an average deviation of ± 5% from the experimental values and Table 14 summarises this deviation. This equation applies to all liquid velocities in the range 0.030 to 0.200 ft./sec., and to all gas velocities greater than 0.17 ft./sec., i.e., for all gas velocities to the right of the vertical line BC in Fig. 14.

For the transition region the absorption efficiency is best obtained by using equation (49) which gives calculated values of E_A within ± 5%

of the experimental result. (See Table 14).

Equation (47) and (49) show that the absorption efficiency can be made to approach 100% by increasing the bed height or by decreasing the pressure. Obviously, absorption efficiencies of 100% or greater are impossible, and when values of more than 100% are calculated from equations (47) and (49) it may be assumed that the water leaving the absorber is almost saturated at the partial pressure of carbon dioxide in the incoming gas.

3.7.6. Concentration gradients in fluidised bubble-beds

Concentration changes through the bubble-bed were determined by taking off liquid samples at various distances above the porous diffuser plate by the sampling technique previously described. The dissolved carbon dioxide in the various samples was obtained by titration. The results are shown in Fig. 19. and the data tabulated in the large table at the back. The results indicate that there are three concentration regions in a fluidised bubble-bed:

1) A region of about $1\frac{1}{2}$ in. close to the porous disc where there is a sharp drop in concentration. A similar "end effect" has been discussed by Geankoplis and Hixon[30] for a countercurrent spray-type extraction column.

2) A region of about 1 ft. above the porous disc where the concentration does not change much with distance. This region probably corresponds to the completely "fluidised" region where the bubbles and liquid are continually recirculated in the direction of flow. This will result in complete mixing and a liquid of uniform composition.

3) A region where the gas leaves and the liquid enters. In this region there is a sharp change in concentration. This may be caused by a stratified layer of water which has not been mixed into the fluidised region.

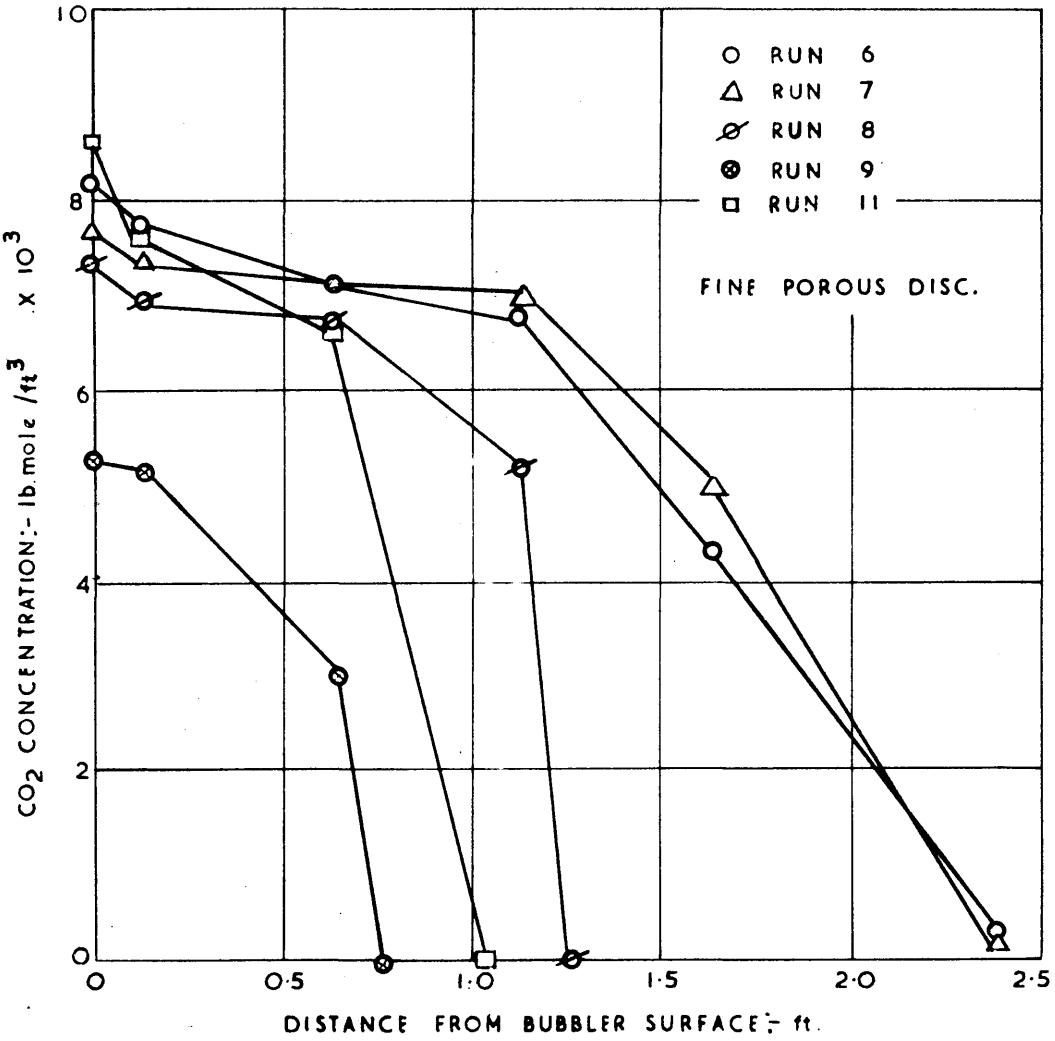

Fig.19. CONCENTRATION GRADIENTS

This sharp break in concentration is observed for bed heights of about 1.5 ft. or less, but for heights greater than this the concentration change is not so sharp but is still apparent.

The presence of a steep concentration gradient above distances of about 1 ft. from the porous disc indicates that for bed height to diameter ratios of greater than 4 there is not complete mixing in the bubble-bed.

3.7.7. The effect of plate porosity

To ascertain the effect of plate porosity, measurements were made of E_A, average $(H.T.U.)_{OL}$ and average K_La, using seven different gas distributors with widely varying porosities. The experiments were carried out at a constant superficial liquid velocity of 0.144 ft./sec., and a constant superficial gas velocity of 0.125 ft./sec.; the results were corrected to a bed height of 1.5 ft., a partial pressure of carbon dioxide of 75 lb./in. abs. and a temperature of 15°C. Table 15 summarises the results.

Table 15 shows that there is no significant effect of porosity up to average pore diameters of 3180 microns. The results for the two arrangements of indented strip (see Fig. 7) are identical, even though one arrangement has more than twice the number of holes in the same area as the other. The results from the indented strip are identical with those from the porous discs, even though the area of the indented strip bubbler was only 0.0214 ft^2 compared with 0.0307 ft^2 for all the porous discs. This would indicate that the area of the bubbler is not a significant factor.

In order to determine the point at which the number and size of the holes in the bubbler significantly affected the absorption rate, discs with 1/8 in. diameter holes and open 3/8 in. pipes were investigated. A plate with only four 1/8 in. diameter holes, spaced 7/8 in. apart at the corners of a square, gave a value of E_A which differed by only 4.5% from the average value of E_A obtained for the indented strip and porous discs

while the single 3/8 in. hole gave values which differed by only 13.3%.

From the investigation of the effect of porosity, the conclusion reached is that the pore size, number and distribution of holes, and the area of the bubbler plate can be varied over a wide range without a profound effect on the absorption rate.

3.8. COMPARISON OF COUNTERCURRENT BUBBLE-TYPE ABSORBERS WITH PACKED TOWERS

Fig. 20 compares absorption rates for packed towers using data available in the literature with absorption rates for bubble-type absorbers obtained in this thesis. For bubble-type absorbers the average K_La values range from 75 to about 500 lb.mole/hr.,ft.^{3},lb.mole/ft.^{3}, while the operating values for packed towers lie in the range 4 to 75 lb.mole/hr.,ft.^{3},lb.mole/ft.^{3} depending upon the liquid velocity, gas velocity and the type of packing[31,32,33]

Fig. 21 compares the data of Cooper, Christl and Peery[12] for the absorption of carbon dioxide in water in a packed tower with the data available at present for the absorption of carbon dioxide in water for countercurrent bubble-type absorbers. The $(H.T.U.)_{OL}$ values for bubble-type absorbers lie in the range 0.75 to 3.5 ft. at an inlet partial pressure of 75 lb./in.^{2} abs., while the average $(H.T.U.)_{OL}$ values for packed towers lie in the range 2.75 to 9 ft.

Shulman and Molstad[16] have made measurements of the rate of absorption of carbon dioxide by water in a 2 in. diameter glass bubble column at atmospheric pressure and three liquid rates. Their results at 1 atm. total pressure and a bed height of 1 ft. are compared with the average $(H.T.U.)_{OL}$ values, obtained in this thesis, at an inlet partial pressure of 5.1 atm. of carbon dioxide and a bed height of 1.5 ft. in Fig. 20. The results in this thesis are somewhat lower than those of Shulman and Molstad because of the higher partial pressure, higher bed heights and because the values are average $(H.T.U.)_{OL}$ values between inlet and outlet gas velocities.

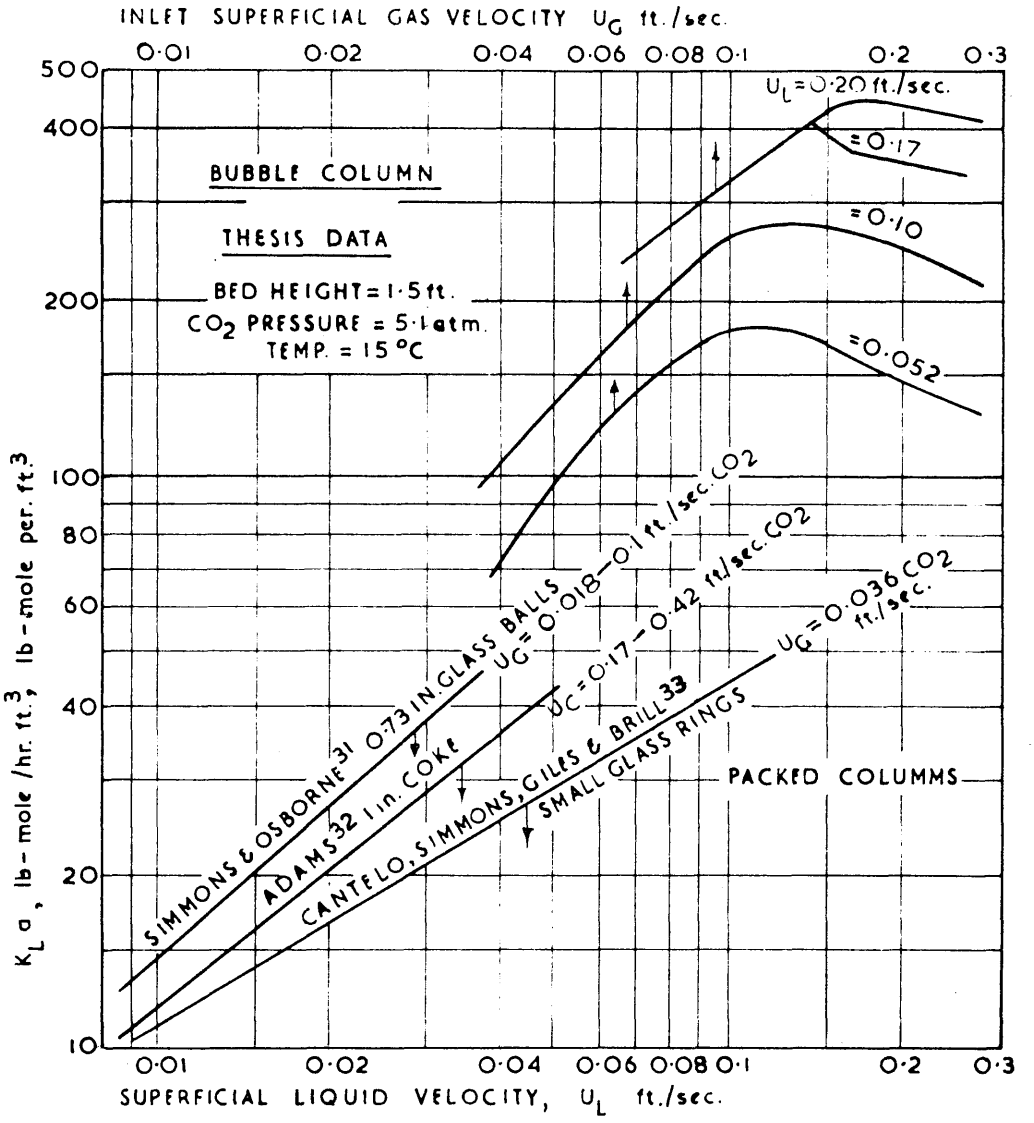

Fig.20 $K_L a$ FOR PACKED COLUMNS & BUBBLE COLUMNS.

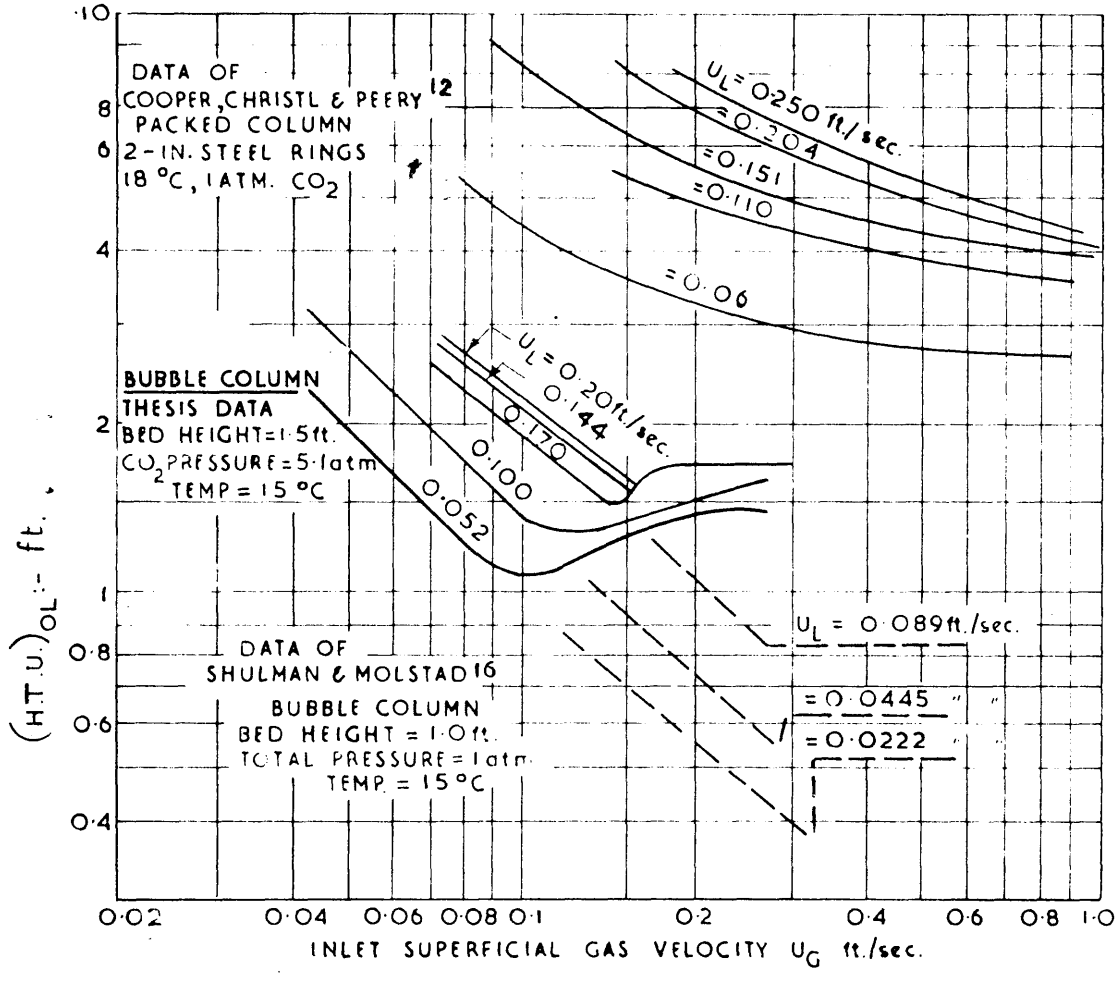

Fig. 21 $(H.T.U)_{OL}$ FOR PACKED COLUMNS AND BUBBLE COLUMNS.

In general it may be concluded that bubble-type absorption towers give absorption rates which are from 3-10-fold greater than those of packed towers.

5.9. DISCUSSION

The objective of this work has been to determine the effects of various operating variables on the behaviour of a bubble-type water scrubber for carbon dioxide under conditions where large quantities of soluble gas are absorbed. The results show that the bubble-type scrubber is superior to the packed tower for the absorption of carbon dioxide in water where the liquid film resistance is believed to control the rate of absorption. The reason for this is undoubtedly connected with the rate of renewal of the liquid film. When a bubble rises it must displace its own volume of liquid as it rises through its own diameter. It may therefore be expected that the liquid film around the bubble is renewed each time it moves through one diameter. In general it can be expected that the volume of a bubble-type tower will be about 1/3rd to 1/10th of the volume of a packed tower for the same amount of absorption depending on the operating pressure. The bubble tower has the additional advantages of better mixing through fluidisation and the relative independence of the performance upon the mechanism of bubble formation and distribution. Investigations of the effect of porosity of the gas distributor plate show that the performance of the absorber is insensitive to changes in the number, size and distribution of the holes in the gas distributor over a wide range. The reason for this behaviour is that the bubbles in the fluidised bed result from the coalescence of two or more bubbles either in the fluidised bed itself or in the region of the gas distributor plate. A recent paper by Helsby and Tuson[34] shows how two or more bubbles leaving a jet may coalesce under viscous solutions of glycerine in water. Evidence will be presented in

Part 4 of this thesis to show that the bubble sizes in a fluidised bed follow a probability distribution and result from the coalescence of two or more bubbles.

The effect of gas rate is to increase the absorption rate in the rising hold-up region. The explanation of this has been ascertained by photographing bubble-beds and measuring the number and size of the bubbles as the gas velocity is increased. For water it was found that the average bubble volume increases only slightly with gas velocity, but the number of bubbles per unit volume increases more rapidly thus causing a rise in the surface area for absorption. The point at which the absorption rate becomes independent of the gas velocity corresponds to the point at which the bubble-bed holds as much gas as it can, and further increases in gas velocity cause the formation of plugs or large bubbles of gas. Observations in the glass column show that there is much turbulence and recirculation at low gas velocities in the rising hold-up region so that it may be incorrect to refer to this region as the "streamline", a term used by Shulman and Molstad.

The effect of liquid velocity upon the absorption rate is best illustrated by the effect of liquid velocity on average K_La. The average K_La increases with increases in both the liquid and gas velocities. The effect of increasing the liquid velocity should be to increase the eddy diffusivity in the liquid film moving round the bubble. Although greater liquid velocities increase the absorption rate the overall effect on E_A is a decrease and on $(H.T.U.)_{OL}$ an increase. The reason for this is that both E_A and $(H.T.U.)_{OL}$ are functions of a liquid rate term other than that involved in the effect of liquid rate on absorption rate. For instance, $(H.T.U.)_{OL}$ is related to K_La by the following equation:

$$(H.T.U.)_{OL} = \frac{L}{\rho_L \cdot K_La} \quad -- \quad -- \quad -- \quad (9)$$

Since the average $K_L a$ in Fig. 20 varies with liquid velocity in proportion to $u_L^{0.56}$ then $(H.T.U.)_{OL}$ should increase with liquid velocity according to $u_L^{0.44}$.

The decrease in absorption rate coefficients with increase in bed height shown in Fig. 16 is a phenomenon which can be explained on the theory that in columns where the bed height to diameter ratio is large, the surface area per unit volume for absorption changes as the distance from the bubbler plate increases. As a bubble rises its volume decreases due to absorption and hence the surface area decreases. If the rate of bubble recirculation in the bed is less than the rate of absorption then there will be a gradual change in bubble volume and surface area for absorption with distance from the bubbler.

The effect of increasing the inlet partial pressure of carbon dioxide is to decrease the absorption rate as shown by Fig. 17. If the absorption of carbon dioxide in water is completely liquid film controlled, then the effect of pressure could be explained by supposing that the diffusion coefficient of dissolved carbon dioxide is influenced by concentration. However, under the highly turbulent conditions in a fluidised bed it is to be expected that the static diffusion coefficient is negligible compared with the eddy diffusivity and it is difficult to visualise how the concentration of dissolved carbon dioxide could influence the eddy diffusivity. Another explanation is that the solution of carbon dioxide in water under pressure is partially controlled by the gas film resistance and the effect of pressure is to increase this resistance.

The effect of increasing the temperature is to increase the absorption rate in both the rising hold-up and the constant hold-up regions, as would be expected for a diffusion controlled mechanism in both regions. However, Shulman and Molstad observed a negative temperature coefficient at atmospheric

pressure for low gas velocities. It may be that the effect of the higher pressures is to increase the proportion of the gas film resistance enough to reverse the temperature coefficient.

The concentration gradient data illustrated by Fig. 19 show that there is a small "end effect" at the bubble plate and a large "end effect" at the water inlet. The end effect at the water inlet can be explained by the presence of a stratified layer of fresh water not completely mixed into the fluidised bed. In order to ascertain the cause of the end effect at the gas bubble plate, experiments were conducted in the glass column of the same dimensions as the pressure unit. In the glass unit a layer of bubbles was observed just below the gas distributor so that absorption would still continue to a slight extent after the liquid had passed the distributor. In addition a few very small bubbles, about 1 mm. in diameter, were observed suspended in the liquid below the bubbler. The sampling point for the water leaving the column was 10 in. below the surface of the bubble plate so that the so called "end effect" in this case could be attributed to a small amount of absorption in this region. It was not possible to obtain samples closer to the bubble plate than about 4 in. since large quantities of gas issued with the liquid from the sampling point and it was impossible to obtain constant material balances.

Finally it can be stated that the bubble-type absorber has proved to be successful for the absorption of large quantities of carbon dioxide from gas mixtures where most of the gas consists of carbon dioxide. The percentage of carbon dioxide absorbed can be made to approach 100% by increasing the bed height in the region 0.5 to 6.0 ft., decreasing the partial pressure of carbon dioxide in the range 2.5 to 14.0 atm., increasing the liquid to gas velocity ratio in the range 0.2 to 2.5 and decreasing the temperature.

PART 4

THE MECHANISM OF FORMATION OF GAS BUBBLE-BEDS

4.1. INTRODUCTION

Recent work shows that in certain cases absorption rates from moving bubbles are greater than absorption rates form moving liquid films such as those present in packed towers.

Shulman and Molstad[16] have described a method for the absorption and desorption of carbon dioxide in dilute mixtures where the gas is bubbled countercurrent to the liquid at atmospheric pressures. The previous section of this thesis (Part 3) has discussed the operation of a bubble column for carbon dioxide at high partial pressures of carbon dioxide where most of the soluble gas is removed. The absorption medium in both cases could be described as a fluidised bubble-bed. The conclusions reached were that rates of absorption in bubble-type absorbers are faster than the rates in packed towers when the rate of absorption is controlled by the liquid film resistance.

In contrast to the fluidised bubble-bed a number of authors have discussed the use of foams for the absorption of gases. Pozin et al[36] have discussed absorption from a foam which flowed across a sieve plate through which the gas was forced. Helsby and Birt[37] have described an apparatus for the absorption of carbon dioxide from dilute mixtures in aqueous ethanolamine solutions where the liquid velocity was so low (0.0005 ft./sec.) that a foam was produced. Dixon and Kiff[38] have discussed the use of perforated and porous plates for the formation of bubbles and foams of 30% monoethanolamine. These authors have discussed the rate of absorption of carbon dioxide in monoethanolamine solutions in relation to the number, size and distribution of holes in the gas distributor.

Very little work has been done on the mechanism of formation and

operation of fluidised and foam beds. Verschoor[39] has measured the densities of various bubble beds as a function of gas velocity using water, methanol and a glycerine-water mixture. Verschoor observed that water and organic liquids all show coalescence of small bubbles emerging from a porous plate and that this coalescence can be suppressed by the addition of small quantities of acetic acid to water. The coalescence of bubbles near jets has recently been confirmed photographically by Helsby and Tuson[34]. However no work has been done on the size, number and distribution of bubbles in the bubble-bed itself in relation to the formation of fluidised and foam beds for the absorption of gases. This aspect of fluidised beds has therefore been studied and leads directly on from the preliminary work done on liquid hold-up for determining the height of the bed in the pressure column.

4.2. EXPERIMENTAL

The apparatus used is shown in Fig. 22. It consists of a 3.14 in. internal diameter glass column in which the liquid to be studied is placed. The gas is bubbled through the liquid using porous metal or glass discs. The gas flow rate is held constant by using the flowmeter, F, and the gas flow leaving the column is accurately measured on a dry gas meter. The bed height, h_B, and the manometer reading, h_L, are read on the same scale so that the bed density can be computed from the equation:

$$\rho_B = \frac{h_L \rho_L}{h_B} \qquad -- \quad -- \quad -- \quad -- \qquad (46)$$

where ρ_L is the density of the liquid being studied. In this way the bed density can be determined over a range of superficial gas velocities.

In order to determine the size, shape and distribution of the bubbles the fluidised bed was photographed using a plate camera in conjunction with an electronic flash.

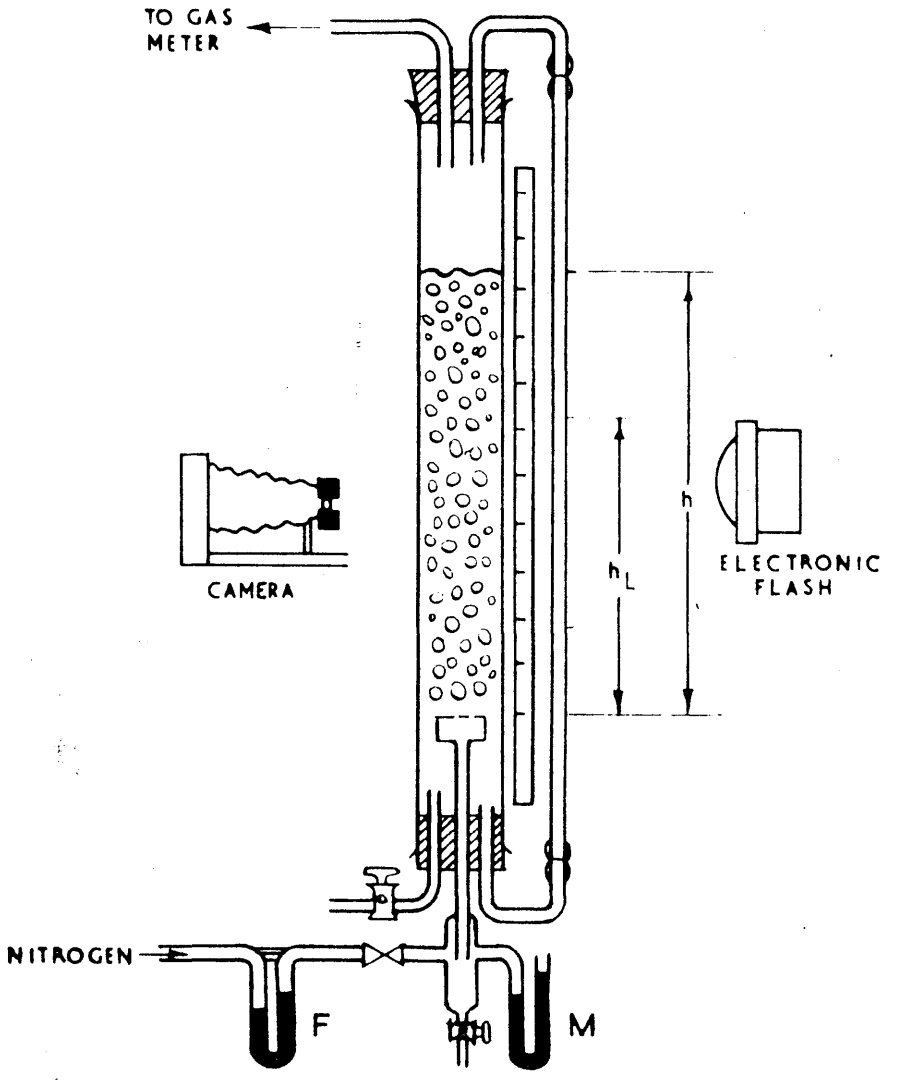

Fig. 22. EQUIPMENT

The liquids studied were acetone, aniline, ethyl acetate, monoethanolamine, water, glycerine, glycerine-water mixtures and solutions of acetic acid in water. The gases used were nitrogen, oxygen and carbon dioxide.

The manometer, M, which contained either water or mercury, was used to measure the pressure drop across the gas distributor at various gas flow rates.

4.3. POROSITY OF GAS DISTRIBUTOR

The plates used for the distribution of the gas through the liquid were either of sintered glass or sintered bronze such that the porosities varied over a wide range. Other types of bubble distributor were the two arrangements of indented nickel strip already described in section 3.4.

The pressure drop across the bubbler or gas distributor is obtained by subtracting the hydrostatic pressure due to the bubble bed from the back pressure read on manometer M.

$$\Delta P = h_M \rho_M - h_B \rho_B \quad -- \quad -- \quad -- \quad (50)$$

The resulting pressure drop ΔP is the sum of the frictional and contractional pressure drops due to the flow of gas through the porous plate, ΔP_f, and the maximum bubble pressure required for the formation of bubbles at the plate surface, ΔP_o.

$$\Delta P = \Delta P_o + \Delta P_f \quad -- \quad -- \quad -- \quad (51)$$

It is well known that during the formation of a bubble at a jet the pressure first increases until the bubble is a hemisphere whose radius is equal to that of the jet, and then decreases as the bubble grows larger. Consequently if the pressure drop across the plate, ΔP, is plotted against gas velocity and the resulting line is extrapolated to zero gas flow then the intercept will be ΔP_o, or the maximum bubble pressure which is independent of gas velocity. The average pore diameter can then be calculated from the equation:

$$d = \frac{4\gamma}{\Delta P_o} \quad -- \quad -- \quad -- \quad -- \quad (52)$$

where γ is the surface tension of the liquid.

Fig. 23 shows typical plots of ΔP against the superficial gas velocity, u_G. It is observed in Fig. 23 that the plots of ΔP versus u_G can be divided into three regions:

1) A region at low gas velocities where ΔP increases rapidly with increases in superficial gas velocity. This region can be ascribed to an increase in the maximum bubble pressure as smaller pores in the bubbler come into operation.

2) A region where ΔP increases less rapidly with gas velocity. This region can be attributed to the streamline flow of gas through the pores.

3) A region where increases in gas velocity have very little effect upon ΔP. This can be attributed to the turbulent flow of gas through the pores.

It was found that if the line for the streamline flow region was extrapolated to zero gas velocity then the pressure drop obtained, ΔP_o, could be used to calculate the average pore diameter with good reproducibility. The pore diameter obtained will be an average value for the case where the maximum number of holes are in operation for the particular liquid used.

Table 16 summarises the porosities obtained by this method for six bronze discs, three glass discs and the two arrangements of indented nickel strip, using water as the liquid in the column. Table 17 gives the porosities of plates P2 and P3 determined for various other liquids and solutions. The results show that the average pore size of a porous plate depends upon the physical properties of the liquid used, in particular the surface tension. In general it would appear that the lower the surface tension of the liquid the lower the average pore size for the same porous plate. However, acetone appears to be an exception since it gives an average pore size which is in

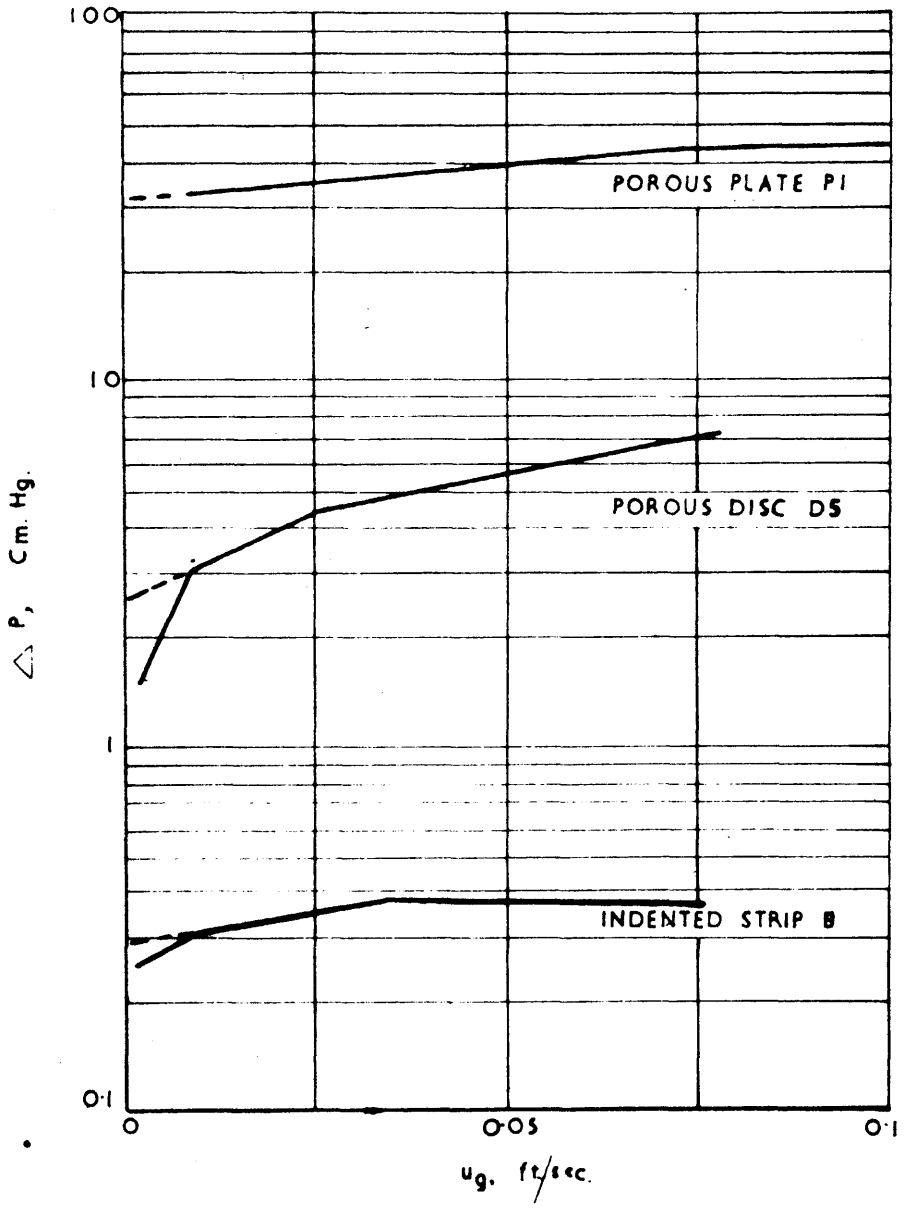

FIG.23. PRESSURE DROP ACROSS GAS DISTRIBUTORS.

agreement with that obtained by pure water, even though the surface tension of acetone is 26 dynes/cm. compared with 72 dynes/cm. for water.

It may be inferred that the pore diameters of a porous plate vary over a wide range and that in general there is a tendency for the largest pores to be used for bubble formation. However, smaller pores may be brought into action by using liquids of lower surface tension.

4.4. BED DENSITIES

Fig 24 shows how the bed densities for various pure liquids vary with superficial gas velocity. All the curves have the same general shape. The bed density decreases and the gas hold-up increases as the superficial gas velocity increases, until a more or less constant value of bed density is reached over the range studied. At this point plugs of gas are formed which cause the bed level to rise and fall as the plugs are discharged at the surface. In the cases of acetic acid and ethyl acetate plug formation causes the bed density to rise from a minimum value, to a constant average value between the maximum and minimum levels. It was ascertained at the beginning of the investigations that the bed density curve was independent of the gases used (O_2, N_2 and CO_2), and independent of the amount of liquid in the column for a particular porous plate and liquid.

The bed densities of various glycerine-water solutions are shown in Fig. 25. The effect of adding glycerine to water is to lower the bed density curve below that for pure water up to concentrations of about 68% by weight of glycerine. At 84 wt.% glycerine the bed density curve lies between those of pure glycerine and those of pure water. It is evident that the bed densities of glycerine solutions bear very little relationship to the bed densities of the pure components. Glycerine solutions containing from 13 to 68 wt.% glycerine have good foaming properties. At low gas velocities in these solutions the bubbles rise to the surface to form stable

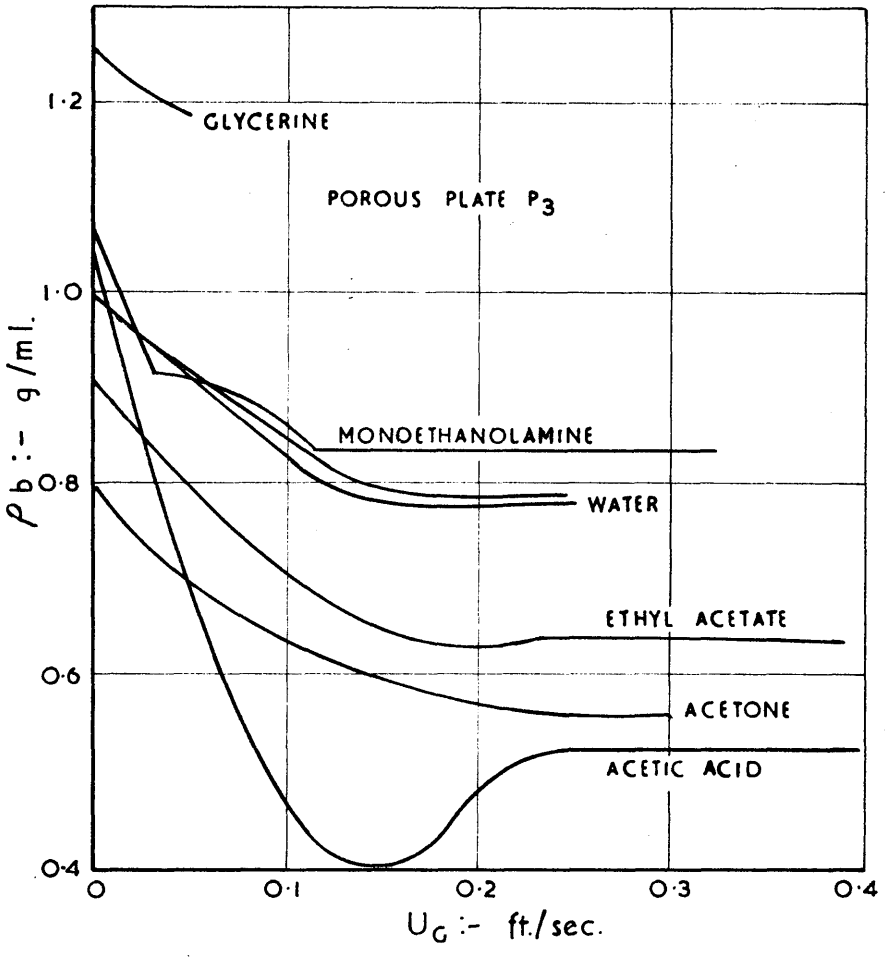

Fig. 24. BED DENSITIES FOR PURE LIQUIDS.

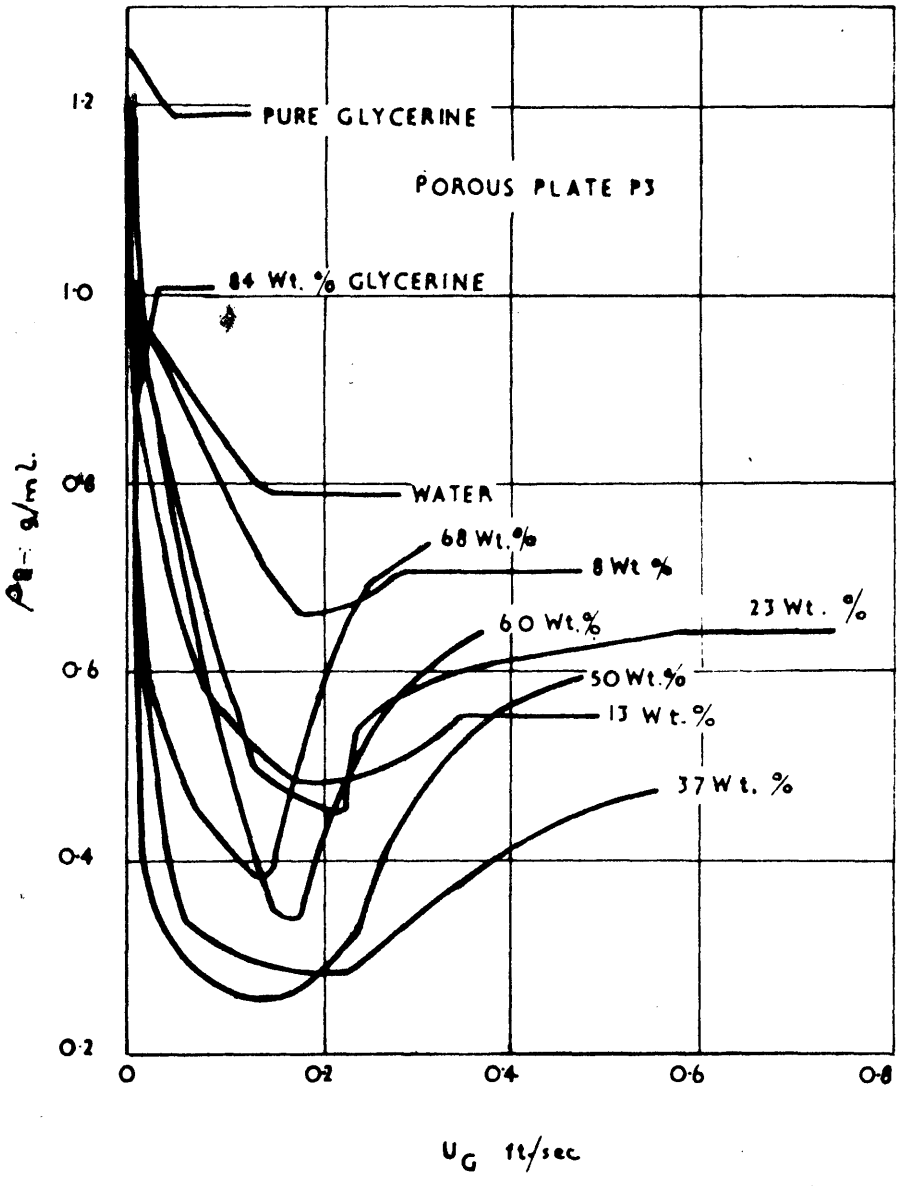

FIG. 25. BED DENSITIES OF AQUEOUS GLYCERINE SOLUTIONS.

bubble rafts on top of a fluidised bubble-bed containing mainly liquid. As the gas velocity is increased the foam raft increases in volume until at a certain gas velocity the whole bed becomes a mass of foam where the gas is the main constituent. Plate IV shows a fluidised bubble-bed consisting mainly of liquid with a foam raft on top consisting mainly of gas. This can be termed a "two-phase" bubble-bed.

Fig. 26 compares the behaviour of acetic acid solutions with that of pure water and pure acetic acid. It is evident that the behaviour of acetic acid solutions is quite out of proportion to the amount of acetic acid present. The behaviour of acetic acid solutions in concentrations as low as 0.04 to 0.42 wt.% is comparable with behaviour of glycerine solutions containing 13 to 68 wt.% glycerine. Further increases in acetic acid concentration from 0.42 to 3.6 wt.% have no noticeable effect upon the bed density. With acetic acid solutions a "two-phase" region was observed at low gas velocities between the fluidised region and the region of complete foam.

Fig. 27 shows the effect of gas velocity on the bed density for sea water compared with fresh water for two porous plates. It is evident that sea water in its behaviour is more akin to that of glycerine-water and acetic acid-water foams than it is to the fluidised beds produced by pure liquids. The sea water curves exhibit a pronounced minimum and bed densities as low as 0.35 g./ml. are observed. The sea water used had a chlorinity of 16 and was obtained from the Firth of Clyde near the entrance to Loch Long. The sea water had a surface tension of 58.7 dynes/cm. at 20°C indicating the presence of surface active agents probably due to the decay of living animal and plant organisms. Fig. 27 also shows that variations in bed densities with gas velocity can be used to detect differences in porosity. The porous glass plates P2 and P3 have average pore

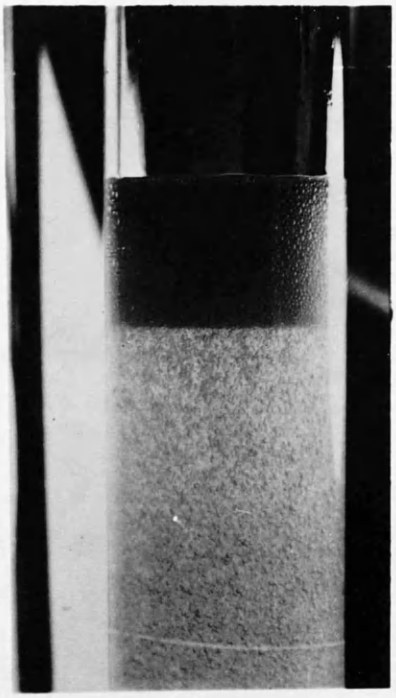

PLATE IV

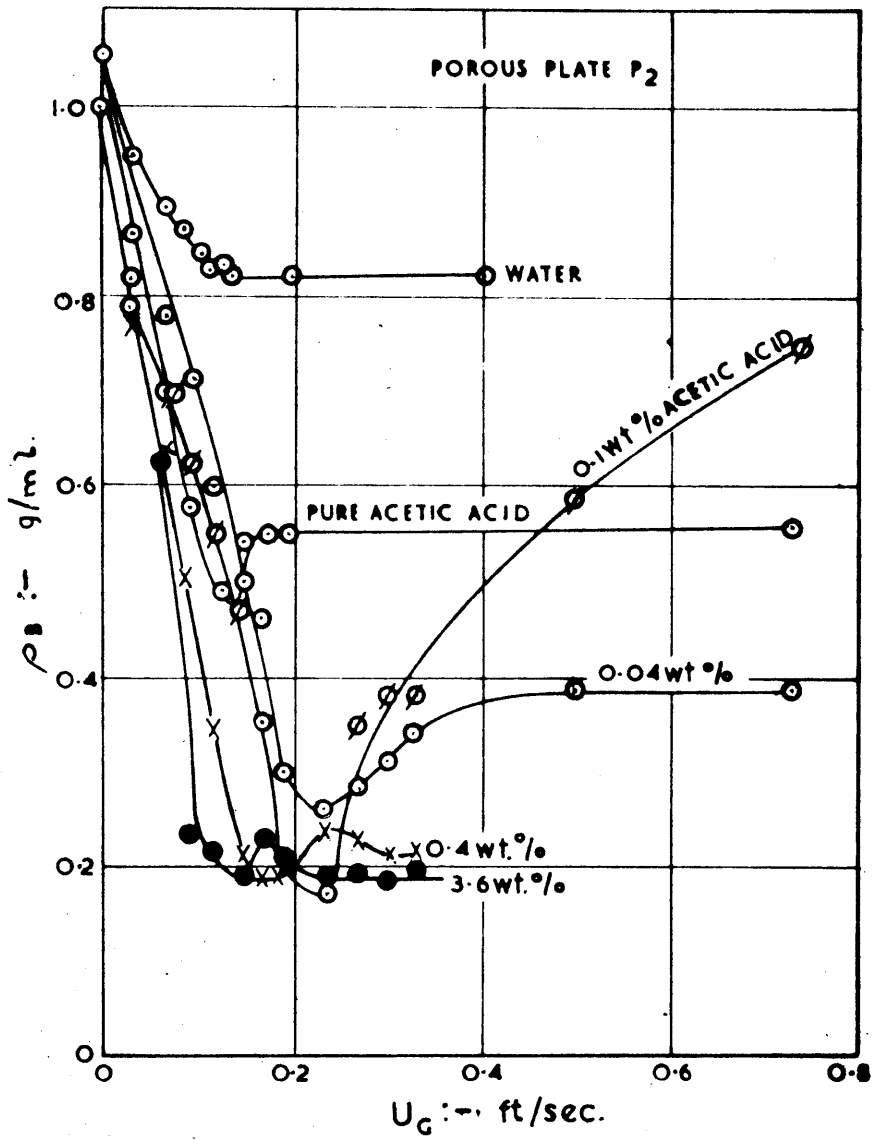

Fig.26. BED DENSITIES OF AQUEOUS ACETIC ACID SOLUTIONS.

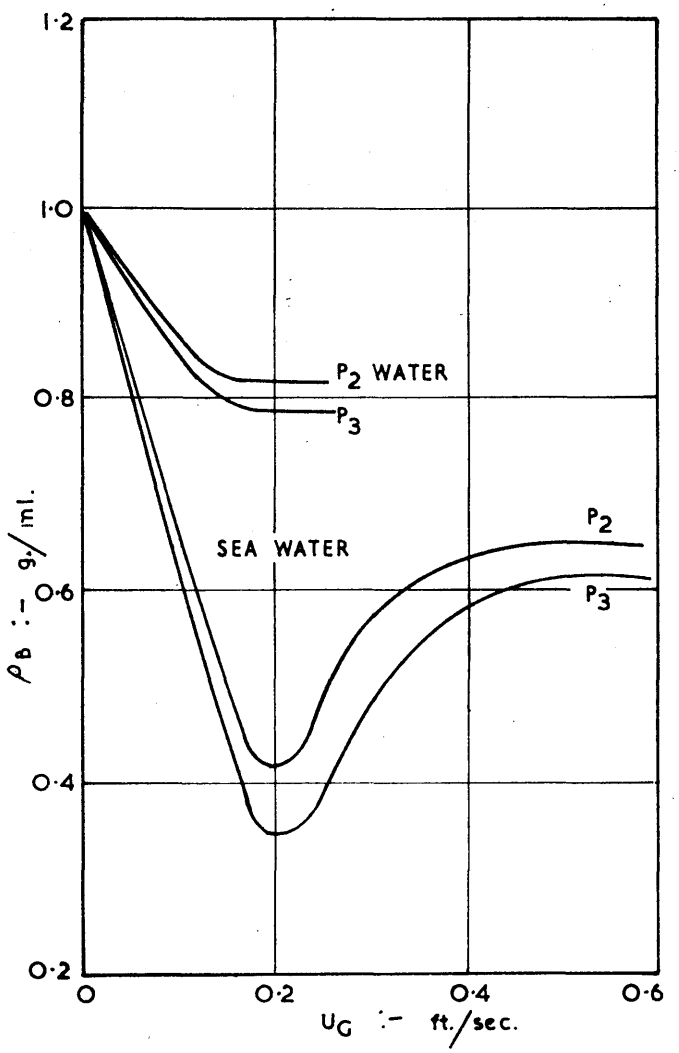

Fig.27. BED DENSITIES OF FRESH SEA WATER.

diameters which differ by about 15% and this difference shows up as a 5% difference in bed density for sea water. A similar difference is observed for different liquids over a wide range of porous plates. In general the more porous plates produce the higher bed densities, but this is not necessarily so since the bed density is a function of both size and the number of bubbles per unit volume of bed.

It is evident that for pure liquids there is a region of rising hold-up where the bed density decreases with increases in gas velocity and a constant hold-up region where the bed holds the maximum amount of gas and further increases in gas flow produce large bubbles or plugs of gas which cause the bed level to rise and fall about some mean value. For solutions, gas bubbles form stable bubble rafts at the surface instead of bursting so that the fluidised bed passes through a "two-phase" region to form a complete mass of foam when further increases in gas velocity cause plugs of gas to form in the foam.

4.5. PLUG FORMATION

The best conditions for plug formation are those in which the rate of bubble formation is very high and the velocity of bubble rise is low. In this respect pure glycerine was found to be the ideal liquid. Plates V(a) to (h) illustrate the mechanism of plug formation in glycerine. At low gas velocities only a few holes in the centre of the porous plate are used and as the flow rate increases a greater proportion of the plate area is used. At higher gas velocities small bubbles collect in groups of approximately the same shape as the large bubble which finally results. These groups coalesce to produce a large bubble or plug which as it rises collects in its wake other smaller bubbles which may or may not be combined with the larger one before the plug reaches the surface of the liquid. Helsby and Tuson[34] have observed a similar phenomenon in the formation of bubbles

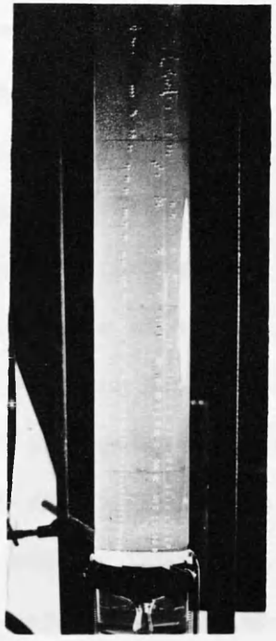

a

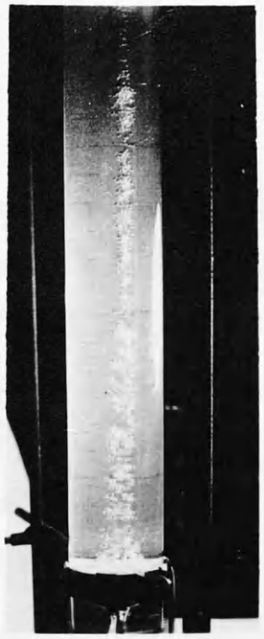

b

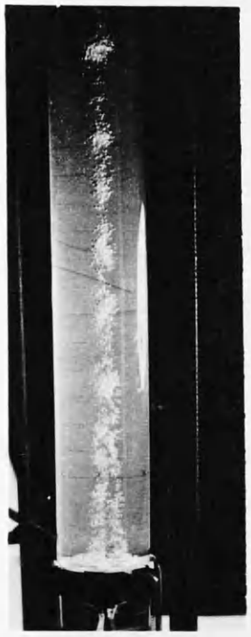

c

d

e

f

g

h

PLATE V

at jets under glycerine solutions. They have shown that during bubble formation at single jets two or more bubbles may coalesce to produce a single bubble within a short distance of the jet at high gas rates. It is evident that coalescence takes place on a large scale in a bubble-bed during plug formation.

4.6. BUBBLE RESULTS

4.6.1. Bubble shapes

By photographing bubble-beds in various stages of development and examining the enlarged photographs it was possible to show the variation in bubble shape with bubble size. In general the shape of most of the bubbles in the fluidised and foam beds observed was that of an oblate spheroid. Fig. 28 is a plot on log-log paper of the major axis b of the oblate spheroid against the minor axis a for bubbles of nitrogen in six different liquids. Each point is an average taken from at least 30 bubbles and the accuracy of measuring the major and minor axes is about ± 5%. For liquids whose viscosities lie in the range 0.5 to 1.3 centipoise, all the bubbles lie on the same straight line indicating that bubble shape is insensitive to viscosity in this range. However, a similar plot for glycerine-water solutions of viscosity 11.6 centipoise also on Fig. 28 shows that the bubbles tend to become spherical as the liquid viscosity increases.

For liquids of viscosities in the range 0.5 to 1.3 cp. the relation between a and b can be simplified to:

$$b = 1.2a \qquad -- \qquad -- \qquad -- \qquad (53)$$

For correlation purposes the equivalent spherical diameter, D_e, has some advantages over either a or b and is the variable most often used in the literature. The diameter of a sphere whose volume is equal to that of an oblate spheroid is given by:

$$D_e = (ab^2)^{1/3} \qquad -- \qquad -- \qquad -- \qquad (54)$$

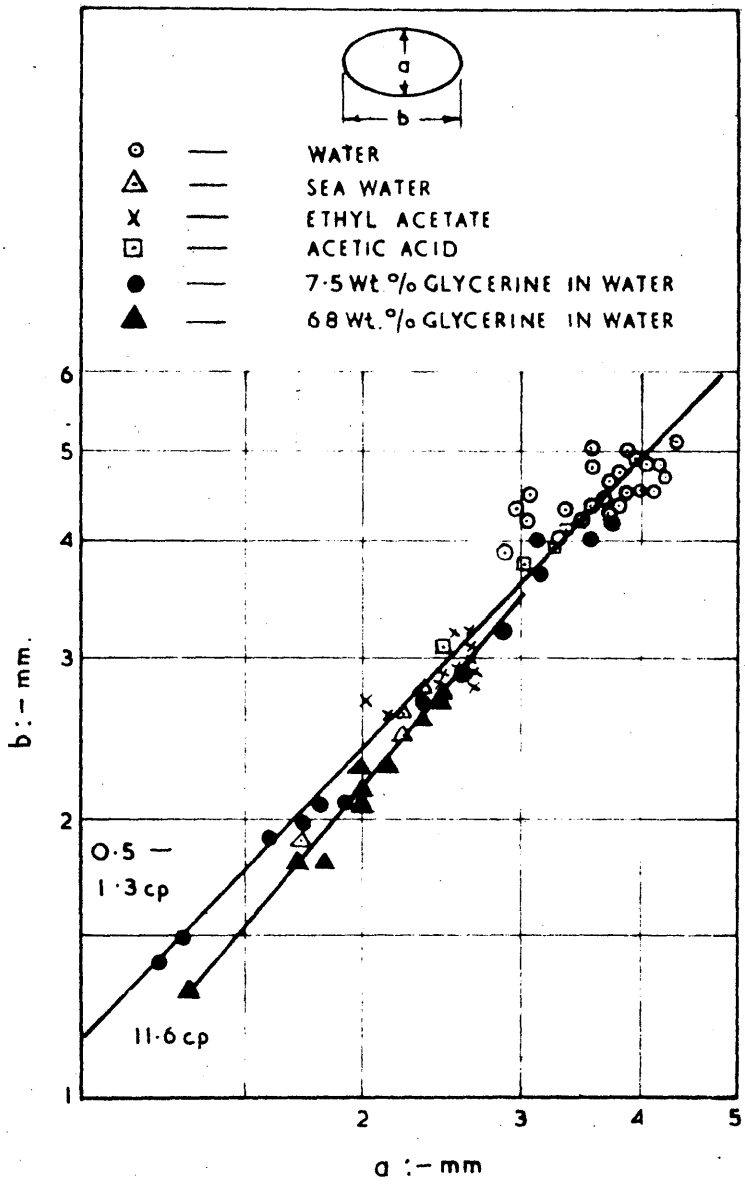

Fig.28. SHAPE OF BUBBLES.

Substituting equation (53) into equation (54) we get:

$$D_e = 1.13a \qquad (55)$$

4.6.2. Bubble size distribution

An examination of enlarged photographs of both fluidised and foam beds shows that the bubble sizes are not uniform. By measuring a large number of bubbles it was possible to ascertain the number of bubbles of each size present in a typical bed. The results are illustrated in Fig. 29 for a fluidised bed of nitrogen bubbles in pure water using disc D5 of porous bronze. It is evident that the bubble sizes follow a typical probability distribution about the most probable size which was found to vary with the porosity of the gas distributor, gas velocity and the properties of the liquid phase. The presence of a probability function was confirmed by plotting the bubble diameter against the cumulative percentage of bubbles with a size lower than this value on log-probability paper. The result was a straight line.

The bubbles smaller than the most probable size observed may have been formed at very small pores or they may have been broken off from other bubbles by the action of the container wall or by collision with other bubbles. The sizes larger than the most probable bubble size could either be produced by larger pores or by coalescence. The probability of coalescence in the body of the liquid seems to be a less likely phenomenon than coalescence close to the bubbler plate since most bubbles seem to coalesce by being sucked upwards into the slip stream of the bubble ahead. The coalescence of bubbles moving in opposite directions appears unlikely since the moving films of liquid around the front and sides would tend to repel other bubbles.

4.6.3. Effect of liquid properties on average bubble diameter

Fig. 30 illustrates the effect of superficial gas velocity upon the

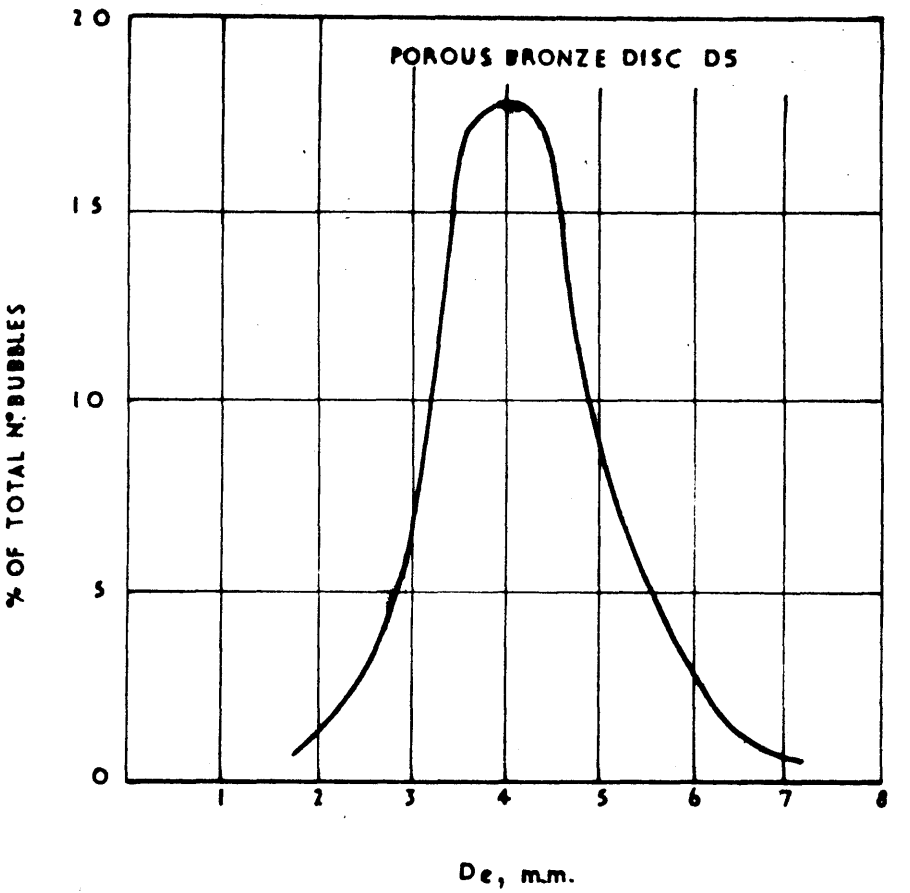

FIG. 29. DISTRIBUTION OF BUBBLE SIZES

average bubble diameter for various pure liquids and for porous plate P2. Each bubble diameter is an average of the diameters of at least thirty bubbles in the bed.

The effect of increasing the gas velocity is to increase the average bubble size but the effect for the pure liquids is very much less than that for the glycerine-water solutions and sea water. For instant in ethyl acetate the equivalent spherical diameter only changes from 2.42 to 2.95 mm. as the velocity increases from 0.0368 to 0.16 ft./sec.; while the bubble diameter in 68 wt.% glycerine in water solution changes from 1.3 to 2.5 mm. in the same range; a much larger effect.

The largest bubbles produced by plate P5 are produced under water and the smallest are produced under 68 wt.% glycerine in water solution, although the surface tension of water is 72 dynes/cm. and that of 68 wt.% glycerine 68 dynes/cm., a difference of only 4 dynes/cm. That surface tension appears to have some effect upon average bubble diameter is illustrated by comparing ethyl acetate, acetic acid and water. Ethyl acetate has a surface tension of 24.6 dynes/cm., acetic acid has a value of 27.8 dynes/cm., water a value of 72 dynes/cm. and the bubble sizes are observed to increase as the surface tension increases, but not proportionally. Table 17 shows that the average pore size for acetic acid and ethyl acetate using plate P2 are about half the average pore size for water so that the smaller average bubble sizes at the lower surface tensions are probably due to the utilization of smaller pores.

Fig. 30 shows that superficial gas velocity has a much more profound effect upon bubbles in foams of 7 wt.% and 68 wt.% glycerine in water than it does for the pure liquids. The reason for the variation in bubble sizes with gas velocity for foams may be that the porous plate produces larger bubbles as the amount of liquid available becomes less or there is a greater

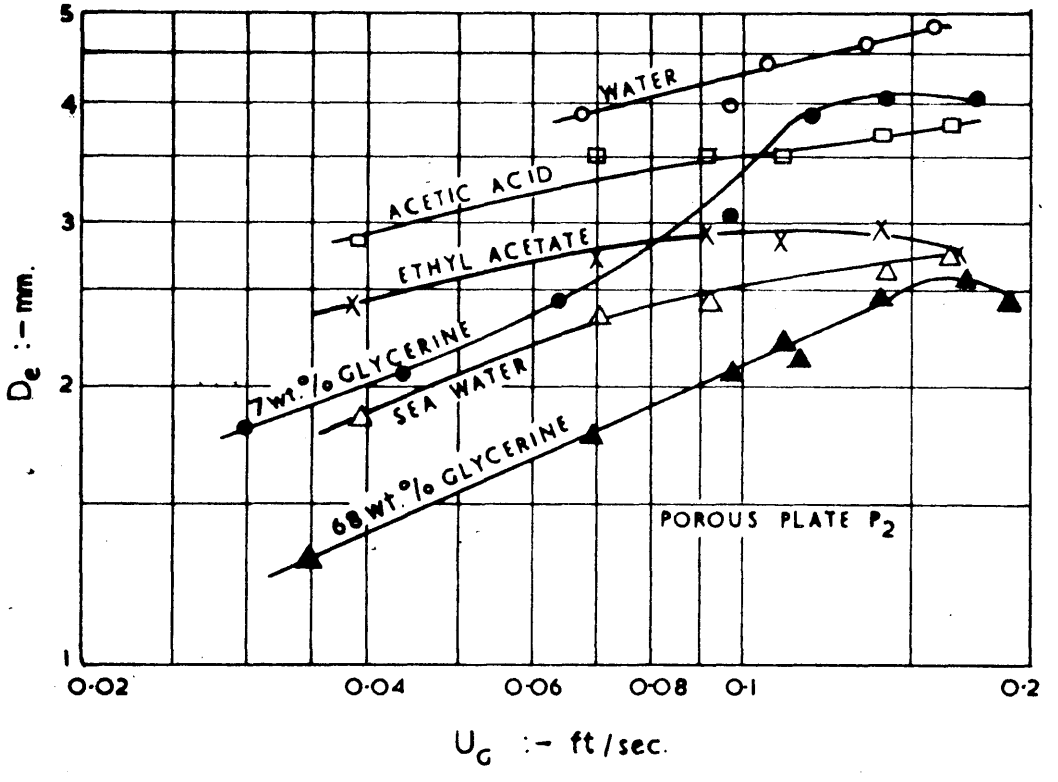

Fig.30 EFFECT OF LIQUID PROPERTIES ON BUBBLE DIAMETER.

rate of coalescence in foams. Observations on single bubbles in a foam shows that foam bubbles once formed are very stable and resistant to coalescence. Hence the most probable explanation for the variation of bubble diameter with gas velocity is that as the ratio of gas to liquid increases in the foam, the film of liquid over the porous plate becomes thinner and a larger bubble is then formed from gas issuing from several adjacent pores.

Fig. 30 also shows that the bubble size in sea water beds increases with gas velocity. This would indicate that a sea water bubble-bed behaves more like a foam than as a fluidised bed, a fact which is confirmed by the much lower bed densities observed with sea water compared with fresh water.

4.6.4. Effect of plate porosity on average bubble diameter

Fig. 31 illustrates the effect of plate porosity on the average bubble size. For the pure liquids, water and ethyl acetate there is no detectable effect within the limits of experimental error for plates P2 and P3. For foams of 7 wt.% and 68 wt.% glycerine in water solutions the bubble sizes produced by plates P2 and P3 differ considerably in the same solution. However, as the superficial gas velocity is increased the average bubble sizes produced by the two plates tend to approach the same value for each solution.

The conclusion reached is that foams are more sensitive to changes in plate porosity than are fluidised bubble beds. Sensitivity to the number and porosity of the holes in the distributor plate may become a serious drawback in the use of foam scrubbers where the pores may become blocked by deposits from solution. The insensitivity of fluidised bubble-beds to the number and porosity of the holes in the distributor plate has been already noted in the absorption column, where the absorption rate is not considerably affected by the size and porosity of the bubbler. (Section 3.7.7.)

4.6.5. Effect of liquid properties on bubble density

The bubble density is defined as the number of bubbles per ml. of

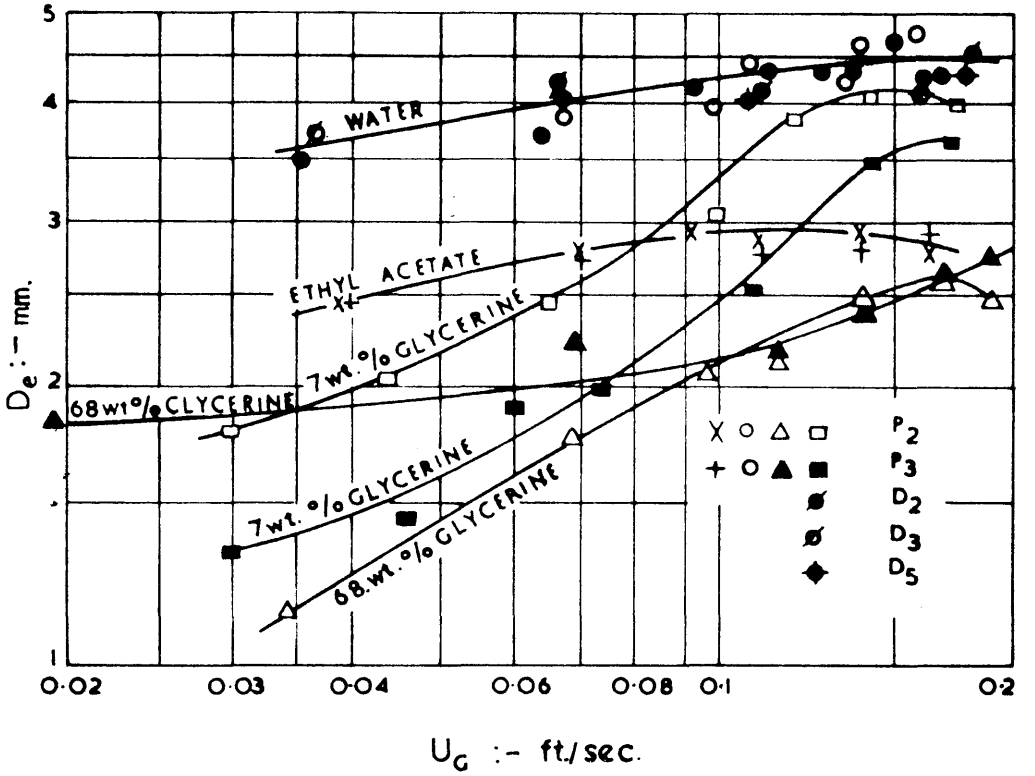

Fig.31. EFFECT OF POROSITY ON BUBBLE DIAMETER.

bubble bed. The number of bubbles per ml. can be calculated from the bed density and the average bubble volume. Plots of bubble density against superficial gas velocity are given in Figs. 32 and 33.

Fig. 32 illustrates the effect of liquid properties on bubble density. The foaming glycerine solutions (7 and 68 wt.%) show a decrease in bubble density with an increase in gas velocity. The 68 wt.% glycerine in water solution shows a very high bubble density of between 50 and 300 bubbles per ml. The decrease in bubble density with increase in gas velocity in foaming media is probably caused by the initial formation of much larger bubbles at the porous plate as the ratio of gas to liquid becomes higher.

For the pure liquids Figs. 32 and 33 show that the effect of increasing the gas velocity is to increase the bubble density at low gas velocities to give a constant bubble density at gas velocities of greater than about 0.1 ft./sec. In the isolated case of porous plate P2 the gas velocity has very little effect upon bubble density. It will be noted that the number of bubbles per ml. of bed for water is of the order 1 to 7 for all the gas distributors, very much lower than the bubble density of foam beds. This is the phenomenon that explains the effect of gas rate on the absorption efficiency. The increase in the bubble density increases the surface area for absorption and thus the absorption rate increases. The point at which the absorption rate becomes independent of the gas velocity corresponds to the point where the bubble bed holds as much gas as it can, i.e., where the curve of bubble density against gas velocity flattens out. See curve for porous disc D5 in Fig. 33, this being the gas distributor used in the experiments on the absorber.

4.6.6. Effect of plate porosity on bubble density

Fig 33 shows that for pure liquids the plate porosity has very little effect upon the number of bubbles per ml. of bed. The porous bronze discs

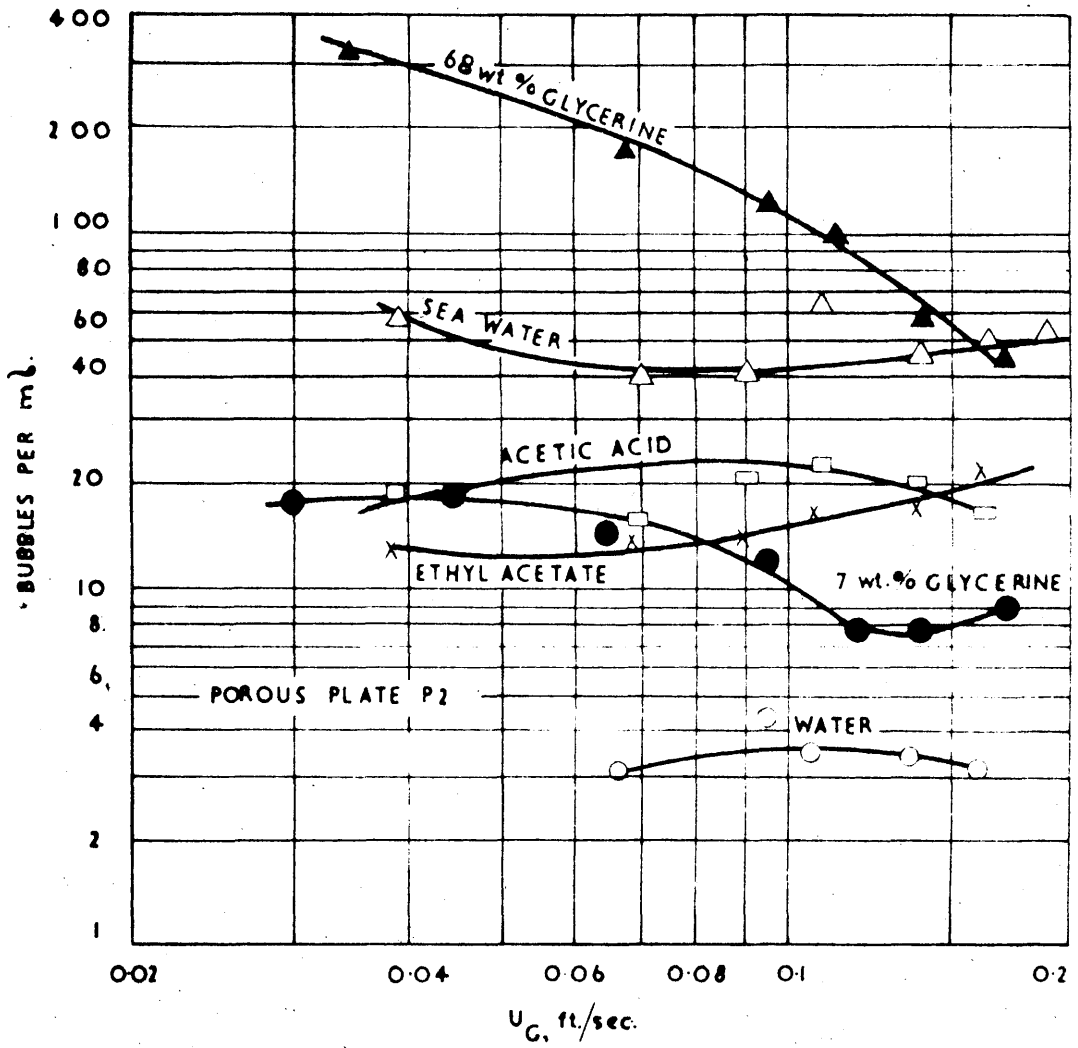

Fig. 32 EFFECT OF LIQUID PROPERTIES ON BUBBLE DENSITY.

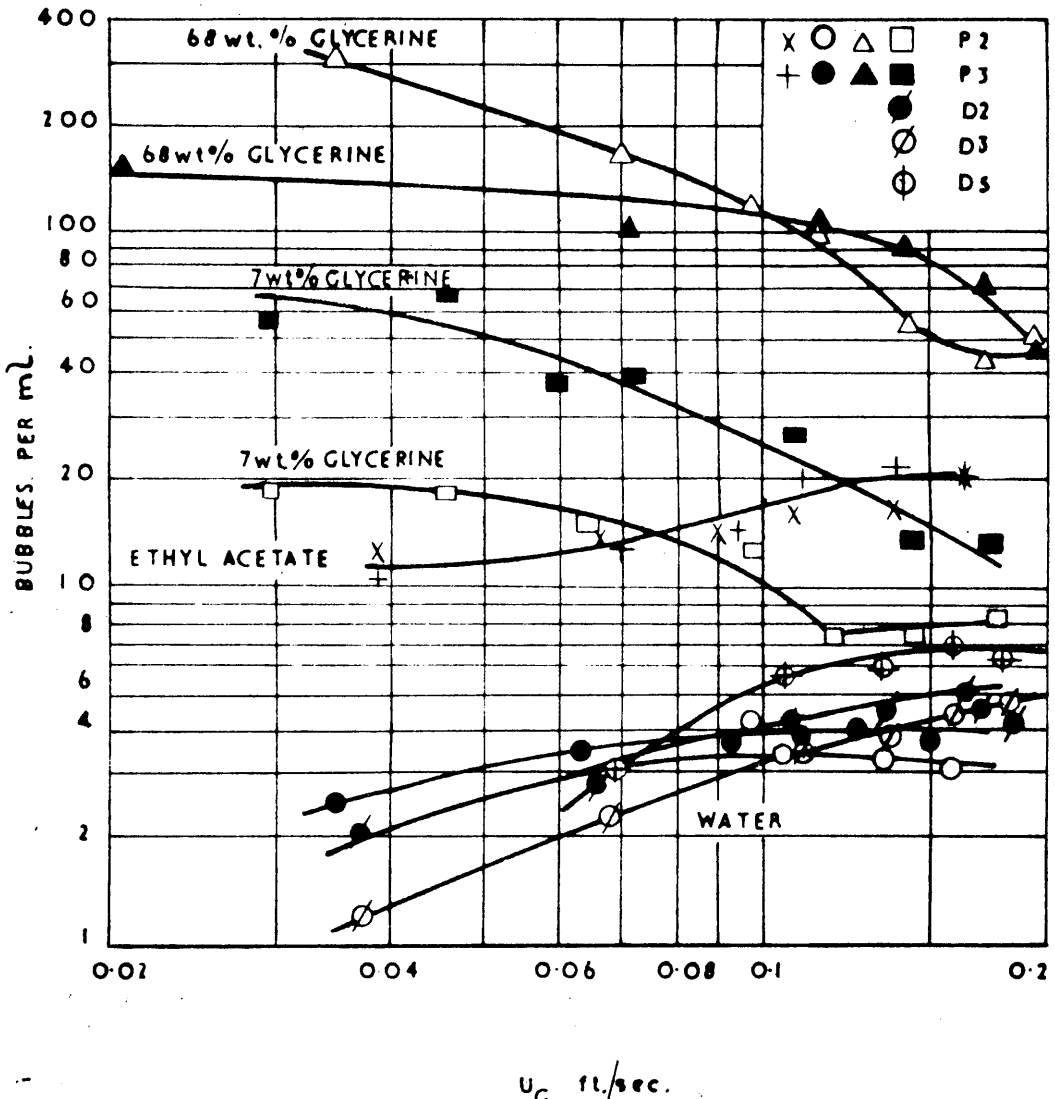

FIG.33. EFFECT OF POROSITY ON BUBBLE DENSITY.

and glass plates give low bubble densities (1 to 7 bubbles per ml.) and show a slight variation of bubble density with porosity. This confirms the relative insensitivity of absorption rate to porosity of the gas distributor (section 3.7.7.)

For the solutions of glycerine in water which form foams even the 15% difference in porosity of plates P2 and P3 can have an appreciable effect on the bubble density.

4.7 VELOCITY OF RISE IN BUBBLE-BEDS

The average velocity of rise of bubbles in a bubble-bed can be computed from the equation:

$$u_B = u_G \left[\frac{\rho_L}{\rho_L - \rho_B} \right] \quad -- \quad -- \quad -- \quad (56)$$

The average velocity of bubble rise is plotted against equivalent spherical bubble diameter in Fig. 34 so that the velocities of rise in bubble beds may be compared with the velocity of rise for single free rising bubbles. However, it must be remembered that the motion of bubbles in a fluidised or foam bed is hindered by the close proximity of other bubbles so that the velocity of rise in a bubble-bed is not constant at a particular bubble size but varies with the density of the bubbles in the bed.

The broken lines in Fig. 34 represents the velocities of rise of single free rising bubbles in an infinite liquid as a function of bubble diameter. The velocities of rise in acetic acid and ethyl acetate were obtained from the data of Peebles and Garber[40]. The velocities of rise of single bubbles in pure water and sea water have been determined by Thomson, Houghton and Ritchie[41] by timing the rise of bubbles produced singly at a jet. It was found that bubbles rising in sea water could exhibit a spiral motion or they could rise without spiral motion even though their diameters were identical. Spiral motion was usually observed when the jet producing the single bubbles was vibrated at the time of bubble break-off. Spiral and

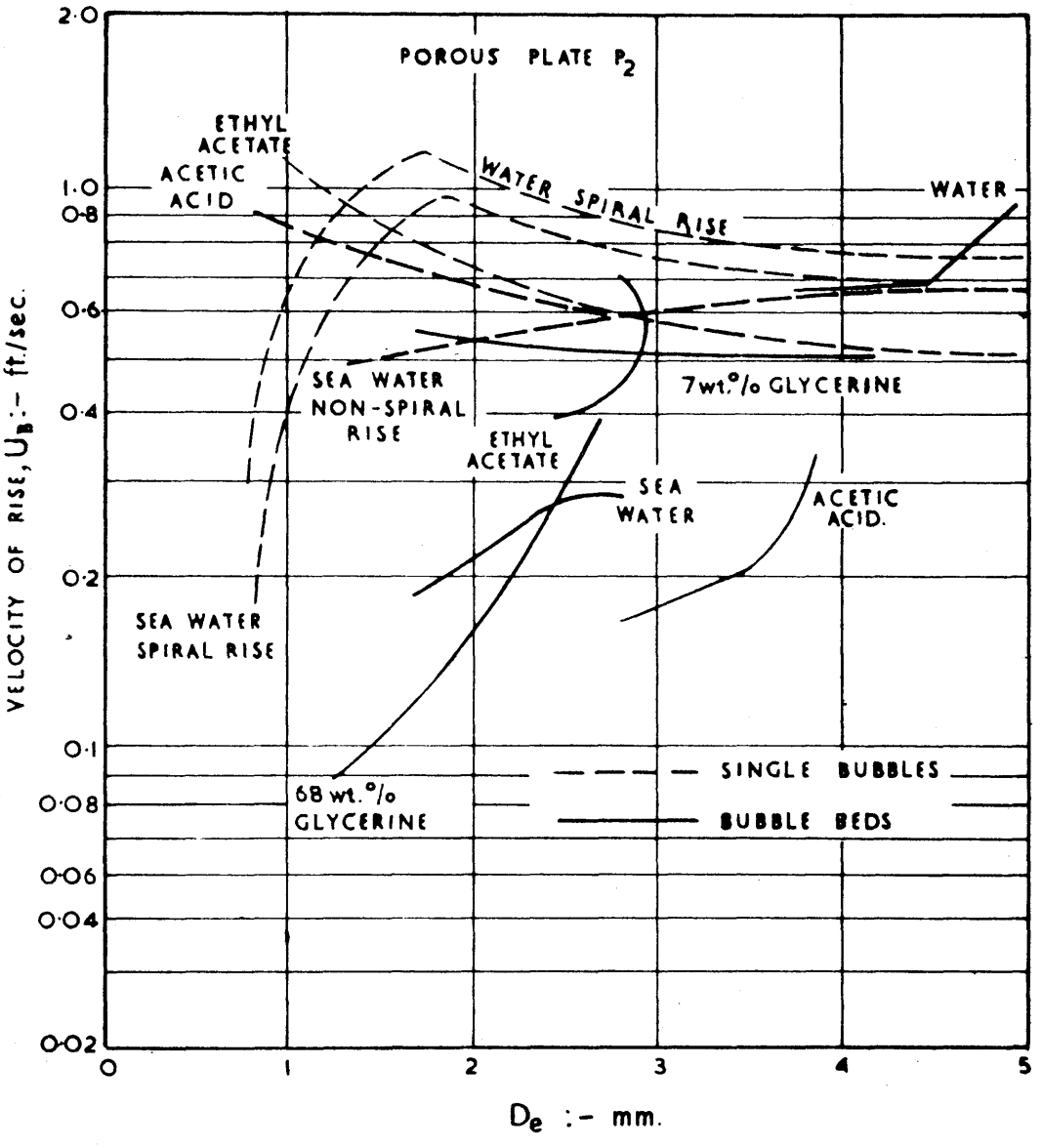

Fig. 34. VELOCITIES OF RISE

non-spiral motions were only observed for bubbles whose diameters were in the range 1 to 4 mm. A similar effect has been observed by Stuke[42] for oxygen bubbles rising in caproic acid solutions. Apparently the effect of dissolved impurities of certain types is to suppress the spiral type of rise.

The curves for spiral and non-spiral rise are plotted on Fig. 34. In sea water the velocity of spiral rise is somewhat less than that in pure water by an amount which cannot be accounted for by the small difference in density and viscosity. Measurements of surface tension showed that of sea water to be 58.7 dynes/cm. compared with 72 dynes/cm. for pure water so that the difference in velocities of rise is undoubtedly connected with the presence of surface active agents.

Comparison of velocities of rise in fluidised and foam beds shows that in general they are lower than the corresponding velocities of rise for single bubbles. This is to be expected due to the hindering effect of the other bubbles in the bed. Sea water has velocities of rise in bubble-beds which are less than half those of single bubbles, which bears out the supposition that sea water bubble-beds are more closely allied to foams than to fluidised beds.

An interesting fact that can be observed in Fig. 34 is that sometimes the velocity of rise in a bubble bed can be greater than the velocity of rise of a single free-rising bubble. This would not be expected on the theory of hindered rise. For instance, the velocities of rise of bubbles in ethyl acetate and water beds are greater than the velocities of rise for single bubbles as is seen from Fig. 34. In other experiments an average bubble velocity of 1.7 ft./sec. was observed in water and 2.7 ft./sec. in ethyl acetate under conditions where the bubble density was very high. Velocities of rise in bubble beds greater than the velocities of rise of

single bubbles of the same diameter can be explained by the formation of plugs of gas in the liquid such that u_g in equation (56) becomes large while the bed density ρ_B remains approximately the same. This is confirmed by the observation that high bubble velocities in beds are always observed in the region of "bumping" where plugs of gas cause the bed level to rise and fall about an average value.

4.8. DISCUSSION.

The bed density at any superficial gas velocity is a function of the number of bubbles per ml. and the average volume of the bubbles. In these respects fluidised and foam beds have been found to behave differently. In fluidised beds the bed density decreases and the gas hold-up increases, because the number of bubbles per ml. increases while the average bubble size remains approximately constant and independent of gas velocity. At higher gas velocities both the number of bubbles per ml. and the bubble diameter tend to become constant. It may therefore be concluded that in the "rising hold-up" region the increase in absorption rate with gas velocity is caused by an increase in surface area for absorption; and in the "constant hold-up" region the surface area becomes constant as does the absorption rate.

In general, foams show a wider change of bed density with gas velocity than do fluidised beds. Foams usually contain a much larger number of bubbles per ml. than do fluidised beds and the bubbles are smaller. The effect of increasing the gas flow rate with foams is to decrease the number of bubbles per ml. and to increase the average bubble size, a behaviour quite different from that of fluidised bubble beds.

Foams are sensitive to the porosity of the gas distributor used for introduction of the gas into the liquid, while fluidised beds are relatively insensitive to the number, size and distribution of the pores.

It is interesting to discuss the stages in the formation of a foam from a fluidised bed. At low gas velocities the bubbles rise more or less independently through the liquid and the bed may be termed "dilute". At higher gas velocities the bed expands further and the bubbles can no longer rise independently but are hindered by the motion of other bubbles. The bed soon becomes a turbulent mass of rising and recirculating bubbles where the term "fluidised" may be correctly applied. Further increases in gas velocity cause plug formation with consequent bumping.

The conversion of a fluidised bed to a foam bed is closely linked with the behaviour of the bubbles when they reach the surface. For pure liquids the bubbles are seen to burst immediately while in the initial stages of foam formation the bubbles collect on the surface in the form of rafts which appear to be quite stable. The rate at which the bubbles burst is very much lower for foams than for fluidised beds. If the rate of bursting is slower than the rate at which the bubbles reach the surface then the foam raft will expand until the rate of bubble formation equals the bursting rate at the surface of the foam. The volume of foam increases as the gas flow increases until the "two-phase" region becomes entirely foam. When the amount of liquid available at the porous plate surface becomes low then plugs of gas are formed in the foam.

Obviously the essential difference between fluidised and foam is bound up with the stability of the bubbles at the liquid surface. It would appear that bubbles are more stable at a liquid surface when they are formed in solutions rather than in pure substances. A very important property when dealing with foam formation is obviously the "elasticity" of the film of liquid around the bubble. In solutions it would appear that the bubble films are more elastic and more resistant to bursting than bubbles formed in pure liquids.

APPENDIX I

POWER REQUIREMENTS FOR A BUBBLE-TYPE ABSORBER UNDER PRESSURE

5.1. INTRODUCTION

The effect of running a bubble-type absorber under pressure as compared with atmospheric pressure is to reduce the diameter of the absorber. A reduction in size will reduce the space occupied by the absorber, if this is important, and may reduce the initial cost of materials and construction. Against this must be balanced the cost of power for compression and pumping to the higher pressure.

5.2. POWER CALCULATIONS

The total power required to operate a pressure scrubber will be the sum of the power required to compress the inlet gas and the power required to pump the water into the column.

a) Gas compression power

The compression power is given by the following equation assuming all compression stages are adiabatic with no clearance and using the overall compressor efficiency E_c:

$$\text{Compression power} = \frac{sGRT}{E_c}\left[\left(\frac{P}{P_G}\right)^{\frac{\gamma-1}{s}} - 1\right] \quad \text{---} \quad (57)$$

If it is possible to recover power by the decompression of the outlet gas from the absorber then the only power required is that for the compression of the gas which is absorbed.

$$\text{Compression power} = \frac{sGy_2zRT}{E_c}\left[\left(\frac{P}{P_G}\right)^{\frac{\gamma-1}{s}} - 1\right] \quad \text{---} \quad (58)$$

where z is the fraction of gas absorbed and y_2 is the mole fraction of the soluble component of the inlet gas stream

b) Water power

The water power can be computed by assuming Henry's law and an overall

absorption efficiency, E_A, based on the inlet gas.

$$\text{ft.}^3 \text{ } CO_2 \text{ at N.T.P./ft.}^3 \text{ water at saturation} = S_t P_{CO_2} \quad -- \quad (59)$$

$$= S_t y_2 P \quad -- \quad (60)$$

$$\text{ft.}^3 \text{ water / lb.mole } CO_2 \text{ absorbed at saturation} = \frac{RT_o}{S_t y_2 P} \quad -- \quad (61)$$

If a fraction z of the incoming soluble gas is absorbed, then

$$\text{lb.mole/sec. } CO_2 \text{ absorbed} = y_2 zG \quad -- \quad -- \quad (62)$$

The amount of water required can be obtained by combining equations (61) and (62).

$$\text{ft./sec. of water} = \frac{RT_o zG}{S_t P} \quad -- \quad -- \quad (63)$$

It is assumed in the derivation of equation (65) that the water leaving the absorber is saturated at the partial pressure of the incoming soluble gas. However, the water will only reach a fraction, E_A, of its saturation value

$$\text{ft./sec. of water} = \frac{RT_o zG}{S_t P E_A} \quad -- \quad -- \quad (64)$$

If the water is available at a pressure P_w, then;

$$\text{water power} = \frac{RT_o zG}{S_t P E_A}(P - P_w) \quad -- \quad -- \quad (65)$$

Taking the overall efficiency of the water pump to be E_p, then;

$$\text{water power} = \frac{RT_o zG}{S_t P E_A E_P}(P - P_w) \quad -- \quad -- \quad (66)$$

c) Total power

The total power requirement is the sum of the water power and the gas compression power.

$$\text{Total power} = \frac{sGy_2 zRT}{E_c}\left[\left(\frac{P}{P_G}\right)^{\frac{\chi - 1}{s}} - 1\right] + \frac{RT_o zG}{S_t P E_A E_P}\left[1 - \frac{P_w}{P}\right] \quad -- \quad (67)$$

5.3. THE FRACTION OF SOLUBLE GAS ABSORBED, z.

For design purposes it is necessary to be able to calculate the amount of soluble gas absorbed quickly and easily. This can readily be achieved

from equation (64) thus;

Transposing equation (64) and letting L be the liquid rate we get

$$z = \frac{LPE_A S_t}{RT_o G} \quad -- \quad -- \quad -- \quad -- \quad (68)$$

now if the ideal gas law and Henry's law are obeyed

$$z = \frac{LTE_A S_t}{T_o GV} \quad -- \quad -- \quad -- \quad -- \quad (69)$$

where $\frac{P}{R} = \frac{T}{V}$ for 1 lb.mole. and GV is the gas rate in ft.^{3}/sec., then;

$$z = E_A \frac{u_L}{u_G} \left(\frac{S_t T}{T_o}\right) \quad -- \quad -- \quad -- \quad -- \quad (70)$$

If the ideal gas law and Henry's law are not obeyed, then the absorption coefficient must be obtained for each partial pressure of soluble gas and a correction made for the compressibility of the gas. The fraction of gas absorbed then becomes

$$z = E_A \frac{u_L}{u_G} \left(\frac{S_{tp} CT}{pT_o}\right) \quad -- \quad -- \quad -- \quad (71)$$

5.4. THE FRACTION OF CARBON DIOXIDE ABSORBED

This thesis has been concerned with the absorption of carbon dioxide from a bubble-type absorber. Section 3.7.5. gives a general correlation equation for the behaviour of the absorption efficiency, E_A, under various operating conditions. If this value for E_A is now substituted in equations (70) and (71), one obtains the fraction of carbon dioxide that this particular absorber will absorb under certain conditions.

For the rising hold-up region and where the gas obeys the ideal law and the solution obeys Henry's law

$$z = 0.86 \left(\frac{S_t T}{T_o}\right) \frac{u_L^{0.52}}{u_G^{0.39}} \left(\frac{h}{p}\right)^{0.33} t^{0.1} \quad -- \quad -- \quad (72)$$

If Henry's law and the ideal gas law are not obeyed then equation (72) must be corrected for the variation of compressibility and solubility with pressure.

$$z = 0.86 \frac{(S_{tp}{}^{CT})}{(pT_o)} \frac{u_L{}^{0.52}}{u_G{}^{0.39}} \frac{(h)}{(p)}^{0.33} t^{0.1} \quad -- \quad -- \quad (73)$$

For the constant hold-up region and an absorber pressure such that the gas obeys the ideal gas law and the solution obeys Henry's law, the following equation can be used to compute the fraction of carbon dioxide absorbed.

$$z = 0.52 \frac{(S_t{}^T)}{(T_o)} \frac{u_L{}^{0.85}}{u_G} \frac{h^{0.22}}{p^{0.33}} t^{0.1} \quad -- \quad -- \quad (74)$$

Equation (74) can be corrected for deviations from the ideal gas law and Henry's law as follows;

$$z = 0.52 \frac{(S_{tp}{}^{CT})}{(pT_o)} \frac{u_L{}^{0.85}}{u_G} \frac{h^{0.22}}{p^{0.33}} t^{0.1} \quad -- \quad -- \quad (75)$$

The compressibilities and solubilities of carbon dioxide can be obtained at various partial pressures and temperatures from Part 2 of this thesis.

Inspection of the above equations shows that the conditions for absorbing almost all of the incoming carbon dioxide are high bed level, low pressures, high absorption coefficient (low temperature) and high liquid to gas velocity ratios for this particular absorber.

5.5. NOMENCLATURE

C	=	compressibility coefficient	
E_A	=	absorption efficiency, fraction of saturation based on inlet gas	
E_C	=	overall compressor efficiency	
E_P	=	overall liquid pump efficiency	
G	=	mass flow rate of gas	lb.mole/sec.
h	=	height of absorption bed	ft.
L	=	volumetric liquid flow rate	$ft.^3$/sec.
p	=	partial pressure of soluble gas	atm.
P	=	total pressure of absorption process	atm.
P_G	=	inlet pressure of gas	atm.
P_W	=	inlet pressure of water	atm.
R	=	universal gas constant	
s	=	number of compression stages	
S_t	=	Bunsen absorption coefficient	vol./vol.
t	=	temperature	$^oC.$
T	=	Temperature	$^oK.$
u_G	=	gas velocity	ft./sec.
u_L	=	liquid velocity	ft./sec.
V	=	molecular volume of gas	$ft.^3$/lb.mole.
y2	=	mole fraction of soluble component in gas stream.	
z	=	fraction of gas absorbed	
χ	=	ratio of specific heats.	

APPENDIX II.

Summary of pressure bubble column data used in part 3 of this thesis.

Effects of liquid and gas velocities. (Figs. 14,15,20 & 21)

Absorption rates corrected to:

$h = 1.5$ ft., $t = 15^{\circ}C$, $p = 5.1$ atm. CO_2.

Run No.	u_G ft./sec. In	Out	E_A	$(H.T.U.)_{OL}$	K_La
$u_L = 0.030$ ft./sec.					
76	0.249	0.232	70.2	1.28	95
$u_L = 0.052$ ft./sec.					
18	0.043	0.035	44.5	2.25	76
62	0.065	0.039	61.0	1.49	129
19	0.086	0.058	70.3	1.20	165
20	0.110	0.082	73.4	1.08	179
21	0.148	0.117	67.5	1.27	167
22	0.168	0.136	66.6	1.33	154
65	0.252	0.226	63.5	1.45	130
$u_L = 0.100$ ft./sec.					
23	0.043	0.019	32.9	3.22	114
24	0.062	0.030	43.0	2.30	154
25	0.104	0.055	63.1	1.34	267
26	0.144	0.090	65.5	1.33	269
27	0.188	0.139	62.6	1.46	252
78	0.249	0.191	63.8	1.58	230

Run No.	u_G ft./sec. In	Out	E_A	$(H.T.U.)_{OL}$	K_La
u_L = 0.144 ft./sec.					
15	0.062	0.018	35.6	2.44	237
61	0.093	0.041	43.4	2.26	232
2	0.113	0.050	49.0	1.93	257
5	0.115	0.049	50.0	2.05	248
3	0.116	0.056	44.7	2.40	212
1	0.119	0.050	48.5	1.99	257
4	0.127	0.052	53.0	1.80	286
59	0.150	0.094	49.4	2.06	254
16	0.183	0.118	53.5	1.85	283
17	0.210	0.140	53.0	1.83	271
u_L = 0.170 ft./sec.					
28	0.075	0.024	40.7	2.30	270
29	0.110	0.044	51.8	1.81	340
30	0.148	0.067	59.9	1.43	432
31	0.164	0.078	56.4	1.65	362
32	0.214	0.119	56.9	1.72	352
u_L = 0.200 ft./sec.					
33	0.082	0.024	38.3	2.65	276
34	0.116	0.029	49.6	1.72	407
35	0.143	0.054	52.1	1.74	410
36	0.181	0.075	56.2	1.57	455
37	0.270	0.111	56.0	1.67	418

Effects of bed height. (Fig. 16)

Absorption rates corrected to:

$p = 5.1$ atm. CO_2 , $t = 15^{\circ}C.$

$u_L = 0.144$ ft./sec., $u_G = 0.106$ ft./sec.

Run	h	E_A	$(H.T.U.)_{OL}$	K_La
12	0.38	28.9	1.05	468
9	0.67	35.4	1.40	372
13	1.28	39.0	2.31	230
5	1.75	50.0	2.23	229
7	2.18	51.0	2.70	190
6	2.89	53.5	3.44	149
60	4.00	61.5	3.74	140
14	5.39	78.4	2.56	198

$u_L = 0.052$ ft./sec., $u_G = 0.065$ ft./sec.

63	0.43	38.6	0.85	218
62	1.50	61.0	1.49	129
64	3.10	76.0	1.92	99

$u_L = 0.052$ ft./sec., $u_G = 0.253$ ft./sec.

66	0.55	50.3	0.78	181
65	1.50	63.5	1.45	130
67	2.75	70.5	2.13	101

Effects of partial pressure. (Fig. 17)

Absorption rates corrected to:

$h = 1.5$ ft., $t = 15^{\circ}C.$

$u_L = 0.144$ ft./sec., $u_G = 0.113$ ft./sec.

Run	p	E_A	$(H.T.U.)_{OL}$	K_La
38	2.90	62.5	1.31	391
58	5.26	50.4	2.04	263
40	8.01	47.2	2.08	254
41	10.88	39.4	2.83	191
42	13.60	34.9	3.35	164

$u_L = 0.052$ ft./sec., $u_G = 0.063$ ft./sec.

68	2.58	70.1	1.07	171
62	5.10	61.0	1.49	129
69	12.10	47.5	2.20	90

$u_L = 0.052$ ft./sec., $u_G = 0.248$ ft./sec.

74	2.86	77.4	0.97	328
65	5.10	63.5	1.45	130
75	6.64	58.7	1.67	106

Effects of temperature. (Fig. 18)

Absorption rates corrected to:

h = 1.5 ft., p = 5.1 atm. CO_2.

u_L = 0.145 ft./sec., u_G = 0.127 ft./sec.

Run	t	E_A	$(H.T.U.)_{OL}$	K_La
1	10	48.2	2.00	257
58	15.5	49.9	1.99	263
54	20	51.1	1.93	274
57	25	52.3	1.93	270
56	29.1	53.5	1.85	286

u_L = 0.052 ft./sec., u_G = 0.063 ft./sec.

70	12	59.9	1.50	128
62	19.1	62.4	1.47	133
72	29.4	64.5	1.38	141

u_L = 0.052 ft./sec., u_G = 0.249 ft./sec.

71	12	65.1	1.41	148
65	18	64.4	1.43	133
73	29.4	68.4	1.27	193
77	15.5	66.7	1.18	178

REFERENCES

1. Cryder and Maloney; Trans. Amer. Inst. chem. Engrs., 1941, 37, 827.
2. Dixon; Trans. Brit. Inst. chem. Engrs., 1954, 32, Supplement No. 1, S85.
3. Chambers and Wall; Ibid., 1954, 32, Supplement No. 1, S96.
4. Dixon and Williams; J. Soc. chem. Ind., 1950, 69, 69.
5. O'Connell; Trans. Amer. Inst. chem. Engrs., 1946, 42, 741.
6. Drickamer and Bradford; Ibid., 1943, 39, 319.
7. Sherwood and Pigford; "Absorption and Extraction" 2nd Ed. McGraw-Hill, 1952, p. 291.
8. Whitman; Chem. Met. Eng., 1923, 29, No. 4.
9. Lewis and Whitman; Industr. engng. Chem., 1924, 16, 1215.
10. Morris and Jackson; "Absorption Towers", Butterworths Scientific Publications, 1953. p. 9.
11. Chilton and Colburn; Industr. engng. Chem., 1935, 27, 255.
12. Cooper, Christl and Peery; Trans. Amer. Inst. chem. Engrs., 1941, 37, 979.
13. Bonnet; Univ. Delaware, Ph.D. Thesis, 1949.
14. Walter and Sherwood; Industr. engng. Chem., 1941, 33, 493.
15. Datta, Napier and Newitt; Trans, Brit. Inst. chem. Engrs., 1950, 28, 14.
16. Shulman and Molstad; Industr. engng. Chem., 1950, 42, 1058.
17. Howard; Trans. Brit. Inst. chem. Engrs., 1954, 32, Supplement No.1, S146.
18. Bohr and Bock; Wied. Ann. Phys. (3), 1899, 68, 503.
19. Zelvinskii; J. chem. Ind. (U.S.S.R.), 1937, 4, 1250.
20. Wiebe and Gaddy; J.Amer. chem. Soc., 1939, 61, 315., 1940, 62, 815.
21. Cawood and Patterson; Trans. Roy. Soc., 1936, A236, 77.
22. Linhart; J. phys. Chem., 1933, 37, 645; 1934, 38, 1091.
23. Michels and Michels; Proc. Roy. Soc., 1936, A 153, 201.

24. Maron and Turnbull; J. Amer. chem. Soc., 1942, 44, 2195.

25. Beattie; Proc. nat. Acad. Sci.,(Wash.), 1930, 16, 14.

26. Amagat; Int. Crit. Tables, Vol. III, p. 11.

27. Andrews; Phil. Trans., 1876, 166, 421.

28. Carey and Williamson; Proc. Inst. mech. Engrs., 1950, 163,(W.E.P. No.56), 41.

29. Van Ardsel; Trans. Amer. Inst. chem. Engrs., 1921-22, 14, 391.

30. Geankoplis and Hixon; Industr. engng. Chem., 1950, 42, 1141.

31. Simmons and Osborne; Ibid., 1934, 26, 529.

32. Adams and Edmonds; Ibid., 1937, 29, 447.

33. Cantello, Simmons, Giles and Brill, Ibid., 1927, 19, 989.

34. Helsby and Tuson; Research, 1955, 8, 270.

35. Holborn and Otto; Zeit. Phys., 1924, 23, 77.

36. Pozin, Mukhlenov, Tumarkina and Tarat; Zh. Prikl. Khim. Leningrad, 1954, 27, (1), 12.

37. Helsby and Birt; J. appl. Chem., 1955, 5, 347.

38. Dixon and Kiff; Ibid., 1955, 5, 390.

39. Verschoor; Trans. Brit. Inst. chem. Engrs., 1950, 28, 52.

40. Peebles and Garber; Chem. engng. Progr., 1953, 49, 88.

41. Thomson, Houghton and Ritchie; The Velocities of Rise and Types of Bubbles in Water; to be published.

42. Stuke; Naturwiss., 1952, 39, 325.

TABLE I

TABLE OF VIRIAL COEFFICIENTS

EQUATION	YEAR	EXPLICIT IN	NO. OF EMPIRICAL CONSTANTS	α_1	α_2	α_3	α_4	α_5	α_6	α_7
VAN DER WAALS	1873	p	2	1	$a_1 + \frac{a_2}{T}$	$\frac{b_1}{T}$	—	—	—	—
BERTHELOT	1897	p	2	1	$a_1 + \frac{a_2}{T^2}$	$\frac{b_1}{T^2}$	—	—	—	—
WOHL	1914	p	3	1	$a_1 + \frac{a_2}{T}$	$\frac{b_1}{T}$	$\frac{c_1}{T}$	—	—	—
LINDE	1905	V	5	K	$a_1 + \frac{a_2}{T^3}$	$b_1 T + \frac{b_2}{T^2}$	—	—	—	—
BEATTIE-BRIDGEMAN	1928	p	5	1	$a_1 + \frac{a_2}{T} + \frac{a_3}{T^3}$	$b_1 + \frac{b_2}{T} + \frac{b_3}{T^3}$	$\frac{c_1}{T^3}$	—	—	—
BEATTIE	1930	V	5	1	$a_1 + \frac{a_2}{T} + \frac{a_3}{T^3}$	$b_1 + \frac{b_2}{T} + \frac{b_3}{T^3}$	$\frac{c_1}{T^3}$	—	—	—
BENEDICT-WEBB-RUBIN	1940	p	8	1	$a_1 + \frac{a_2}{T} + \frac{a_3}{T^3}$	$b_1 + \frac{b_2}{T} + \frac{b_3 e^{-\gamma/V^2}}{T^3}$	—	$\frac{d_1 e^{-1/V^2}}{T^3}$	$\frac{e_1}{T}$	—
BUREAU OF STANDARDS	1923	V	10	K	$a_1 + \frac{a_2}{T^3} + \frac{a_3}{T^{11}}$	$b_1 T + \frac{b_2}{T^{10}}$	$c_1 T^2$	$d_1 T^3$	—	$\frac{f_1}{T^{14}}$
MARON-TURNBULL	1942	V	12	1	$a_1 + \frac{a_2}{T} + \frac{a_3}{T^3}$	$\frac{b_1}{T} + \frac{b_2}{T^3} + \frac{b_3}{T^5}$	$c_1 + \frac{c_2}{T^2} + \frac{c_3}{T^4}$	$d_1 T + \frac{d_2}{T} + \frac{d_3}{T^2}$	—	—

TABLE 2a

Showing the deviation of calculated volumes from the experimental volumes of carbon dioxide using the Beattie equation and the new explicit volume equation of state.

Experimental data : Michels and Michels, Proc.Roy.Soc.(London), 1936, A 153, 201.

Temp. °C	Pressure atm.	Exptl. volume V_e litres	Beattie equation		New equation	
			$\Delta V = V_c - V_e$	% dev.	$\Delta V = V_c - V_e$	% dev.
0.000	16.5488	1.187255	+0.019848	+ 1.672	-0.004099	-0.345
	26.0553	0.679060	+0.036257	+ 5.339	-0.002039	-0.300
	33.4202	0.472396	+0.055206	+11.686	+0.001449	+0.307
25.053	18.5374	1.187257	+0.011422	+ 0.962	-0.000133	-0.011
	26.3707	0.790083	+0.018026	+ 2.282	-0.000244	-0.031
	33.3074	0.591653	+0.024594	+ 4.157	-0.001577	-0.267
31.037	19.0023	1.187263	+0.010337	+ 0.872	+0.000402	+0.054
	27.1155	0.790088	+0.015990	+ 2.024	-0.000159	-0.020
	34.3530	0.591659	+0.021850	+ 3.693	-0.001686	-0.285
40.105	19.7049	1.187261	+0.008912	+ 0.751	+0.000894	+0.075
	28.2269	0.790084	+0.013706	+ 1.735	+0.000167	+0.021
	35.9178	0.591658	+0.018482	+ 3.124	-0.001629	-0.275
75.260	22.3956	1.187257	+0.005953	+ 0.501	+0.001959	+0.165
	27.5246	0.948858	+0.007104	+ 0.749	+0.001466	+0.155
	32.4664	0.790086	+0.008386	+ 1.061	+0.000844	+0.107
99.767	24.2483	1.187265	+0.005334	+ 0.448	+0.002651	+0.223
	29.8914	0.948856	+0.005887	+ 0.621	+0.002143	+0.226
	35.3693	0.790086	+0.006569	+ 0.831	+0.001469	+0.186

TABLE 2b

Deviation summary.

	total no. of pts.	overall average	+ve points		-ve points		maxm. +ve	maxm. -ve
			no.	average	no.	average		
Beattie equation	18	2.361	18	2.361	-	-	11.686	-
New equation	18	0.169	10	0.150	8	0.192	0.307	0.345

TABLE 3a

Showing the deviation of calculated volumes from the experimental volumes of carbon dioxide using the Beattie equation and the new explicit volume equation of state.

Experimental data : Andrews, Phil.Trans., 1876,166,421.
(pressure values being corrected for the compressibility of air)

Temp.	Press., atm.		Exptl. volume	Beattie equation		New equation	
°C	Ands.	Crtd.	V_e, litres	$\Delta V = V_c - V_e$	%dev.	$\Delta V = V_c - V_e$	%dev.
6.89	12.01	11.94	1.763302	+0.021410	+1.214	+0.006562	+0.372
6.90	13.22	13.13	1.590110	+0.019859	+1.249	+0.004128	+0.259
6.90	14.68	14.57	1.416696	+0.020719	+1.462	+0.003811	+0.269
6.62	31.06	30.59	0.576340	+0.037567	+6.518	−0.001093	−0.190
63.86	17.60	17.44	1.485038	+0.009442	+0.635	+0.005841	+0.393
63.79	22.56	22.30	1.138210	+0.010968	+0.964	+0.005104	+0.448
63.83	31.39	30.91	0.792495	+0.012772	+1.612	+0.003841	+0.485
100.39	17.42	17.26	1.698077	+0.007838	+0.462	+0.006325	+0.372
100.41	22.37	22.11	1.308953	+0.007944	+0.607	+0.006015	+0.460
100.64	31.06	30.59	0.925617	+0.008903	+0.962	+0.004900	+0.529

TABLE 3b

Deviation summary.

	total no. of pts.	overall average	+ve points		-ve points		maxm. +ve	maxm. -ve
			no.	average	no.	average		
Beattie equation	10	1.569	10	1.569	-	-	6.518	-
New equation	10	0.378	9	0.399	1	0.190	0.529	0.190

TABLE 4

Test examples - showing the deviation of calculated volumes from random experimental volumes of carbon dioxide using the new explicit volume equation of state.

Temp. °C	Pressure atm.	Experimental volume V_e, litres	$\Delta V = V_c - V_e$	% deviation	Data Source
0.000	1.0000	22.261137	-0.013298	-0.060	Gram Mol. Volume
29.900	23.0572	0.948857	+0.000279	+0.029	Michels & Michels
49.712	25.0260	0.948859	+0.000887	+0.093	
6.05	27.31	0.667610	-0.000255	-0.038	Andrews (pressure corrected)
6.79	19.89	0.991955	+0.001417	+0.143	

TABLE 5

Compressibility factors, C, and fugacity coefficients, f/p, for carbon dioxide.

Pressure range 0-36 atm. Temperature range 0-100°C.

P atm.	0°C		10°C		15°C	
	C	f/p	C	f/p	C	f/p
0	1.000000	1.00000	1.000000	1.00000	1.000000	1.00000
1	0.992631	0.99266	0.993590	0.99362	0.993996	0.99400
2	0.985273	0.98536	0.987190	0.98724	0.988003	0.98806
4	0.970552	0.97098	0.974395	0.97470	0.976024	0.97630
6	0.955759	0.95676	0.961557	0.96230	0.964014	0.96464
8	0.940821	0.94275	0.948685	0.95004	0.951925	0.95314
10	0.925667	0.92886	0.935586	0.93768	0.939719	0.94174
12	0.910218	0.91512	0.922240	0.92584	0.927316	0.93042
14	0.894400	0.90146	0.908680	0.91398	0.914698	0.91918
16	0.878141	0.88792	0.894799	0.90198	0.901807	0.90796
18	0.861363	0.87442	0.880542	0.89016	0.888595	0.89690
20	0.843995	0.86097	0.865852	0.87836	0.875012	0.88580
22	0.825961	0.84753	0.850675	0.86657	0.861010	0.87474
24	0.807186	0.83413	0.834954	0.85483	0.846542	0.86370
26	0.787595	0.82073	0.818633	0.84305	0.831558	0.85263
28	0.767117	0.80751	0.801657	0.83130	0.816010	0.84160
30	0.745674	0.79387	0.783970	0.81950	0.799848	0.83055
32	0.723192	0.78039	0.765516	0.80770	0.783027	0.81941
34	-	-	0.746239	0.79583	0.765494	0.80830
36	-	-	0.726083	0.78393	0.747203	0.79715

	20°C		25°C		35°C	
0	1.000000	1.00000	1.000000	1.00000	1.000000	1.00000
1	0.994365	0.99436	0.994700	0.99472	0.995293	0.99533
2	0.988740	0.98880	0.989412	0.98946	0.990595	0.99066
4	0.977501	0.97772	0.978846	0.97904	0.981214	0.98136
6	0.966239	0.96678	0.968265	0.96874	0.971829	0.97218
8	0.954913	0.95596	0.957633	0.95854	0.962411	0.96310
10	0.943480	0.94524	0.946911	0.94844	0.952933	0.95410
12	0.931899	0.93458	0.936065	0.93840	0.943365	0.94516
14	0.920127	0.92402	0.925056	0.92842	0.933680	0.93624
16	0.908123	0.91350	0.913848	0.91852	0.923849	0.92738
18	0.895842	0.90302	0.902404	0.90864	0.913844	0.91856
20	0.883244	0.89258	0.890686	0.89882	0.903638	0.90980
22	0.870286	0.88218	0.878660	0.88900	0.893199	0.90106
24	0.856927	0.87178	0.866286	0.87918	0.882504	0.89230
26	0.843122	0.86140	0.853529	0.86940	0.871581	0.88356
28	0.828831	0.85100	0.840352	0.85960	0.860281	0.87484
30	0.814010	0.84058	0.826716	0.84976	0.848579	0.86610
32	0.798619	0.83013	0.812587	0.83995	0.836565	0.85755
34	0.782615	0.81967	0.797927	0.83010	0.824149	0.84857
36	0.765955	0.80917	0.782699	0.82021	0.811316	0.83979

	50°C		75°C		100°C	
0	1.000000	1.00000	1.000000	1.00000	1.000000	1.00000
1	0.996026	0.99602	0.996962	0.99696	0.997658	0.99764
2	0.992060	0.99208	0.993929	0.99394	0.995322	0.99534
4	0.984143	0.98424	0.987881	0.98794	0.990660	0.99070
6	0.976234	0.97646	0.981843	0.98196	0.986011	0.98606
8	0.968308	0.96876	0.975805	0.97604	0.981365	0.98150
10	0.960350	0.96112	0.969757	0.97014	0.976721	0.97692
12	0.952338	0.95352	0.963689	0.96432	0.972068	0.97240
14	0.944255	0.94596	0.957589	0.95850	0.967402	0.96736
16	0.936079	0.93844	0.951446	0.95268	0.962717	0.96358
18	0.927794	0.93098	0.945252	0.94682	0.958009	0.95890
20	0.919378	0.92350	0.938994	0.94116	0.953269	0.95442
22	0.910813	0.91606	0.932662	0.93542	0.948491	0.94996
24	0.902078	0.90866	0.926246	0.92972	0.943671	0.94554
26	0.893156	0.90134	0.919734	0.92402	0.938800	0.94108
28	0.884028	0.89384	0.913118	0.91832	0.933875	0.93668
30	0.874672	0.88644	0.906384	0.91260	0.928888	0.93234
32	0.865070	0.87902	0.899520	0.90688	0.923834	0.92794
34	0.855203	0.87160	0.892527	0.90102	0.918706	0.92345
36	0.845051	0.86417	0.885381	0.89530	0.913498	0.91898

TABLE 6

The solubility of carbon dioxide in water.
Temperature range 0-100°C. Pressure range 0-36 atm.

A comparison of Zelvinskii's solubility data with the data calculated from Henry's law and the fugacity correction to Henry's law.

Isotherm 0°C

P atm.	Zelvinskii's data			data of Bohr and Bock				
				Henry's law		Fugacity correction		
	Sol. S vol/vol	mole fraction $x \times 10^3$	exptl. m.f. $x \times 10^3$	$x \times 10^3$	% dev.	fugacity atm.	$x \times 10^3$	% dev.
0	0.000	0.000		0.000			0.000	
1	1.815	1.467	1.445	1.385*	- 5.6	0.9927	1.385	- 5,6
2	3.580	2.889		2.770	- 4.1	1.9714	2.750	- 4.8
4	6.960	5.602		5.540	- 1.1	3.9840	5.418	- 3.3
5	8.575	6.893	6.593	6.925	+ 0.5	4.8190	6.723	- 2.5
6	10.140	8.140		8.310	+ 2.1	5.7408	8.008	- 1.6
8	13.120	10.508		11.080	+ 5.5	7.5424	10.522	+ 0.1
10	15.900	12.706	12.610	13.850	+ 9.0	9.2890	12.958	+ 2.0
12	18.480	14.737		16.620	+12.8	10.9812	15.319	+ 3.9
14	20.860	16.604		19.390	+16.8	12.6210	17.606	+ 6.0
15	21.975	17.477	17.240	20.775	+18.9	13.4190	18.730	+ 7.1
16	23.043	18.307		22.160	+21.0	14.2064	19.818	+ 8.3
18	25.020	19.849		24.930	+25.6	15.7392	21.956	+10.6
20	26.800	21.231	20.880	27.700	+30.5	17.2200	24.022	+13.1
22	28.380	22.455		30.470	+35.7	18.6450	26.010	+15.9
24	29.760	23.523		33.240	+42.2	20.0184	27.926	+19.5
25	30.375	23.997	23.900	34.625	+44.2	20.6825	28.852	+20.3
26	30.940	24.431		36.010	+47.5	21.3382	29.767	+21.9
28	31.920	25.185		38.780	+53.9	22.6044	31.533	+25.2
30	32.700	25.785	25.950	41.550	+61.2	23.8170	33.225	+28.9
32	33.280	26.230		44.320	+68.9	24.9728	34.837	+32.8
33	33.495	26.395		45.705	+73.1	25.5387	35.626	+35.0

Isotherm 25°C

0	0.000	0.000		0.000			0.000	
1	0.749	0.608		0.616*	+ 1.3	0.9947	0.616	+ 1.32
2	1.489	1.207		1.232	+ 3.1	1.9790	1.225	+ 1.49
4	2.945	2.385		2.464	+ 3.3	3.9160	2.424	+ 1.64
6	4.367	3.532		3.696	+ 4.6	5.8122	3.598	+ 1.87
8	5.755	4.650		4.928	+ 6.0	7.6680	4.746	+ 2.07
10	7.110	5.738		6.160	+ 7.4	9.4840	5.871	+ 2.32
10.98	7.762	6.261	6.226	6.764	+ 8.0	10.3596	6.413	+ 2.43
10.98			6.106					
12	8.431	6.797		7.329	+ 8.8	11.2608	6.970	+ 2.52
14	9.720	7.828		8.624	+10.2	12.9976	8.046	+ 2.78
16	10.974	8.829		9.865	+11.6	14.6960	9.097	+ 3.05
18	12.195	9.802		11.088	+13.1	16.3548	10.124	+ 3.29
20	13.383	10.746		12.320	+14.7	17.9760	11.127	+ 3.54
21.75	14.394	11.549	11.830	13.398	+16.0	19.3619	11.985	+ 3.78
22	14.536	11.662		13.552	+16.2	19.5580	12.106	+ 3.81
22.92	15.057	12.074	12.399	14.119	+16.9	20.2682	12.546	+ 3.91
24	15.657	12.550		14.784	+17.8	21.1008	13.061	+ 4.07
24.65	16.014	12.832	12.714	15.184	+18.3	21.5934	13.366	+ 4.16
26	16.744	13.409	13.427	16.016	+19.4	23.0044	13.992	+ 4.35
28	17.248	14.241		17.248	+21.1	24.0686	14.899	+ 4.62
30	18.817	15.045		18.480	+22.8	25.4940	15.781	+ 4.88
31.40	19.511	15.511	15.570	19.342	+24.1	26.4608	16.379	+ 5.06
32	19.804	15.821		19.712	+24.6	26.8800	16.639	+ 5.16
34	20.757	16.570		20.944	+26.4	28.2234	17.470	+ 5.43
34.36	20.924	16.701	16.604	21.166	+26.7	28.4570	17.615	+ 5.47
36	21.676	17.291		23.176	+28.3	29.5272	18.277	+ 5.70

(* experimental value)

TABLE 6(cont.)

Zelvinskii's data for the isotherms 10, 15 and 20°C have been calculated from equations interpolated from Fig. 1.

P atm.	Zelvinskii's data		data of Bohr and Bock				
	sol. S vol/vol	mole fraction $x \times 10^3$	Henry's law		Fugacity correction		
			$x \times 10^3$	% dev.	fugacity atm.	$x \times 10^3$	% dev.
Isotherm 10°C							
0	0.000	0.000	0.000			0.000	
1	1.218	0.985	0.966*	- 1.9	0.9936	0.966	- 1.9
2	2.409	1.946	1.932	- 0.7	1.9744	1.919	-.1.4
4	4.710	3.799	3.864	+ 1.7	3.8988	3.790	- 0.2
6	6.906	5.560	5.796	+ 4.3	5.7738	5.612	+ 0.2
8	8.996	7.230	7 728	+ 6.9	7.6000	7.387	+ 2.2
10	10.978	8.810	9.660	+ 9.7	9.3790	9.116	+ 3.5
12	12.855	10.300	11.591	+12.5	11.1096	10.798	+ 4.8
14	14.625	11.701	13.524	+15.4	12.7946	12.436	+ 6.3
16	16.289	13.015	15.456	+18.8	14.4320	14.028	+ 7.8
18	17.847	14.242	17.388	+22.1	16.0236	15.575	+ 9.5
20	19.297	15.382	19.320	+25.6	17.5680	17.076	+11.0
22	20.642	16.437	21.252	+29.3	19.0652	18.531	+12.7
24	21.880	17.405	23.184	+33.2	20.5152	19.941	+14.6
26	23.012	18.289	25.116	+37.3	21.9206	21.307	+16.5
28	24.038	19.089	27.048	+41.7	23.2764	22.625	+18.6
30	24.957	19.804	28.980	+46.3	24.5850	23.897	+20.7
32	25.769	20.436	30.912	+51.2	25.8464	25.123	+22.9
34	26.475	20.984	32.844	+56.5	27.0572	26.300	+25.4
36	27.075	21.449	34.776	+62.2	28.2204	27.430	+27.9
Isotherm 15°C							
0	0.000	0.000	0.000			0.000	
1	0.990	0.802	0.825*	+ 2.8	0.9940	0.825	+ 2.8
2	1.963	1.587	1.650	+ 4.0	1.9762	1.640	+ 3.3
4	3.855	3.113	3.300	+ 6.0	3.9052	3.241	+ 4.1
6	5.676	4.577	4.950	+ 8.1	5.7876	4.804	+ 5.0
8	7.425	5.978	6.600	+10.4	7.6248	6.329	+ 5.9
10	9.103	7.320	8.250	+12.7	9.4170	7.816	+ 6.8
12	10.710	8.601	9.900	+15.1	11.1648	9.267	+ 7.8
14	12.247	9.823	11.550	+17.6	12.8688	10.681	+ 8.7
16	13.718	10.990	13.200	+20.1	14.5280	12.058	+ 9.7
18	15.105	12.088	14.850	+22.9	16.1442	13.400	+10.9
20	16.428	13.133	16.500	+25.6	17.7160	14.704	+12.0
22	17.679	14.119	18.150	+28.6	19.2434	15.972	+13.1
24	18.860	15.048	19.800	+31.5	20.7288	17.205	+14.3
26	19.969	15.919	21.450	+34.8	22.1676	18.399	+15.6
28	21.006	16.732	23.100	+38.1	23.5648	19.559	+16.9
30	21.994	17.489	24.750	+41.6	24.9150	20.679	+18.3
32	22.869	18.188	26.400	+45.2	26.2208	21.763	+19.7
34	23.694	18.832	28.050	+48.9	27.4822	22.810	+21.1
36	24.449	19.420	29.700	+53.0	28.6956	23.817	+22.7
Isotherm 20°C							
0	0.000	0.000	0.000			0.000	
1	0.855	0.692	0.711*	+ 2.8	0.9944	0.711	+ 2.8
2	1.697	1.374	1.422	+ 4.2	1.9776	1.414	+ 2.9
4	3.345	2.704	2.844	+ 5.2	3.9108	2.796	+ 3.4
6	4.944	3.992	4.266	+ 6.9	5.8008	4.148	+ 3.9
8	6.495	5.239	5.688	+ 8.6	7.6480	5.468	+ 4.4
10	7.997	6.442	7.110	+10.4	9.4520	6.758	+ 4.9
12	9.450	7.604	8.532	+12.2	11.2152	8.019	+ 5.5
14	10.854	8.724	9.954	+14.1	12.9360	9.249	+ 6.0
16	12.210	9.806	11.376	+16.0	14.6160	10.450	+ 6.6
18	13.518	10.841	12.798	+18.1	16.2540	11.622	+ 7.2
20	14.776	11.838	14.220	+20.1	17.8520	12.764	+ 7.8
22	15.986	12.795	15.642	+22.3	19.4084	13.877	+ 8.5
24	17.126	13.695	17.064	+24.6	20.9232	14.960	+ 9.2
26	18.258	14.587	18.468	+26.8	22.3964	16.013	+ 9.8
28	19.322	15.425	19.908	+29.1	23.8280	17.037	+10.5
30	20.337	16.221	21.330	+31.5	25.2180	18.031	+11.2
32	21.303	16.979	22.752	+34.0	26.5632	18.993	+11.8
34	22.220	17.696	24.174	+36.6	27.8698	19.927	+12.6
36	22.988	18.297	25.596	+39.9	29.1312	20.829	+13.8

(* experimental value)

TABLE 6(cont.)

Isotherm 35°C

(Zelvinskii's data interpolated from Fig. 1)

P	Zelvinskii's data			data of Bohr and Bock					Wiebe&Gaddy	
	Sol. S	mole fraction	exptl. m.f.	Henry's law		Fugacity correction				
atm.	vol/vol	$x \times 10^3$	$x \times 10^3$	$x \times 10^3$	%dev.	fugacity atm.	$x \times 10^3$	%dev.	$x \times 10^3$	%dev.
0	0.000	0.000		0.000			0.000		0.000	
1	0.581	0.473		*0.482	+ 1.8	0.9953	0.482	+1.84	0.466	-1.48
2	1.159	0.943		0.964	+ 2.2	1.9812	0.959	+1.70	0.927	-1.09
4	2.299	1.868		1.928	+ 3.2	3.9256	1.900	+1.72	1.837	-1.66
6	3.418	2.775		2.892	+ 4.2	5.8332	2.823	+1.73	2.730	-1.62
8	4.518	3.665		3.856	+ 5.2	7.7048	3.729	+1.75	3.606	-1.61
10	5.597	4.537		4.820	+ 6.2	9.5410	4.618	+1.78	4.465	-1.59
12	6.657	5.391		5.784	+ 7.3	11.3424	5.490	+1.84	5.508	-1.54
14	7.697	6.228		6.748	+ 8.4	13.1068	6.344	+1.87	6.134	-1.51
16	8.717	7.047		7.712	+ 9.4	14.8384	7.182	+1.92	6.944	-1.46
18	9,717	7.850		8.676	+10.5	16.5348	8.003	+1.95	7.738	-1.43
20	10.697	8.635		9.640	+11.6	18.1960	8,807	+1.99	8.516	-1.38
22	11.658	9.402		10.604	+12.8	19.8242	9.595	+2.05	9.287	-1.32
24	12.598	10.153		11.568	+14.0	21.4152	10.365	+2.08	10.022	-1.29
24.94	13.034	10.502		12.053	+14.5	22.1548	10.723	+2.11	*10.369	-1.27
26	13.519	10.887		12.532	+15.1	22.9756	11.119	+2.13	10.752	-1.24
28	14.420	11.604		13.496	+16.3	24.4944	11.855	+2.16	11.463	-1.21
30	15.301	12.304		14.460	+17.5	25.9830	12.576	+2.21	12.160	-1.17
32	16.162	12.988		15.424	+18.7	27.4368	13.279	+2.24	12.840	-1.14
34	17.003	13.654		16.388	+20.0	28.8524	13.965	+2.28	13.503	-1.11
36	17.824	14.304		17.352	+21.3	30.2328	14.635	+2.30	14.149	-1.08

Isotherm 50°C

0	0.000	0.000		0.000			0.000		0.000	
1	0.418	0.342		*0.357	+ 4.3	0.9960	0.357	+4.29	0.345	+0.70
2	0.834	0.683		0.714	+ 4.5	1.9842	0.710	+3.96	0.687	+0.59
4	1.655	1.354		1.428	+ 5.5	3.9368	1.409	+4.07	1.363	+0.66
6	2.465	2.015		2.142	+ 6.3	5.8590	2.098	+4.11	2.028	+0.65
8	3.261	2.664		2.856	+ 7.2	7.7504	2.775	+4.17	2.682	+0.68
10	4.046	3.303		3.570	+ 8.1	9.6110	3.441	+4.18	3.326	+0.70
12	4.817	3.930		4.284	+ 9.0	11.4420	4.096	+4.22	3.960	+0.76
14	5.577	4.547		4.998	+ 9.9	13.2440	4.741	+4.26	4.584	+0.81
16	6.325	5.154		5.712	+10.8	15.0144	5.375	+4.29	5.196	+0.81
18	7.062	5.751		6.462	+11.7	16.7580	5.999	+4.31	5.800	+0.85
19.14	7.475	6.085	6.226	6.833	+12.3	17.7390	6.351	+4.36	6.139	+0.89
19.14			6.322							
19.16	7.481	6.090	6.146	6.840	+12.3	17.7517	6.355	+4.35	6.144	+0.89
20	7.783	6.335		7.140	+12.7	18.4700	6.612	+4.37	6.392	+0.90
22	8.494	6.909		7.854	+13.8	20.1542	7.215	+4.43	6.975	+0.93
24	9.191	7.472		8.568	+14.7	21.8088	7.808	+4.49	7.548	+0.99
24.88	9.494	7.716		8.881	+15.1	22.5178	8.061	+4.47	*7.794	+1.01
26	9.877	8.026		9.282	+15.7	23.4512	8.388	+4.50	8.110	+1.05
28	10.551	8.568		9.996	+16.7	25.0264	8.959	+4.56	8.662	+1.10
30	11.212	9.100		10.710	+17.7	26.5920	9.520	+4.61	9.203	+1.13
32	11.861	9.622		11.424	+18.7	28.1280	10.070	+4.66	9.735	+1.17
32.57	12.043	9.768	9.961	11.627	+19.0	28.5574	10.224	+4.66	9.884	+1.19
32.58	12.047	9.772	9.770	11.631	+19.0	28.5629	10.226	+4.64	9.886	+1.17
32.80	12.117	9.828	9.858	11.710	+19.2	28.7328	10.286	+4.66	9.944	+1.18
34	12.498	10.133		12.138	+19.8	29.6344	10.609	+4.70	10.256	+1.21
36	13.121	10.634		12.852	+20.9	31.1112	11.138	+4.74	10.768	+1.26

(* experimental value)

TABLE C (cont.)

Isotherm 75°C

P	Zelvinskii's data					data of Wiebe & Gaddy		
	Sol. S	mole fraction	exptl. m.f.	Henry's law		Fugacity correction		
atm.	vol/vol	$x \times 10^3$	$x \times 10^3$	$x \times 10^3$	% dev.	fugacity atm.	$x \times 10^3$	% dev.
0	0.000	0.000		0.000			0.000	
1	0.299	0.248		0.248	0.00	0.9970	0.239	-3.41
2	0.597	0.495		0.496	+ 0.20	1.9878	0.477	-3.64
4	1.187	0.984		0.992	+ 0.81	3.9516	0.949	-3.56
6	1.768	1.465		1.488	+ 1.57	5.8920	1.415	-3.42
8	2.342	1.941		1.984	+ 2.32	7.8080	1.875	-3.40
10	2.908	2.409		2.480	+ 2.94	9.7010	2.330	-3.28
12	3.468	2.871		2.976	+ 3.66	11.5716	2.779	-3.21
14	4.020	3.326		3.472	+ 4.39	13.4190	3.223	-3.10
16	4.564	3.775		3.968	+ 5.11	15.2432	3.661	-3.03
18	5.100	4.216		4.464	+ 5.88	17.0442	4.094	-2.90
18.82	5.319	4.396	4.456	4.667	+ 6.17	17.7755	4.270	-2.86
18.86	5.328	4.404	4.368	4.677	+ 6.20	17.8095	4.278	-2.86
19	5.366	4.435	4.384	4.712	+ 6.25	17.9841	4.308	-2.86
20	5.630	4.652		4.960	+ 6.62	18.8240	4.522	-2.80
22	6.150	5.080		5.456	+ 7.40	20.5788	4.943	-2.70
24	6.665	5.503		5.952	+ 8.16	22.3128	5.360	-2.60
24.61	6.821	5.631		6.104	+ 8.40	22.8365	5.485*	-2.59
26	7.171	5.918		6.448	+ 8.95	24.0240	5.771	-2.39
28	7.670	6.328		6.944	+ 9.74	25.7124	6.176	-2.40
30	8.162	6.730		7.440	+10.54	27.3780	6.576	-2.29
32	8.646	7.126		7.936	+11.35	29.0208	6.971	-2.18
32.20	8.693	7.165	7.168	7.986	+11.45	29.1861	7.011	-2.15
32.68	8.807	7.259	7.272	8.105	+11.64	29.5754	7.104	-2.14
34	9.131	7.516		8.432	+12.18	30.6408	7.360	-2.08
36	9.590	7.899		8.928	+13.00	32.2580	7.744	-1.96

Isotherm 100°C

0	0.000	0.000		0.000			0.000	
1	0.221	0.187		0.187	0.00	0.9976	0.190	+1.71
2	0.442	0.375		0.374	+0.27	1.9906	0.379	+1.01
4	0.881	0.743		0.748	+0.67	3.9628	0.755	+1.61
6	1.317	1.111		1.122	+0.99	5.9166	1.128	+1.54
8	1.751	1.477		1.496	+1.29	7.8520	1.497	+1.35
10	2.183	1.841		1.870	+1.58	9.7690	1.862	+1.14
12	2.613	2.202		2.244	+1.91	11.6689	2.224	+1.00
14	3.039	2.560		2.618	+2.27	13.5506	2.583	+0.90
16	3.464	2.917		2.992	+2.57	15.4144	2.938	+0.72
18	3.886	3.271		3.366	+2.91	17.2602	3.290	+0.58
19.09	4.115	3.463	3.477	3.570	+3.09	18.2539	3.480	+0.49
19.27	4.151	3.493	3.460	3.603	+3.16	18.4133	3.511	+0.52
20	4.305	3.622		3.740	+3.26	19.0880	3.639	+0.47
22	4.722	3.972		4.114	+3.58	20.9000	3.984	+0.30
23.98	5.133	4.315		4.485	+3.94	22.6774	4.323*	+0.19
26	5.548	4.663		4.862	+4.26	24.4636	4.664	+0.02
28	5.958	5.006		5.236	+4.59	26.2276	5.000	-0.13
30	6.364	5.346		5.610	+4.95	27.9660	5.331	-0.38
32	6,769	5.684		5.984	+5.28	29.6896	5.660	-0.42
32.67	6.904	5.797	5.826	6.109	+5.38	30.2590	5.768	-0.50
32.78	6.926	5.815	5.778	6.130	+5.42	30.3543	5.786	-0.50
34	7.171	6.020		6.358	+5.62	31.3956	5.985	-0.58
36	7.571	6.353		6.732	+5.97	33.0840	6.307	-0.72

(* experimental value)

TABLE 7

Deviation summary of the solubility results shown in TABLE 6

Henry's law - data of Bohr and Bock (*Zelvinskii's data).

Temp. °C	total no. of pts.	overall average	+ve points		-ve points		maxm. +ve	maxm. -ve
			no.	ave.	no.	ave.		
0	21	27.6	18	31.6	3	3.6	73.1	5.6
10	19	25.2	17	29.7	2	1.3	62.2	1.9
15	19	24.6	19	24.6	-	-	53.0	-
20	19	19.1	19	19.1	-	-	39.9	-
25	25	14.8	25	14.8	-	-	28.3	-
35	20	11.0	20	11.0	-	-	21.3	-
50	25	13.0	25	13.0	-	-	20.9	-
75 *	25	6.6	24	6.9	-	-	13.0	-
100 *	23	3.3	22	3.4	-	-	6.0	-

Fugacity correction to Henry's law - data of Bohr and Bock.

0	21	12.8	16	15.7	5	3.6	35.0	5.6
10	19	11.0	16	12.7	3	1.2	27.9	1.9
15	19	11.5	19	11.5	-	-	22.7	-
20	19	7.0	19	7.0	-	-	13.8	-
25	25	3.6	25	3.6	-	-	5.7	-
35	20	2.0	20	2.0	-	-	2.3	-
50	25	4.4	25	4.4	-	-	4.7	-

Fugacity correction to Henry's law - data of Wiebe and Gaddy.

35	20	1.4	-	-	20	1.4	-	1.7
50	25	0.9	25	0.9	-	-	1.3	-
75	25	2.8	-	-	25	2.8	-	3.6
100	23	0.8	16	0.9	7	0.4	1.7	0.7

TABLE 8

Comparison of Henry's law and the fugacity correction to Henry's law with Zelvinskii's results.

Temp.	Henry's law		Fugacity correction to Henry's law			
	Bohr and Bock		Bohr and Bock		Wiebe and Gaddy	
°C	ave. %dev.	maxm. dev.	ave. %dev.	maxm. dev.	ave. %dev.	maxm. dev.
0	27.6	73.1	12.8	35.0	-	-
10	25.2	62.2	11.0	27.9	-	-
15	24.6	53.0	11.5	22.7	-	-
20	19.1	39.9	7.0	13.8	-	-
25	14.8	28.3	3.6	5.7	-	-
35	11.0	21.3	2.0	2.3	1.4	1.7
50	13.0	20.9	4.4	4.7	0.9	1.3
75	6.6*	13.0	-	-	2.8	3.6
100	3.3*	6.0	-	-	0.8	1.7

(* based on Zelvinskii's calculated solubility at 1 atm.)

TABLE 9

Comparison of Zelvinskii's experimental and calculated solubilities of carbon dioxide in water with the data of Bohr and Bock at a partial pressure of 1 atmosphere.

Temp. °C	Zelvinskii data			Bohr & Bock data		% deviation
	exptl.S vol./vol.	calcd.S vol./vol.	m.frac. x 10^3	exptl.S vol./vol.	m.frac. x 10^3	
0	1.80	1.815	1.467	1.713	1.385	-5.58
10		1.218	0.985	1.194	0.966	-1.93
15		0.990	0.802	1.019	0.825	+2.79
20		0.855	0.692	0.878	0.711	+2.75
25		0.749	0.608	0.759	0.616	+1.32
35		0.581	0.473	0.592	0.482	+1.84
50		0.418	0.342	0.436	0.357	+4.29

TABLE 10

Comparison of interpolated solubilities from Zelvinskii's equations with experimental solubilities.

Temp. °C	partial pressure atm.	intpld.S vol./vol.	exptl.S vol./vol.	Reference	% deviation
12.43	25	20.25	20.31	Zelvinskii	-0.30
18	24.9792	18.39	19.48	Wiebe & Gaddy	-5.70
31.04	24.9547	14.35	14.12	Wiebe & Gaddy	+1.63
35	24.9435	13.04	12.87	Wiebe & Gaddy	+1.32
40	24.9259	11.80	11.53	Wiebe & Gaddy	+2.34
50	24.8760	9.49	9.59	Wiebe & Gaddy	-1.04
75	24.6136	6.82	6.64	Wiebe & Gaddy	+2.71
100	23.9820	5.13	5.14	Wiebe & Gaddy	-0.19

TABLE 11

Properties of porous discs.

Distributor	Thickness in.	Surface Area $ft.^2$	No. of holes	Porosity μ micron
Fine bronze	0.123	0.0307	-	72
Medium bronze	0.126	0.0307	-	408
Coarse bronze	0.121	0.0307	-	634

Properties of other gas distributors.

Indented strip A	1.0	0.0214	441	1150
Indented strip B	1.0	0.0214	903	810
Brass plate drilled with $\frac{1}{8}$" dia. holes	1/16	0.0307	4	3180
$\frac{3}{8}$" dia. pipe	-	-	1	9540

TABLE 12

Calculation of $(N.T.U.)_{OL}$

Run	Gas comp. %		$(N.T.U.)_{OL}$				
	In	Out	Graphical integration	Log. mean		Method of Carey and Williamson.	
				$(N.T.U.)_{OL}$	%dev.	$(N.T.U.)_{OL}$	%dev.
3	84.3	67.7	0.607	0.626	+ 3.1	0.607	0
14	83.7	28.9	2.07	3.25	+57	2.04	-1.5
15	77.5	22.8	0.591	0.780	+32	0.614	+3.9
28	82.8	38.0	0.614	0.723	+18	0.609	-0.8
29	84.8	56.8	0.809	0.870	+ 7.5	0.811	+0.3
33	84.5	45.1	0.534	0.619	+16	0.539	+0.9
34	83.9	42.1	0.811	0.925	+14	0.782	-3.6

TABLE 13

Deviation summary of the values of E_A calculated from equation (47) with the experimental values of E_A for the rising hold-up region.

Run No.	E_A(calc.) 1.	E_A(exp.) 2.	1. - 2.	% dev.
1	50.1	48.2	+1.9	+ 3.9
2	48.7	47.3	+0.4	+ 0.8
3	48.8	43.0	+5.3	+12.3
4	48.8	50.6	-1.8	- 3.6
5	51.1	48.2	+2.9	+ 6.0
6	60.5	52.8	+7.7	+14.6
7	55.3	50.3	+5.0	+ 9.9
9	34.1	35.0	-0.9	- 2.6
12	30.8	28.3	+2.5	+ 8.7
13	39.5	38.9	+0.6	+ 1.5
14	80.9	79.8	+1.1	+ 1.4
15	32.8	34.5	-1.7	- 4.9
18	45.8	44.1	+1.7	+ 3.9
19	68.6	69.2	-0.6	- 0.9
23	32.5	32.0	+0.5	+ 1.6
24	40.0	41.3	-1.3	- 3.1
25	57.3	62.5	-5.2	- 8.3
28	34.8	39.3	-4.5	-11.4
29	44.8	50.3	-5.5	-10.9
33	34.1	36.8	-2.7	- 7.3
34	42.5	48.2	-5.7	-11.8
35	49.5	52.1	-2.6	- 5.0
38	60.9	61.7	-0.8	- 1.3
40	42.9	47.4	-4.5	- 9.5
41	39.7	39.8	-0.1	- 0.3
42	34.5	34.5	-	-
54	54.7	51.3	+3.4	+ 6.6
56	58.5	53.9	+4.6	+ 8.5
57	59.0	52.6	+6.4	+12.2
58	55.2	50.0	+5.2	+10.4
60	68.4	61.9	+6.5	+10.5
61	45.4	44.3	+1.1	+ 2.5
62	59.5	61.7	-2.2	- 3.6
63	39.1	39.1	-	-
64	75.1	76.9	-1.8	- 2.3
68	73.5	72.1	+1.4	+ 1.9
69	44.5	49.0	-4.5	- 9.2
70	55.1	60.1	-5.0	- 8.3
72	61.0	64.4	-3.4	- 5.3

No. of points = 39 ; average deviation = 5.8%

No. of +ve pts. = 18 ; ave. deviation (+ve) = 5.5%

No. of -ve pts. = 19 ; ave. deviation (-ve) = 6.5%

Maxm. +ve dev. = 14.6% ; Maxm. -ve dev. = 11.8%

TABLE 14

Deviation summary of the values of E_A calculated from equation (49) for the transition and constant hold-up regions.

Run No.	E_A(calc.) 1.	E_A(exp.) 2.	1. - 2.	% dev.
8	53.5	48.9	+4.6	+9.4
10	47.7	48.6	-0.9	-1.9
11	50.9	52.9	-2.0	-3.8
16	52.4	53.9	-1.5	-2.8
17	57.9	53.7	+4.2	+7.8
20	66.5	72.8	-6.3	-8.7
21	67.2	69.2	-2.0	-2.9
22	66.3	67.0	-0.7	-1.0
26	60.2	65.1	-4.9	-7.5
27	61.2	63.6	-2.4	-3.8
30	56.5	59.9	-3.4	-5.7
31	55.9	55.7	+0.2	+0.4
32	56.5	57.1	-0.6	-1.0
36	55.4	56.8	-1.4	-2.5
37	55.4	56.8	-1.4	-2.5
39	70.6	72.3	-1.7	-2.4
44	57.2	55.9	+1.3	+2.3
65	68.5	64.5	+4.0	+6.2
66	55.0	51.6	+3.4	+6.6
67	77.5	71.8	+5.7	+7.9
71	64.6	64.4	+0.2	+0.3
73	70.6	67.2	+3.4	+5.1
74	82.0	78.4	+3.6	+4.6
75	61.6	58.9	+2.7	+4.6
76	67.5	69.3	-1.8	-2.6
77	67.5	65.3	+2.2	+3.4
78	61.7	61.9	-0.2	-0.3

No. of points = 27 ; average deviation = 4.0%

No. of +ve pts. = 12 ; ave. deviation (+ve) = 4.9%

No. of -ve pts. = 17 ; ave. deviation (-ve) = 2.9%

Maxm. +ve deviation = 9.4% ; maxm. -ve dev. = 8.7%

TABLE 15

Effect of porosity on absorption rate.

Run	Distributor	Porosity μ microns	E_A %	average $(H.T.U.)_{OL}$	average $K_L a$
4	fine bronze disc	72	53.0	1.80	286
45	medium bronze disc	408	55.4	1.61	325
46	coarse bronze disc	634	55.3	1.67	317
47	indented strip A	1150	52.9	1.77	266
48	indented strip B	810	53.1	1.75	287
49	1 x $\frac{3}{8}$in. dia. hole	9540	40.8	2.66	198
50	1 x $\frac{3}{8}$in. dia. hole	9540	40.4	2.49	208
51	4 x $\frac{1}{8}$in. dia. hole	3180	49.4	2.06	254

Where the absorption rate has been corrected to :-

h = 1.5 ft. p = 5.1 atm. CO_2 t = 15°C

u_L = 0.144 ft./sec. u_G = 0.135 ft./sec.

TABLE 16

Porosities of gas distributors using water.

Distributor	Thickness in.	Area $ft.^2$	Porosity μ microns
Porous glass P1	0.160	0.029	7.3
P2	0.160	0.026	81
P3	0.160	0.030	114
Porous bronze D1	0.123	0.0307	1330
D2	0.123	0.0307	634
D3	0.126	0.0307	408
D4	0.126	0.0307	364
D5	0.121	0.0307	72
D6	0.121	0.0307	170
Indented strip A.	1.00	0.0214	1150
Indented strip B.	1.00	0.0214	810

TABLE 17.

Effect of liquid properties on porosity.

Liquid.	Surface tension dynes/cm.	Porosity, microns	
		P2	P3
Water	72.9	81	114
Sea water	58.7	75	107
Acetone	26.2	82	76
Acetic acid	27.8	49	56
Ethyl acetate	24.6	45	74
23 wt.% glycerine	72.3	80	93
37 wt.% glycerine	71.3	83	88
49 wt.% glycerine	70.0	81	89
58 wt.% glycerine	69.0	80	89

PRESSURE ABSORBER - BUBBLE TYPE

DATA SHEET

ABSORBER HEIGHT - 8 FT. ; CROSS-SECTIONAL AREA = 0.0513 FT^2 ; ABSORPTION MEDIUM - FRESH WATER

Run Number	Gas Distributor	Total Absorber Pressure atm.	Pressure Drop Across Distributor p.s.i.	Temperature °C	Estimated Bed Height ft.	Inlet Gas: Total Rate lb.mole/hr.	Inlet Gas: Velocity ft./sec.	Inlet Gas: Composition % CO_2	Inlet Gas: CO_2 Rate lb.mole/hr.	Inlet Gas: N_2 Rate lb.mole/hr.	Exit Gas: Total Rate lb.mole/hr.	Exit Gas: Velocity ft./sec.	Exit Gas: Composition % CO_2	Exit Gas: CO_2 Rate lb.mole/hr.	CO_2 Absorbed lb.mole/hr.	% CO_2 Absorbed	Liquid Phase: Flow Rate c.f.m.	Liquid Phase: Flow Rate lb.mole/hr.	Liquid Phase: Velocity ft./sec.	Conc. of CO_2 in Solution, Inlet Liquid: m.f. x 10^3	Inlet Liquid: lb.mole/ft^3 x 10^3	Exit Liquid: m.f. x 10^3	Exit Liquid: lb.mole/ft^3 x 10^3	Equilibrium CO_2 Conc., Inlet Gas Conditions: α vol./vol.	Inlet Gas: m.f. x 10^3	Inlet Gas: lb.mole/ft^3 x 10^3	Outlet Gas Conditions: α vol./vol.	Outlet Gas: m.f. x 10^3	Outlet Gas: lb.mole/ft^3 x 10^3	E_A Absorption Efficiency (% Saturation) Based on Inlet Gas	E_A Based on Outlet Gas	CO_2 Material Balance %	Inlet E_A corrected† to 100% CO_2 Material Balance	Carry Over % CO_2	Run Number
1	D5	6.11	10	10.0	1.56	0.373	0.119	86.8	0.324	0.049	0.155	0.050	67.8	0.105	0.219	67.6	0.444	92.3	0.144	0.02	0.08	2.35	8.15	6.14	4.91	17.10	4.86	3.90	13.54	47.6	60.0	98.8	48.2	-	1
2		6.11	10	9.9	1.49	0.357	0.113	84.1	0.300	0.057	0.153	0.050	63.4	0.097	0.203	67.7	0.444	92.3	0.144	0.03	0.09	2.42	8.40	5.99	4.80	16.70	4.58	3.68	12.76	50.1	65.5	106.0	47.3	-	2
3		6.12	10	10.0	1.48	0.362	0.116	84.3	0.305	0.057	0.173	0.056	67.7	0.117	0.188	61.7	0.441	91.8	0.144	0.03	0.09	2.07	7.19	5.97	4.78	16.64	4.86	3.90	13.54	43.0	52.8	100.0	43.0	-	3
4		6.12	10	9.2	1.49	0.403	0.127	85.4	0.344	0.059	0.164	0.052	64.1	0.105	0.239	69.5	0.446	92.8	0.145	0.03	0.09	2.49	8.65	6.28	5.03	17.50	4.80	3.86	13.38	48.2	64.3	97.4	50.6	-	4
5		6.12	10	10.1	1.75	0.365	0.115	85.2	0.311	0.054	0.152	0.049	64.5	0.098	0.213	68.5	0.444	92.3	0.144	0.03	0.09	2.37	8.24	6.02	4.82	16.78	4.64	3.73	12.92	48.8	63.3	101.3	48.2	-	5
6		6.11	10	11.4	2.89	0.340	0.109	81.5	0.277	0.063	0.129	0.042	50.4	0.065	0.212	76.6	0.441	91.8	0.144	0.02	0.08	2.35	8.16	5.49	4.40	15.30	3.46	2.78	9.64	53.2	84.4	100.3	52.8	-	6
7		6.11	10	11.4	2.18	0.340	0.109	80.9	0.275	0.065	0.139	0.045	53.3	0.074	0.201	73.1	0.441	91.8	0.144	0.03	0.11	2.21	7.67	5.47	4.38	15.25	3.66	2.94	10.21	50.1	74.9	99.6	50.3	-	7
8		6.10	10	13.0	1.17	0.459	0.148	87.5	0.401	0.058	0.259	0.085	77.2	0.200	0.201	50.1	0.446	92.8	0.145	0.02	0.08	2.13	7.34	5.51	4.41	15.37	4.90	3.93	13.64	48.1	54.0	98.4	48.9	-	8
9		6.09	10	11.6	0.67	0.293	0.096	81.8	0.240	0.053	0.153	0.051	65.4	0.100	0.140	58.4	0.446	92.8	0.145	0.03	0.12	1.52	5.27	5.44	4.33	15.07	4.46	3.58	12.43	34.7	42.0	99.2	35.0	-	9
10		6.10	10	12.4	0.72	0.424	0.138	87.3	0.370	0.054	0.237	0.078	71.8	0.170	0.200	54.1	0.446	92.8	0.145	0.02	0.08	2.19	7.58	5.63	4.51	15.68	4.68	3.76	13.03	48.8	58.5	100.3	48.6	-	10
11	D5	6.10	10	12.0	0.99	0.425	0.138	87.1	0.370	0.055	0.203	0.067	69.0	0.140	0.230	62.2	0.446	92.8	0.145	0.03	0.10	2.46	8.55	5.71	4.58	15.92	4.58	3.68	12.76	52.3	66.6	98.9	52.9	-	11
12		6.10	10	12.2	0.38	0.347	0.113	85.0	0.295	0.052	0.240	0.079	76.7	0.184	0.111	37.7	0.446	92.8	0.145	0.03	0.10	1.30	4.48	5.53	4.43	15.41	5.02	4.03	13.99	28.9	31.8	102.1	28.3	-	12
13		6.11	10	13.5	1.28	0.254	0.082	81.1	0.206	0.048	0.109	0.031	55.0	0.060	0.146	70.9	0.446	92.8	0.145	0.03	0.10	1.56	5.41	5.03	4.04	14.02	3.47	2.79	9.67	38.2	55.5	98.1	38.9	-	13
14		6.11	10	16.0	5.39	0.362	0.119	83.7	0.303	0.059	0.083	0.028	28.9	0.024	0.279	92.1	0.435	90.7	0.142	0.03	0.12	3.07	10.67	4.84	3.89	13.49	1.35	1.09	3.76	78.8	100+	98.8	79.8	-	14
15		6.11	10	12.4	1.31	0.191	0.062	77.5	0.148	0.043	0.057	0.018	22.8	0.013	0.135	91.2	0.471	97.8	0.153	0.03	0.12	1.38	4.77	5.04	4.05	14.05	1.31	1.07	3.65	33.6	100+	98.0	34.5	-	15
16		6.11	10	13.8	1.62	0.564	0.183	86.8	0.489	0.075	0.354	0.118	76.8	0.272	0.217	44.4	0.449	93.4	0.146	0.03	0.12	2.28	7.91	5.30	4.26	14.78	4.72	3.80	13.16	53.2	59.7	98.6	53.9	-	16
17		6.12	10	14.1	1.65	0.653	0.210	86.8	0.566	0.087	0.429	0.140	79.0	0.339	0.209*	36.9	0.446	92.8	0.145	0.03	0.12	2.28	7.91	5.25	4.22	14.63	4.80	3.86	13.38	53.7	58.8	96.7	53.7	3.3	17
18		6.08	10	15.7	1.34	0.127	0.043	74.8	0.095	0.032	0.079	0.027	58.2	0.046	0.049	51.6	0.160	33.3	0.052	0.03	0.11	1.55	5.37	4.25	3.41	11.83	3.36	2.70	9.37	45.0	56.9	102.0	44.1	-	18
19		6.11	10	17.4	1.39	0.262	0.086	84.4	0.221	0.041	0.174	0.058	76.4	0.133	0.088	39.8	0.160	33.3	0.052	0.03	0.11	2.51	8.70	4.60	3.70	12.82	4.18	3.36	11.65	67.6	74.5	97.8	69.2	-	19
20		6.11	10	17.6	1.42	0.335	0.110	85.4	0.268	0.049	0.247	0.082	79.0	0.195	0.091	31.8	0.160	33.3	0.052	0.03	0.11	2.71	9.40	4.62	3.73	12.87	4.29	3.45	11.85	72.4	78.4	99.7	72.6	-	20
21	D5	6.12	10	17.8	1.53	0.453	0.148	87.7	0.397	0.056	0.360	0.117	83.3	0.300	0.097	24.5	0.160	33.3	0.052	0.03	0.11	2.56	8.94	4.73	3.80	13.18	4.50	3.62	12.53	67.1	72.5	97.0	69.2	-	21
22		6.10	10	16.2	1.57	0.507	0.168	89.1	0.452	0.055	0.412	0.136	86.3	0.356	0.096	21.2	0.160	33.3	0.052	0.03	0.11	2.65	9.20	5.00	4.02	13.93	4.85	3.90	13.52	65.7	67.7	98.2	67.0	-	22
23		6.12	10	17.0	1.30	0.132	0.043	81.8	0.108	0.024	0.060	0.019	56.7	0.034	0.074	68.5	0.307	63.8	0.100	0.03	0.12	1.17	4.03	4.53	3.64	12.62	3.18	2.56	8.87	31.4	45.1	98.2	32.0	-	23
24		6.10	10	15.2	1.33	0.190	0.062	83.2	0.158	0.032	0.090	0.030	62.2	0.056	0.102	64.5	0.307	63.8	0.100	0.03	0.12	1.59	5.53	4.80	3.86	13.38	3.66	2.94	10.21	40.7	53.7	98.8	41.3	-	24
25		6.10	10	15.7	1.43	0.316	0.104	83.6	0.264	0.052	0.166	0.055	68.7	0.114	0.150	56.8	0.307	63.8	0.100	0.03	0.12	2.42	8.39	4.77	3.83	13.29	3.95	3.17	11.00	62.9	75.4	100.6	62.5	-	25
26		6.10	10	15.3	1.55	0.441	0.144	89.5	0.395	0.046	0.274	0.090	82.5	0.226	0.169	42.8	0.307	63.8	0.100	0.03	0.12	2.70	9.36	5.14	4.12	14.31	4.76	3.83	13.28	65.3	70.3	100.3	65.1	-	26
27		6.09	10	16.5	1.63	0.582	0.188	89.8	0.523	0.059	0.421	0.139	85.5	0.360	0.163	31.2	0.307	63.8	0.100	0.03	0.12	2.56	8.87	4.98	4.00	13.88	4.76	3.83	13.28	63.4	66.6	99.7	63.6	-	27
28		6.09	10	15.2	1.31	0.227	0.075	82.2	0.188	0.039	0.071	0.024	38.0	0.027	0.161	85.7	0.520	108.3	0.170	0.03	0.10	1.49	5.16	4.78	3.84	13.32	2.24	1.78	6.24	38.6	83.4	98.4	39.3	-	28
29		6.09	10	16.0	1.39	0.334	0.110	84.8	0.283	0.051	0.132	0.044	56.8	0.075	0.208	73.6	0.520	108.3	0.170	0.03	0.10	1.96	6.80	4.79	3.85	13.35	3.26	2.62	9.08	50.5	74.5	100.3	50.3	-	29
30		6.10	10	16.3	1.50	0.451	0.148	86.0	0.388	0.063	0.201	0.067	67.2	0.135	0.253	65.2	0.520	108.3	0.170	0.03	0.10	2.29	7.94	4.82	3.88	13.43	3.81	3.06	10.61	58.7	74.6	98.0	59.9	-	30
31	D5	6.10	10	15.0	1.52	0.502	0.164	88.2	0.443	0.059	0.236	0.078	75.0	0.177	0.246*	49.0	0.520	108.3	0.170	0.03	0.10	2.30	7.99	5.11	4.11	14.24	4.37	3.51	12.19	55.7	65.3	95.5	55.7	4.5	31
32		6.10	10	16.0	1.58	0.654	0.214	89.2	0.583	0.071	0.363	0.119	81.3	0.295	0.249*	39.1	0.520	108.3	0.170	0.03	0.10	2.33	8.10	5.05	4.06	14.08	4.62	3.71	12.88	57.1	62.5	93.6	57.1	6.4	32
33		6.10	10	15.8	1.32	0.251	0.082	84.5	0.212	0.039	0.071	0.024	45.1	0.032	0.180	84.9	0.614	127.8	0.200	0.03	0.12	1.42	4.92	4.80	3.86	13.38	2.62	2.11	7.30	36.3	66.8	98.7	36.8	-	33
34		6.12	10	15.0	1.39	0.329	0.116	83.9	0.276	0.053	0.088	0.029	42.1	0.037	0.239	86.6	0.614	127.8	0.200	0.03	0.12	1.89	6.55	4.88	3.92	13.59	2.51	2.02	6.99	47.8	93.5	99.3	48.2	-	34
35		6.12	10	16.8	1.48	0.440	0.143	87.3	0.384	0.056	0.164	0.054	66.5	0.109	0.257*	69.6	0.614	127.8	0.200	0.03	0.12	2.04	7.09	4.84	3.89	13.49	3.78	3.04	10.53	52.1	66.8	95.3	52.1	4.7	35
36		6.12	10	16.5	1.55	0.559	0.181	86.3	0.482	0.077	0.228	0.075	67.6	0.154	0.279*	57.9	0.614	127.8	0.200	0.03	0.12	2.22	7.71	4.93	3.99	13.46	3.83	3.07	10.67	56.8	72.1	88.9	56.8	10.1	36
37		6.10	10	16.5	1.64	0.825	0.270	90.4	0.746	0.079	0.336	0.111	80.1	0.269	0.290*	38.9	0.614	127.8	0.200	0.03	0.12	2.31	8.00	5.03	4.04	14.02	4.48	3.60	12.48	56.8	63.9	74.8	56.8	25.2	37
38		3.39	8	15.5	1.45	0.192	0.114	85.4	0.164	0.028	0.069	0.041	59.4	0.041	0.123	75.0	0.441	91.8	0.144	0.03	0.12	1.42	4.91	2.77	2.23	7.72	1.95	1.57	5.44	63.2	90.3	102.5	61.7	-	38
39		3.39	8	15.3	1.54	0.252	0.149	84.9	0.214	0.038	0.106	0.063	63.2	0.067	0.147	68.7	0.441	91.8	0.144	0.03	0.12	1.59	5.50	2.77	2.23	7.72	2.08	1.67	5.80	70.9	95.2	98.2	72.3	-	39
40		9.51	10	16.7	1.47	0.524	0.109	84.4	0.442	0.082	0.271	0.057	68.7	0.186	0.256	57.9	0.441	91.8	0.144	0.03	0.12	2.78	9.65	7.13	5.88	19.87	5.87	4.70	16.35	47.0	58.8	99.2	47.4	-	40
41	D5	12.91	10	16.3	1.50	0.758	0.114	84.2	0.638	0.120	0.474	0.071	74.3	0.352	0.286	44.8	0.441	91.8	0.144	0.03	0.12	2.96	10.25	9.51	7.59	26.50	8.49	6.79	23.65	38.8	43.3	97.7	39.8	-	41
42	D5	16.32	10	15.9	1.46	0.867	0.101	85.4	0.723	0.144	0.562	0.066	73.6	0.414	0.309	42.7	0.441	91.8	0.144	0.03	0.11	3.11	10.79	11.51	9.20	32.10	10.49	8.38	29.25	33.6	36.9	96.9	34.5	-	42
43	D5	1.00	5	13.2	1.90	0.448	0.906	100.0	0.448	-	0.385	0.779	99.5	0.383	0.054*	12.1	0.449	93.4	0.146	0.03	0.12	0.62	2.13	1.07	0.86	2.98	1.07	0.86	2.98	71.1	71.1	97.6	71.1	2.4	43
44	D5	6.11	10	13.2	1.96	0.438	0.141	100.0	0.438	-	0.177	0.057	99.5	0.176	0.264	66.7	0.449	93.4	0.146	0.03	0.12	2.76	9.57	6.23	4.99	17.37	6.19	4.96	17.23	55.0	55.4	98.4	55.9	-	44
45	D3	6.11	10	16.4	1.60	0.384	0.125	82.5	0.317	0.067	0.197	0.065	64.5	0.127	0.190	59.9	0.441	91.8	0.144	0.03	0.11	2.08	7.21	4.63	3.73	12.90	3.66	2.94	10.21	55.4	70.5	98.4	55.7	-	45
46	D2	6.11	10	16.2	1.63	0.384	0.125	82.5	0.317	0.067	0.194	0.064	63.9	0.124	0.193	60.9	0.441	91.8	0.144	0.03	0.11	2.09	7.27	4.65	3.74	12.95	3.64	2.93	10.15	55.6	71.1	98.8	56.3	-	46
47	A	6.11	8	17.2	1.64	0.377	0.123	84.1	0.317	0.060	0.201	0.067	67.6	0.136	0.181	57.1	0.441	91.8	0.144	0.03	0.11	1.96	6.80	4.61	3.71	12.85	3.74	3.00	10.42	52.4	65.0	98.8	52.9	-	47
48	B	6.10	8	16.4	1.69	0.376	0.123	84.6	0.318	0.058	0.199	0.066	68.4	0.136	0.182	57.3	0.441	91.8	0.144	0.03	0.11	1.98	6.88	4.73	3.80	13.18	3.86	3.08	10.75	51.7	63.9	99.0	52.2	-	48
49	C	6.10	3	17.2	1.50	0.374	0.123	84.0	0.314	0.060	0.235	0.078	74.1	0.174	0.140	44.6	0.441	91.8	0.144	0.03	0.11	1.54	5.36	4.60	3.70	12.82	4.08	3.28	11.37	41.2	46.5	99.7	41.3	-	49
50	C	6.09	3	17.0	1.50	0.394	0.131	86.1	0.339	0.055	0.258	0.086	77.9	0.201	0.138	40.7	0.441	91.8	0.144	0.03	0.11	1.57	5.44	4.73	3.80	13.18	4.29	3.46	11.95	40.9	45.0	100.8	40.6	-	50
51	E	6.09	5	18.0	1.53	0.449	0.150	85.6	0.384	0.065	0.280	0.094	76.8	0.215	0.169	44.0	0.441	91.8	0.144	0.02	0.08	1.85	6.42	4.58	3.68	12.76	4.12	3.31	11.48	50.0	56.1	100.2	49.9	-	51
54	D5	6.10	10	20.0	1.63	0.373	0.124	86.1	0.321	0.052	0.209	0.069	74.2	0.155	0.166	51.7	0.446	92.8	0.145	0.02	0.08	1.82	6.31	4.35	3.49	12.13	3.76	3.02	10.48	51.8	60.0	101.0	51.3	-	54
56		6.10	10	29.1	1.63	0.378	0.129	86.0	0.325	0.053	0.236	0.080	77.6	0.183	0.142	47.7	0.446	92.8	0.145	0.02	0.08	1.51	5.24	3.49	2.80	9.72	3.15	2.53	8.78	53.6	59.4	99.5	53.9	-	56
57		6.10	10	25.0	1.60	0.399	0.134	86.5	0.345	0.054	0.249	0.085	78.4	0.195	0.150	43.5	0.446	92.8	0.145	0.02	0.08	1.65	5.72	3.85	3.09	10.72	3.50	2.81	9.74	53.2	58.5	101.2	52.6	-	57
58		6.10	10	15.5	1.58	0.395	0.129	86.3	0.341	0.054	0.208	0.068	73.6	0.153	0.188	55.2	0.446	92.8	0.145	0.02	0.08	1.98	6.87	4.94	3.97	13.76	4.25	3.41	11.83	49.4	57.8	98.8	50.0	-	58
60		6.09	10	18.0	4.00	0.326	0.109	84.9	0.277	0.049	0.119	0.040	58.8	0.070	0.207	74.8	0.441	91.8	0.144	0.02	0.08	2.24	7.76	4.54	3.65	12.64	3.18	2.56	8.87	61.7	87.5	99.7	61.9	-	60
61	D5	6.09	10	17.2	1.51	0.277	0.093	85.2	0.236	0.041	0.122	0.041	66.4	0.081	0.155	65.7	0.441	91.8	0.144	0.02	0.08	1.65	5.72	4.66	3.75	12.98	3.67	2.95	10.24	43.7	55.7	98.8	44.3	-	61
62		6.10	10	19.1	1.52	0.191	0.065	85.7	0.164	0.027	0.116	0.039	76.8	0.089	0.075	45.8	0.160	33.3	0.052	0.02	0.08	2.22	7.70	4.49	3.61	12.51	3.99	3.21	11.12	61.4	69.0	99.5	61.7	-	62
63		6.10	10	19.1	0.43	0.191	0.065	85.7	0.164	0.027	0.145	0.049	81.4	0.118	0.046	28.1	0.160	33.3	0.052	0.02	0.08	1.44	5.00	4.49	3.61	12.51	4.22	3.39	11.77	39.6	42.2	101.2	39.1	-	63
64		6.10	10	19.1	3.10	0.191	0.065	85.7	0.164	0.027	0.097	0.033	72.2	0.070	0.094	57.4	0.160	33.3	0.052	0.02	0.08	2.71	9.40	4.49	3.61	12.51	3.80	3.05	10.58	75.0	88.8	97.5	76.9	-	64
65		6.09	10	18.0	1.55	0.755	0.252	85.4	0.645	0.110	0.676	0.226	83.6	0.565	0.080	12.4	0.160	33.3	0.052	0.02	0.08	2.38	8.19	4.57	3.67	12.73	4.47	3.59	12.46	64.4	66.1	99.8	64.5	-	65
66		6.10	10	20.0	0.55	0.757	0.253	85.6	0.648	0.109	0.713	0.234	84.6	0.603	0.045	6.3	0.160	33.3	0.052	0.02	0.08	1.84	6.38	4.32	3.47	12.04	4.27	3.43	11.89	52.8	53.4	102.4	51.6	-	66
67		6.09	10	18.3	2.75	0.757	0.253	85.5	0.647	0.110	0.658	0.220	81.9	0.547	0.100	16.5	0.160	33.3	0.052	0.02	0.08	2.55	8.84	4.52	3.63	12.60	4.34	3.48	12.10	70.1	73.1	97.7	71.8	-	67
68		3.04	8	18.0	1.52	0.093	0.062	84.9	0.079	0.014	0.049	0.034	71.4	0.035	0.044	55.7	0.160	33.3	0.052	0.02	0.08	1.38	4.77	2.31	1.86	6.44	1.95	1.57	5.44	73.9	87.8	102.5	72.1	-	68
69		14.27	10	18.0	1.54	0.460	0.063	84.8	0.390	0.070	0.321	0.045	78.2	0.251	0.139	35.7	0.160	33.3	0.052	0.02	0.08	3.84	13.32	10.03	8.06	27.95	9.31	7.48	25.95	47.6	51.2	97.2	49.0	-	69
70		6.10	10	12.0	1.53	0.191	0.062	85.8	0.164	0.027	0.100	0.032	73.0	0.073	0.091	55.5	0.160	33.3	0.052	0.02	0.08	2.70	9.36	5.63	4.51	15.68	4.82	3.88	13.43	59.7	69.2	99.4	60.1	-	70
71	D5	6.10	10	12.0	1.49	0.757	0.245	85.6	0.648	0.109	0.651	0.211	83.1	0.541	0.107	16.5	0.160	33.3	0.052	0.02	0.08	2.85	9.88	5.62	4.50	15.65	5.46	4.37	15.19	63.2	64.7	98.2	64.4	-	71
72		6.10	10	29.4	1.53	0.187	0.063	85.6	0.160	0.027	0.126	0.043	78.6	0.099	0.061	38.2	0.160	33.3	0.052	0.02	0.08	1.77	6.14	3.45	2.77	9.61	3.18	2.56	8.86	63.6	68.4	98.8	64.4	-	72
73		6.10	10	29.4	1.48	0.750	0.251	85.9	0.644	0.106	0.670	0.255	84.0	0.563	0.081	12.6	0.160	33.3	0.052	0.02	0.08	1.83	6.35	3.46	2.78	9.64	3.38	2.72	9.42	65.6	67.1	97.7	67.2	-	73
74		3.36	8	16.7	1.51	0.415	0.250	85.0	0.353	0.062	0.351	0.212	82.3	0.289	0.062	17.7	0.160	33.3	0.052	0.02	0.08	1.62	5.62	2.64	2.12	7.36	2.56	2.06	7.14	76.2	78.4	97.2	78.4	-	74
75		6.64	10	16.2	1.47	0.802	0.241	100.0	0.802	-	0.699	0.210	100.0	0.699	0.103	12.9	0.160	33.3	0.052	0.02	0.08	3.30	11.43	6.90	5.54	19.21	6.90	5.54	19.21	59.4	59.4	100.9	58.9	-	75
76		6.09	10	15.5	1.50	0.747	0.249	85.1	0.636	0.111	0.689	0.232	83.9	0.578	0.058	8.2	0.093	19.5	0.030	0.02	0.08	2.69	9.33	4.86	3.90	13.54	4.79	3.85	13.35	68.8	69.8	99.0	69.3	-	76
77		6.09	10	15.5	1.52	0.747	0.249	85.1	0.636	0.111	0.654	0.218	82.9	0.542	0.094	14.8	0.160	33.3	0.052	0.02	0.08	2.51	8.70	4.86	3.90	13.54	4.75	3.82	13.24	64.2	65.5	98.4	65.3	-	77
78		6.09	10	15.5	1.52	0.747	0.249	85.1	0.636	0.111	0.575	0.191	79.1	0.465	0.150	23.6	0.307	63.8	0.100	0.02	0.08	2.34	8.11	4.86	3.90	13.54	4.54	3.65	12.64	59.8	64.0	96.6	61.9	-	78

CONCENTRATION GRADIENT DATA

Run Number	Height Above Gas Distributor ft.	CO_2 Content lb.mole/ft^3 x 10^3
6	0.00	8.16
	0.13	7.69
	0.63	7.07
	1.13	6.76
	1.63	4.27
	2.38	0.23
7	0.00	7.67
	0.13	7.36
	0.63	7.07
	1.13	6.89
	1.63	5.00
8	0.00	7.34
	0.13	6.89
	0.63	6.69
	1.13	5.21
9	0.00	5.27
	0.13	5.17
	0.63	3.01
10	0.00	7.58
	0.13	7.12
	0.63	5.53
11	0.00	8.55
	0.13	7.55
	0.63	6.60
13	0.00	5.41
	0.13	5.06
	0.63	3.35
	1.13	2.15

GAS DISTRIBUTORS :-

	Distributor	Porosity Microns	No of Holes	Area ft^2
A	Indented Strip A	1150	441	0.0214
B	Indented Strip B	810	903	0.0214
C	3/8" Dia. Hole	9540	1	0.0031
D2	Sintered Bronze Disc	634	-	0.0307
D3	Sintered Bronze Disc	408	-	0.0307
D5	Sintered Bronze Disc	72	-	0.0307
E	1/8" Dia. Hole	3180	4	0.0307

NOTES :-

* Absorption rates calculated from liquid phase carbon dioxide concentrations.

† Absorption efficiencies, E_A, corrected to various operating conditions as used in plotting thesis graphs, are shown in Appendix II of this thesis. The corresponding $(H.T.U.)_{OL}$ and K_La values are also shown in Appendix II.